

Global structure of conformal theories in the $SU(3)$ gauge theoryK.-I. Ishikawa,¹ Y. Iwasaki,² Yu Nakayama,³ and T. Yoshie²¹*Graduate School of Science, Hiroshima University, Higashi-Hiroshima, Hiroshima 739-8526, Japan*²*Center for Computational Sciences, University of Tsukuba, Tsukuba, Ibaraki 305-8577, Japan*³*Kavli Institute for the Physics and Mathematics of the Universe (WPI), Todai Institutes for Advanced Study, Kashiwa, Chiba 277-8583, Japan*

(Received 29 October 2013; published 9 June 2014)

We investigate $SU(3)$ gauge theories in four dimensions with N_f fundamental fermions on a lattice using the Wilson fermion. Clarifying the vacuum structure in terms of Polyakov loops in spatial directions and properties of temporal propagators using a new method that we call “local analysis,” we conjecture that the “conformal region” exists together with the confining region and the deconfining region in the phase structure parametrized by β and K , both in the cases of the large N_f QCD within the conformal window (referred as conformal QCD) with an IR cutoff and small N_f QCD at $T/T_c > 1$ with T_c being the chiral transition temperature (referred to as high-temperature QCD). Our numerical simulation on a lattice of the size $16^3 \times 64$ shows the following evidence of the conjecture. In the conformal region, we find that the vacuum is the nontrivial $Z(3)$ twisted vacuum modified by nonperturbative effects and that temporal propagators of mesons behave at large t as a power-law-corrected Yukawa-type decaying form. The transition from the conformal region to the deconfining region or the confining region is a sharp transition between different vacua, and therefore, it suggests a first-order transition both in conformal QCD and high-temperature QCD. To confirm the conjecture and distinguish it from the possibility of crossover phenomena, we need to take the continuum/thermodynamic limit, which we do not attempt in this work. Within our fixed-lattice simulation, we find that there is a precise correspondence between conformal QCD and high-temperature QCD in the temporal propagators under the change of the parameters N_f and T/T_c , respectively: one boundary is close to meson states, and the other is close to free quark states. In particular, conformal QCD with $N_f = 7$ corresponds to high-temperature QCD with $N_f = 2$ at $T \sim 2T_c$, both of which are in close relation to a meson unparticle model. From this, we estimate the anomalous mass dimension $\gamma^* = 1.2(1)$ for $N_f = 7$. We also show that the asymptotic state in the limit $T/T_c \rightarrow \infty$ is a free quark state in the $Z(3)$ twisted vacuum. The approach to a free quark state is very slow; even at $T/T_c \sim 10^5$, the state is affected by nonperturbative effects. This is possibly connected with the slow approach of the free energy to the Stefan-Boltzmann ideal gas limit.

DOI: 10.1103/PhysRevD.89.114503

PACS numbers: 12.38.Gc, 11.25.Hf

I. INTRODUCTION

Recently, much attention has been paid to conformal theories in the $d = 4$ dimension since conformal theories or nearly conformal theories are attractive candidates for the beyond standard model. In the evolution of the Universe, conformal theories might play key ingredients in many aspects, presumably more than we know today. All conformal field theories have their own distinct features. To confront the nature, it is important to understand each conformal theory, and for this purpose, it is urgent to clarify the global structure of conformal theories [1].

One important class of simple conformal field theories in $d = 4$ is realized by the so-called Banks-Zaks fixed point [2] in many flavor gauge theories. The possibility of the existence of a conformal theory in $SU(3)$ gauge theory with N_f flavors in the fundamental representation was first pointed out by W. Caswell in [3].

From the perturbative computation of the beta function, we believe that the upper critical number of flavors N_f for

the existence of an infrared (IR) fixed point in $SU(3)$ gauge theory is 16. We denote the lower critical number of flavors by N_f^c . The region of $N_f(N_f^c \leq N_f \leq 16)$ that has the IR fixed point is called the conformal window.

In the case of $N_f \simeq 16$, the coupling constant at the IR fixed point is small, and therefore, the perturbation theory may be applicable. However, in the case of $N_f \sim N_f^c$, nonperturbative effects are important, and nonperturbative tools are essential.

Lattice gauge theories are systematic and nonperturbative tools for investigating issues such as the lower critical number of flavors N_f^c , the anomalous mass dimension and the spectrum. Many lattice studies were indeed performed [4–54]. Numerical tools such as the step-scaling scheme [55] and the Monte Carlo renormalisation group (MCRG) method, as well as the calculation of mass spectrum and the analysis of the phase structure, have been used in order to identify the IR fixed point and the conformal window [1].

However, the determination of the lower critical number of flavors N_f^c is still much controversial. One possible

reason for the controversy arises from the fact that pinpointing the IR fixed point for N_f^c is the strong coupling problem and technically it is hard to reach such a region even with the step-scaling scheme. Another possible reason, when the mass spectrum is used to find the N_f^c , is that the suitable mass region for the investigation of conformal properties is limited, as is clarified in this article. However, in many calculations the mass spectrum outside of this region is used.

In our previous paper [4], we conjectured that the lower critical number of flavor $N_f^c = 7$. In Appendix A, we report a brief summary of the paper with some updates. In this article, we do not assume a particular value of N_f^c in general discussions. The aim of this paper is to establish the properties intrinsic to the conformal window such as the vacuum structure and specific behaviors of temporal propagators. We would like to check these properties for various N_f , including $N_f = 7$, and we verify whether our conjecture of $N_f^c = 7$ is consistent with them.

A. Strategy and objectives

In this article, we discuss the following two categories in $SU(3)$ gauge theories with N_f flavors in the fundamental representation, which possess an IR fixed point:

- (i) Large N_f ($N_f^c \leq N_f \leq 16$) QCD within the conformal window (referred as conformal QCD)
- (ii) Small N_f ($2 \leq N_f \leq N_f^c - 1$) QCD at temperature $T/T_c > 1$ with T_c being the critical temperature (referred as high-temperature QCD)

The existence of an IR fixed point in conformal QCD is well known as the Banks-Zaks IR fixed point [2], as mentioned above. In high-temperature QCD, the existence of an IR fixed point has been recently pointed out in Ref. [56]. We clarify the precise relation between the IR fixed point and the ‘‘conformal symmetry’’ in detail below since this is not literally true at first sight (e.g., the non-vanishing trace anomaly for high-temperature QCD; see also Appendix B for a brief review of our argument in [56]).

Let us further consider the case where there is an IR cutoff in the theory which possesses an IR fixed point. In the case of conformal QCD in the continuum limit, the compact space and/or time gives an IR cutoff. In the case of high-temperature QCD, the temperature T plays a role of an IR cutoff together with a cutoff due to possible compact space, depending on how to take the continuum limit. We note that any lattice calculation is performed on a finite lattice. Thus, any calculation on a lattice possesses an IR cutoff.

In case there is an IR cutoff, we introduce a new concept, ‘‘conformal theories with an IR cutoff’’: In the ‘‘conformal region,’’ where the quark mass is smaller than the critical value, temporal propagators $G_H(t)$ of meson behave at large t as a power-law-corrected Yukawa-type decaying form instead of the exponential decaying form observed in the ‘‘confining region’’ and ‘‘deconfining region.’’ We note

the exponential decay form in the deconfining region is approximate due to the finiteness of the t region. This point is discussed in some detail below. One of the objectives of this article is to verify the existence of the conformal region and a power-law-corrected Yukawa-type decaying form instead of the exponential decaying form of meson propagators in the conformal region on a finite lattice with a fixed size of $16^3 \times 64$.

We stress that QCD in compact space and/or time is a conformal theory with an IR cutoff for $\beta \geq \beta^c$, as is discussed below. Here the β^c is the critical bare coupling constant ($\beta = 6/g_0^2$) at which a chiral transition occurs for the massless quark. In the case of the compact space, the temperature may be defined by $1/N_t a$ as usual.

On the other hand, one of our final goals is the verification of the conjecture of the conformal theory with an IR cutoff for the case of the thermodynamical limit of high-temperature QCD in the flat space, in addition to the continuum limit of the conformal QCD in the flat space at zero temperature. Since we define the conformal region from the properties of the temporal propagators, we need a lattice with large N_t in order to verify the idea of the conformal theories with an IR cutoff. Therefore, we take the same lattice size $16^3 \times 64$ for the simulation of high-temperature QCD.

We understand that our quantitative predictions for thermodynamic properties for high-temperature QCD will be affected by the small spatial lattice size. However, since our theoretical argument only relies on the vanishing beta function and the existence of an IR cutoff (either by a temporal one or a spatial one), this lattice size does not spoil our objective to investigate qualitatively the behavior of propagators. If we could confirm our concepts of conformal field theories with an IR cutoff on this size lattice, we would be able to naturally conjecture that our proposal will be realized on a larger spatial lattice such as $256^3 \times 64$. Testing our conjecture on a larger lattice in order to take the thermodynamic limit is important if we would like to compare our results with the experiment. However, it is beyond the scope of this article. We will make a small comment in Sec. XII.

After verification of the existence of the conformal region and a power-law-corrected Yukawa-type decaying form on the lattice with a size of $16^3 \times 64$, we would like to reveal the properties of the conformal region and the temporal propagators in all cases of conformal QCD and high-temperature QCD as a whole. In particular, we would like to clarify the underlying physics leading to the behavior of the characteristic form of the propagators and extract the physical properties of each theory.

We utilize two tools to investigate the issues: One is a new method of analyzing the propagators of mesons which we call the local analysis of propagators. The other is the analysis of the vacuum in terms of the Polyakov loops in spatial directions.

We find that the vacuum corresponding to the conformal region is the nontrivial $Z(3)$ twisted vacuum modified by nonperturbative effects. Clarifying the relation between the vacuum structure and properties of temporal propagators in each vacuum, we show that the transition from the power-law-corrected Yukawa-type decaying form to the exponential decay is a transition between different vacua, and therefore, it is a first-order transition both in conformal QCD and high-temperature QCD.

Finally, we argue from our theoretical analysis based on the renormalization group (RG) flow and our numerical simulations that there is a precise correspondence between the conformal QCD and high-temperature QCD within the conformal region. The correspondence between the two sets of conformal theories with an IR cutoff is realized between a continuous parameter T/T_c and a discrete parameter N_f : one boundary is close to meson states, and the other is close to free quark states.

In particular, conformal QCD with $N_f = 7$ corresponds to high-temperature QCD with $N_f = 2$ at $T \sim 2T_c$ both of which are in close relation to a meson unparticle model. From this, we estimate the anomalous mass dimension $\gamma^* = 1.2(1)$ for $N_f = 7$. We also show that the asymptotic state in the limit $T/T_c \rightarrow \infty$ is a free quark state in the $Z(3)$ twisted vacuum. The approach to a free quark state is very slow; even at $T/T_c \sim 10^5$, the state is affected by nonperturbative effects. We believe that this is related with the slow approach of the free energy to the Stefan-Boltzmann ideal gas limit. To conclude the precise relation, we need to perform a similar analysis in the thermodynamical limit.

The fact above is consistent with our conjecture that the lower critical flavor number $N_f^c = 7$ [57].

B. Outline of the paper

The rest of the paper is organized as follows. In Sec. II, we provide theoretical and numerical background to study an IR fixed point in lattice QCD. In Sec. III, we introduce the new concept of conformal theories with an IR cutoff and discuss its implications. In Sec. IV, we study the structure of propagators to confirm the existence of conformal regions. In Sec. V, we study the vacuum structure of lattice QCD. In Sec. VI, we analyze the propagators in each vacuum. In Sec. VII, we discuss the detailed relation between the vacuum structure and the existence of conformal region. In Sec. VIII, we analyze the effects of boundary conditions on the structure of vacuum. In Sec. IX, we introduce the concept of unparticle models as an effective description in the conformal region. In Sec. X, we propose the correspondence between conformal QCD and high-temperature QCD. In Sec. XI, the correspondence is further studied to predict the mass anomalous dimensions. In Sec. XII, we conclude the paper with further discussions.

We have six appendixes. In Appendix A, we review the history of our previous works. In Appendix B, we review

the (finite temperature) beta function and its relation to trace anomaly. In Appendix C, we derive the unparticle propagators. In Appendix D, we report the computation of one-loop vacuum energy in lattice QCD with various boundary conditions. In Appendix E, we review our viewpoint on the chiral phase transition in $N_f = 2$ QCD. We collect the figures not listed in the main text in Appendix F.

II. BACKGROUND

A. Action and observables

We define continuous gauge theories as the continuum limit of lattice gauge theories, defined on the Euclidean lattice of the size $N_x = N_y = N_z = N$ and N_t . To obtain the thermodynamic interpretation, we in general impose an antiperiodic boundary condition in the time direction for fermion fields and periodic boundary conditions otherwise. We also discuss the case when antiperiodic boundary conditions in spatial directions for fermion fields are imposed.

Our general argument that follows can be applied to any gauge theories with (vectorlike) fermions in arbitrary representations, but to be specific, we focus on $SU(3)$ gauge theories with N_f fundamental fermions (quarks). We employ the Wilson quark action and the standard one-plaquette gauge action. The theory is defined by two parameters: the bare coupling constant g_0 and the bare degenerate quark mass m_0 at ultraviolet (UV) cutoff. We also use, instead of g_0 and m_0 , $\beta = 6/g_0^2$ and the hopping parameter $K = 1/2(m_0 a + 4)$.

We measure, together with the plaquette and the Polyakov loop in each space-time direction, the quark mass m_q defined through Ward-Takahashi identities [58,59]

$$m_q = \frac{\langle 0 | \nabla_4 A_4 | \text{PS} \rangle}{2 \langle 0 | P | \text{PS} \rangle}, \quad (1)$$

where P is the pseudoscalar (PS) density and A_4 is the fourth component of the local axial vector current, with renormalization constants being suppressed. The quark mass m_q thus defined only depends on β and K and does not depend on whether it is in the confining region or the deconfining region up to order a corrections [60].

In addition to them, we investigate in detail the t dependence of the propagator of the local meson operator in the H channel:

$$G_H(t) = \sum_x \langle \bar{\psi} \gamma_H \psi(x, t) \bar{\psi} \gamma_H \psi(0) \rangle, \quad (2)$$

where the summation is over the spatial lattice points. In this paper, we mostly focus on the PS channel $H = PS$, but we also measure other channels and use the vector channel to see the chiral symmetry.

B. Simulations

We make numerical simulations for $N_f = 7, 8, 12, 16$ as candidates of conformal QCD and for $N_f = 2$ as high-temperature QCD on a lattice with a fixed size of $16^3 \times 64$.

The algorithms we employ are the blocked hybrid Monte Carlo (HMC) algorithm [61] in the case $N_f = 2\mathbb{N}$ and the rational HMC algorithm [62] for $N_f = 1$ in the case of $N_f = 2\mathbb{N} + 1$.

We specify the coupling constant $\beta = 11.5$ for $N_f = 16$, taking account of the fact that the IR fixed point for $N_f = 16$ is $\beta = 11.48$ in two-loop approximation (see Sec. II D), while $\beta = 6.0$ for $N_f = 7, 8, 12, 16$, varying the hopping parameter K so that the quark mass takes the value from 0.40 to 0.0, except for a few cases in the deconfining region or the confining region for comparison. We further perform simulations for $N_f = 12$ at $\beta = 8.0$.

For high-temperature QCD, identifying the chiral transition around $K = 0.151$ at $\beta = 6.0$ on a lattice $16^3 \times 64$ by the “on-Kc method” in Ref. [63], we choose the following values of β s: $\beta = 6.5, 7.0, 8.0, 10.0$, and 15.0 .

If we formally estimate the temperatures based on $\Delta\beta \sim 0.5$ for the scale change of a factor two from the beta function in the one-loop approximation with $N_f = 2$, we obtain $T/T_c \sim 2, T/T_c \sim 4, T/T_c \sim 16, T/T_c \sim 100$, and $T/T_c \sim 10^5$, respectively. We take several values of K for each β in such a way that the quark masses m'_q take values $0.00 \leq m'_q \leq 0.30$, except for a few cases.

We show the parameters for simulations and the numerical results in Tables I–VII. All results for masses of mesons and the quarks are expressed in units of the inverse of the lattice spacing a^{-1} in the text and the tables.

We choose the run parameters in such a way that the acceptance of the global metropolis test is about 70%. The statistics are 1,000 molecular dynamics (MD) trajectories for thermalization and 1,000 MD trajectories for the measurement or 500 MD trajectories for thermalization and 500 ~ 900 MD trajectories for the measurement. We estimate the errors by the jackknife method with a bin size corresponding to 100 HMC trajectories.

C. Continuum limit

The continuum limit of a lattice theory is defined by taking the lattice space $a \rightarrow 0$ with $N \rightarrow \infty$ and $N_t \rightarrow \infty$, keeping $L = Na$ and $L_t = N_t a$ fixed.

When $N_f \leq 16$, the point $g_0 = 0$ and $m_0 = 0$ in the two parameter space (g_0, m_0) is a UV fixed point. Therefore, a theory governed by this fixed point is an asymptotically free theory. We restrict ourselves to the theory defined by this UV fixed point in this article.

There are four cases in the continuum limit:

- (1) L and L_t are finite: the space is the three-torus \mathbb{T}^3 , finite temperature $T = 1/L_t$.
- (2) L is finite and L_t is ∞ : the space is \mathbb{T}^3 , zero temperature.
- (3) L is ∞ and L_t is finite: the space is the Euclidean plane \mathbb{R}^3 , finite temperature $T = 1/L_t$.
- (4) L and L_t are ∞ : the space is \mathbb{R}^3 , zero temperature.

When L and/or L_t are finite, the system is bounded by an IR cutoff Λ_{IR} . In numerical simulations, to achieve the limit corresponding to case 3, we can first take the limit N_t infinity (thermodynamical limit) and then we take the limit N infinity. On the other hand, to achieve the limit

TABLE I. Numerical results for $N_f = 16$: “s” in the second column represents the initial status. The continuation is from the lower K (l) or from the higher K (h). The third column is the number of trajectories for measurement. The fourth column is the plaquette value. The m_q in the fifth column is the quark mass defined in Eq. (1). m in the sixth and seventh columns are the mass of PS and V channels in the case of the exponential decay defined in Eq. (7). The \tilde{m} in eighth and tenth columns and α in the ninth and 11th columns are, respectively, the “mass” and the exponent of PS and V channels in the case of the Yukawa-type decay defined in Eq. (9).

K	s	$N_f = 16$			$\beta = 11.5$					
		N_{tra}	plaq	m_q	m_π	m_V	\tilde{m}_π	α_π	\tilde{m}_V	α_V
0.120	l	1000	0.820199(7)	0.3995(1)	0.7930(5)	0.7931(5)
0.121	l	500	0.820543(7)	0.3672(2)	0.7451(19)	0.7458(20)
0.122	l	500	0.820856(7)	0.3346(1)	0.6844(8)	0.6847(8)
0.123	l	500	0.821214(6)	0.3039(1)	0.6389(9)	0.6397(11)
0.124	l	500	0.821560(7)	0.2733(1)	0.5858(8)	0.5930(18)
0.125	l	1000	0.821918(05)	0.2435(1)	0.5401(27)	0.5411(25)
0.125	h	1000	0.821927(06)	0.2498(1)	...	-	0.615(5)	1.37(5)	0.615(6)	1.34(6)
0.1255	l	1000	0.822127(06)	0.2348(1)	0.599(3)	1.28(3)	0.601(3)	1.23(3)
0.126	l	1000	0.822324(07)	0.2158(1)	0.504(3)	0.99(9)	0.502(3)	0.99(19)
0.1262	h	1000	0.822411(04)	0.2122(3)	0.522(9)	1.72(7)	0.532(7)	1.5(4)
0.1264	l	500	0.822497(11)	0.2072(1)	0.548(12)	1.45(13)	0.545(13)	1.5(15)
0.1266	h	1000	0.822577(06)	0.2010(1)	0.534(3)	1.44(8)	0.533(4)	1.4(5)
0.127	h	1000	0.822745(08)	0.1864(1)	0.451(5)	1.29(10)	0.446(6)	1.34(14)
0.130	h	1000	0.824107(06)	0.0998(2)	0.425(4)	1.19(2)	0.411(7)	1.48(8)
0.1315	h	1000	0.824866(09)	0.0552(4)	0.397(4)	1.15(2)	0.394(7)	1.23(9)
0.13322	h	1000	0.825790(08)	0.0029(4)	0.390(5)	1.09(4)	0.396(8)	1.02(14)

TABLE II. Numerical results for $N_f = 7$: the meanings of the columns are the same as $N_f = 16$.

K	s	$N_f = 7$			$\beta = 6.0$					
		N_{tra}	plaq	m_q	m_π	m_V	\tilde{m}_π	α_π	\tilde{m}_V	α_V
0.1300	l	1000	0.615510(20)	0.5500(3)	1.2216(10)	1.2263(11)
0.1370	l	1000	0.623238(15)	0.3081(3)	0.8443(25)	0.8501(27)
0.1380	l	1000	0.624511(16)	0.2777(2)	0.7979(19)	0.8032(24)
0.1390	l	1000	0.625859(17)	0.2475(2)	0.7358(27)	0.7431(31)
0.1400	l	1000	0.627285(23)	0.2181(2)	0.6824(31)	0.6916(33)
0.1410	l	900	0.628794(14)	0.1889(2)	0.6304(26)	0.6394(32)
0.1412	l	1000	0.629129(20)	0.1833(2)	0.6250(21)	0.6356(23)
0.1412	h	1000	0.629037(12)	0.1814(2)	0.557(5)	0.78(5)	0.560(5)	0.80(7)
0.1413	l	500	0.629228(12)	0.1794(3)	0.5978(30)	0.6022(33)
0.1413	h	1000	0.62927(12)	0.1780(4)	0.512(9)	1.39(8)	0.514(9)	1.36(7)
0.1415	h	600	0.629559(13)	0.1721(2)	0.513(3)	1.09(7)	0.516(3)	1.10(11)
0.1420	h	1000	0.630328(21)	0.1587(4)	0.525(13)	1.05(14)	0.522(15)	1.21(16)
0.1430	h	700	0.631951(20)	0.1309(2)	0.523(6)	0.39(10)	0.529(07)	0.51(11)
0.1446	h	1000	0.634723(22)	0.0842(5)	0.472(6)	0.46(6)	0.483(05)	0.54(03)
0.1452	h	500	0.635759(19)	0.0614(1)	0.426(12)	0.80(1)	0.426(12)	1.03(02)
0.1459	h	1000	0.637062(17)	0.0450(2)	0.410(11)	0.80(14)	0.413(14)	1.01(18)
0.1464	h	700	0.637981(17)	0.0303(2)	0.381(8)	0.64(13)	0.393(09)	0.73(14)
0.1472	h	1000	0.639496(15)	0.0060(2)	0.405(8)	0.75(10)	0.406(09)	1.06(10)

TABLE III. Numerical results for $N_f = 8$ at $\beta = 6.0$: the meanings of the columns are the same as $N_f = 16$.

K	s	$N_f = 8$			$\beta = 6.0$					
		N_{tra}	plaq	m_q	m_π	m_V	\tilde{m}_π	α_π	\tilde{m}_V	α_V
0.1446	h	1000	0.634723(22)	0.0738(1)	0.422(8)	0.79(9)	0.430(9)	0.84(12)
0.1457	h	1000	0.637062(17)	0.0342(2)	0.386(5)	0.78(7)	0.385(7)	1.05(12)

TABLE IV. Numerical results for $N_f = 12$ at $\beta = 6.0$: the meanings of the columns are the same as $N_f = 16$.

K	s	$N_f = 12$			$\beta = 6.0$					
		N_{tra}	plaq	m_q	m_π	m_V	\tilde{m}_π	α_π	\tilde{m}_V	α_V
0.120	l	500	0.616908(25)	0.9515(73)	1.632(12)	0.1635(12)
0.125	l	900	0.622451(14)	0.7035(71)	1.388(19)	0.1390(21)
0.130	l	500	0.629336(94)	0.4944(98)	1.123((19)	1.125(18)
0.135	l	500	0.637354(48)	0.3184(27)	0.8534(26)	0.8574(20)
0.136	l	1000	0.639298(10)	0.2854(3)	0.7960(41)	0.8004(45)
0.136	h	1000	0.639307(11)	0.2850(1)	0.781(4)	0.72(5)	0.769(3)	0.75(5)
0.137	h	500	0.641257(21)	0.2521(47)	0.687(10)	1.11(12)	0.688(10)	1.16(11)
0.140	h	500	0.647566(24)	0.1576(17)	0.550(5)	0.83(7)	0.546(5)	1.00(11)
0.1425	h	500	0.653517(15)	0.0781(2)	0.371(10)	1.32(14)	0.364(0)	1.49(19)
0.144	h	500	0.657296(17)	0.0304(22)	0.406(5)	0.62(11)	0.406(6)	0.99(5)

corresponding to case 4, we can put $N = rN_t$ with r an aspect ratio, and finally, we take the limit N infinity simultaneously keeping r fixed.

When we take the continuum limit, we have to fix the physical scale. In confining QCD, the natural choice is to fix the mass of the hadron by demanding

$$L \cdot m_{PS} > c \tag{3}$$

and take $L \rightarrow \infty$ limit, where the value $c \sim 5$ is typically used in the literature. For the conformal QCD, this choice turns out to be subtle because there should be no scale in conformal field theories after taking the continuum limit.

TABLE V. Numerical results for $N_f = 12$ at $\beta = 8.0$. The meanings of the columns are the same as $N_f = 16$.

K	s	$N_f = 12$			$\beta = 8.0$					
		N_{tra}	plaq	m_q	m_π	m_V	\tilde{m}_π	α_π	\tilde{m}_V	α_V
0.120	l	600	0.730676(9)	0.5685(3)	1.0882(11)	1.0881(11)
0.125	l	600	0.733366(10)	0.3940(1)	0.8293(7)	0.8297(6)
0.128	l	500	0.735300(9)	0.3002(1)	0.6680(5)	0.6690(4)
0.129	l	500	0.736007(10)	0.2705(1)	0.6186(22)	0.6207(23)
0.129	h	500	0.736011(16)	0.2784(2)	0.685(5)	1.27(7)	0.686(6)	1.27(8)
0.130	h	700	0.736759(9)	0.2485(2)	0.668(4)	0.86(5)	0.670(4)	0.85(6)
0.133	h	1000	0.739240(14)	0.1598(2)	0.411(12)	0.80(1)	0.413(11)	1.01(18)
0.135	h	800	0.741071(7)	0.1008(3)	0.389(24)	1.52(22)	0.378(35)	1.73(43)
0.138	h	600	0.741081(9)	0.01261(1)	0.381(6)	1.06(8)	0.370(15)	1.33(22)

TABLE VI. Numerical results for $N_f = 2$. The symbols a, b, and c in the second column at $\beta = 100.0$ and $K = 0.1258$ mean that the state is close to $(1/3, 1/3, 1/3)$, $(0, 1/3, 1/3, 0)$, and $(0, 0, 1/3)$, respectively (see Sec. VA for the definition of state). Otherwise, the meanings of the columns are the same as $N_f = 16$.

K	s	$N_f = 2$								
		N_{tra}	plaq	m_q	m_π	m_V	\tilde{m}_π	α_π	\tilde{m}_V	α_V
0.152	l	1000	0.602192(18)	0.0332(1)	0.3280(60)	$\beta = 5.9$ 0.4492(59)
0.110	l	500	0.596366(17)	1.6932(23)	2.1372(15)	$\beta = 6.5$ 2.1398(15)
0.145	l	1000	0.648107(13)	0.0587(2)	0.4249(45)	0.4414(49)
0.1455	l	600	0.648321(13)	0.0465(3)	0.4112(56)	0.4194(70)
0.146	l	1000	0.648546(14)	0.0337(3)	0.371(9)	0.71(8)	0.371(12)	0.98(14)
0.1465	l	1000	0.648799(14)	0.0213(4)	0.286(19)	0.73(19)	0.279(14)	1.08(26)
0.147	l	1000	0.649046(14)	0.0083(2)	0.295(16)	1.00(16)	0.286(6)	1.41(20)
0.142	l	700	0.678445(09)	0.0592(3)	...	$\beta = 7.0$...	0.386(13)	0.74(15)	0.402(11)	0.66(10)
0.143	l	500	0.678788(10)	0.0333(4)	0.360(13)	0.69(22)	0.356(10)	0.94(23)
0.144	l	600	0.679108(16)	0.0074(2)	0.354(14)	1.02(14)	0.320(14)	1.87(18)
0.139	l	700	0.725022(14)	0.0345(2)	...	$\beta = 8.0$...	0.318(12)	0.97(14)	0.299(12)	1.41(21)
0.140	l	800	0.725140(91)	0.0084(1)	0.376(7)	1.02(7)	0.403(6)	0.67(9)
0.110	l	600	0.783954(05)	0.8644(2)	1.3959(5)	$\beta = 10.0$ 1.3953(5)
0.125	l	600	0.784657(10)	0.3046(1)	0.6518(16)	0.6520(16)
0.130	l	700	0.785016(08)	0.1626(1)	0.3887(5)	0.3907(7)
0.130	h	900	0.785036(11)	0.1676(1)	0.495(11)	1.40(11)	0.498(10)	1.32(11)
0.135	l	1000	0.785549(08)	0.0280(2)	0.372(69)	1.11(6)	0.373(3)	1.14(10)
0.130	l	1000	0.860880(03)	0.0455(1)	...	$\beta = 15.0$...	0.385(55)	1.21(4)	0.3972(6)	1.00(9)
0.100	l	1000	0.979878(01)	1.0054(1)	...	$\beta = 100.0$...	1.466(1)	1.14(1)	1.467(1)	1.11(1)
0.120	l	600	0.979884(01)	0.1860(1)	0.519(1)	1.35(1)	0.510(4)	1.49(7)
0.122	l	800	0.979885(01)	0.1227(1)	0.454(2)	1.25(1)	0.447(4)	1.36(7)
0.125	l	900	0.979888(01)	0.2741(1)	0.389(10)	1.29(12)	0.415(5)	0.825(65)
0.1258	a	1000	0.979889(01)	0.0016(1)	0.373(7)	1.39(6)	0.346(16)	1.87(22)
0.1258	b	1000	0.979889(01)	0.0014(1)	0.318(3)	0.79(2)	0.326(14)	0.65(23)
0.1258	c	1000	0.979889(01)	0.0012(1)	0.224(3)	0.45(2)	0.238(10)	0.24(16)
0.125	l	800	0.9979990(01)	0.0031(1)	...	$\beta = 1000.0$...	0.396(4)	1.19(4)	0.441(6)	0.37(4)

TABLE VII. Numerical results with antiperiodic and periodic boundary conditions in spatial directions for $N_f = 7$ at $\beta = 6.0$: the meanings of the columns are the same as $N_f = 16$, except for the second column.

K	s	$N_f = 7$			$\beta = 6.0$					
		N_{tra}	plaq	m_q	m_π	m_V	\tilde{m}_π	α_π	\tilde{m}_V	α_V
0.1446	pb	1000	0.634723(22)	0.0842(5)	0.4726(46)	0.46(6)	0.4834(47)	0.54(3)
0.1446	apbc	1000	0.634656(33)	0.0880(3)	0.5462(41)	0.5690(49)
0.1459	pb	1000	0.637062(17)	0.0450(2)	0.4106(117)	0.80(14)	0.4131(135)	1.01(18)
0.1459	apbc	1000	0.637104(21)	0.0479(1)	0.5479(19)	0.5690(32)

As we argue, the choice of c leads to different phases in the continuum limit. We also evaluate the upper limit value of c to retain the conformal behavior in the continuum limit.

D. Banks-Zaks fixed point

Within the perturbation theory, the zero-temperature beta function for the $SU(3)$ gauge coupling constant can be computed as

$$\mathcal{B}(g) = -\frac{(33 - 2N_f)}{48\pi^2} g^3 - \frac{(102 - \frac{38}{3}N_f)}{(16\pi^2)^2} g^5 + \mathcal{O}(g^7). \quad (4)$$

The fixed-point $\mathcal{B}(g^*) = 0$ exists for $8.05 < N_f < 16.5$ with the two-loop approximation. Of course, the two-loop result is not trustworthy for lower values of N_f , so the lower bound of the conformal window cannot be obtained from the perturbation theory.

As we review in Appendix B, the beta function is related to the trace anomaly. The trace of the energy-momentum tensor in massless QCD is given by

$$T^\mu{}_\mu = \mathcal{B}(g)\text{Tr}F_{\mu\nu}^2 \quad (5)$$

as an operator identity. It vanishes when the theory is at the IR fixed point $g = g^*$, and vanishing of the trace anomaly means that it is conformal invariant.

At the conformal fixed point, one may compute the anomalous mass dimension. The perturbation theory predicts

$$\gamma_m = \frac{1}{2\pi^2} g^2, \quad (6)$$

which should be compared with the lattice simulation after establishing how to read the anomalous mass dimension from the temporal propagators, as we show later. For reference, for $N_f = 16$, the fixed point value from (4) is $\beta_0 = 11.48$, and the mass anomalous dimension is $\gamma^* = 0.026$. We further note that the conserved current operator is not renormalized. Therefore, the anomalous dimension vanishes.

E. Phase structure

In order to investigate properties of the theory in the continuum limit, it is vital to clarify the phase structure of lattice QCD.

Although we would like to extract the phase diagram in the continuum limit, we have to perform simulations at finite N . Therefore, the phase diagram is a three-dimensional space parameterized by g_0 , m_0 , and N . Thus, first of all, one has to make clear what kind of phases there are in this three-dimensional space.

We claim that we are able to classify the phase space into three regions: (1) the confining region, (2) the deconfining region, and (3) the conformal region.

Let us first recall that there are no order parameters that distinguish the deconfining phase from the confining phase, except for the two limits; in the limit $m_q \rightarrow \infty$, the Polyakov loop for the t direction can be used at the deconfining phase transition, and in the limit $m_q \rightarrow 0$, the chiral scalar density can be used at the chiral transition. Therefore, it is not possible in principle to state which phase is realized at the intermediate quark mass m_q . However, in the $3 \leq N_f \leq 6$ case, there is a first-order transition line from the chiral transition point toward heavier quark mass. In such a case, one may state that either the chiral symmetry is restored or the chiral symmetry is broken, depending on the region it belongs to.

The deconfining transition is a first-order phase transition, and similar to above, there is a first-order transition line from the deconfining transition point to lighter quark mass. In this case, one may say either the quark confinement or deconfinement, depending on the region. However, in the intermediate quark mass region, the first-order transition becomes weak and probably disappears. Thus, the confining region and the deconfining region are connected; therefore, in strict meaning, both regions belong to one phase.

We use the terminology confining region instead of the confining phase since, as mentioned above, there is no order parameter in general.

When there is a Banks-Zaks IR fixed point [2] at finite coupling constant g on the massless line which starts from the UV fixed point, the long-distance behavior is determined by the IR fixed point. This defines a conformal theory. The meaning of the conformal theory is discussed later. We recall that the region of N_f for the existence of the

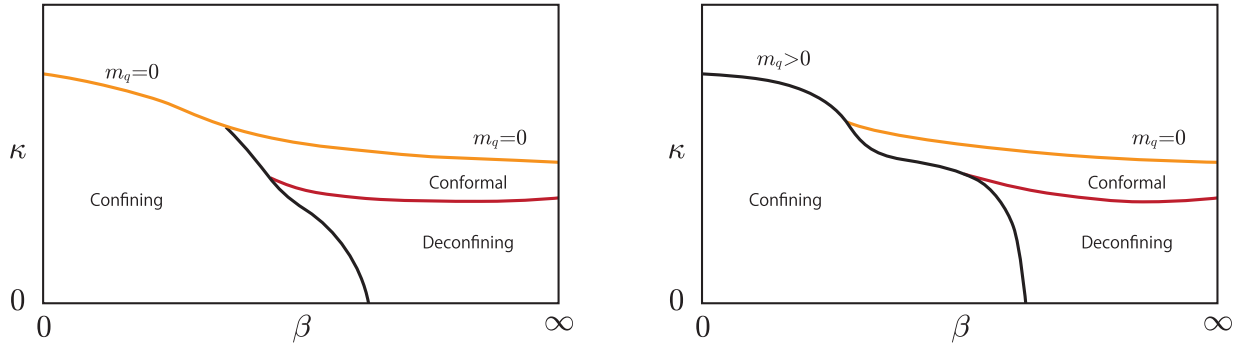


FIG. 1 (color online). Phase diagram on a finite lattice: (left) $1 \leq N_f \leq N_f^c - 1$ and (right) $N_f^c \leq N_f \leq 16$. In the case $N_f^c \leq N_f \leq 16$, the massless quark line originating from the UV fixed point hits the bulk transition point at finite β , and no massless line exists in the confining region. The region above the bulk transition corresponds to the doublers of the Wilson fermion. On the other hand, in the case $1 \leq N_f \leq N_f^c - 1$ on the massless quark line, there is a chiral phase transition on the quark massless line $m_q = 0$. Below the critical point the massless line is in the confining region.

IR fixed point $N_f^c \leq N_f \leq 16$ is called the conformal window.

On the other hand, when $1 \leq N_f \leq N_f^c - 1$, the beta function does not possess an IR fixed point in the continuum limit with infinite space-time, which implies the quark confinement. When the lattice size is finite, the vicinity of the point $g_0 = 0$ along $m_q = 0$ is the chiral symmetric phase, and there is a chiral phase transition on the quark massless line $m_q = 0$.

The scenario above is a common lore, although there is an alternative possibility that in between the confinement (chiral symmetry broken) region and the chiral symmetric conformal region at zero temperature, a new phase like the magnetic phase may exist.

In this article, we propose a new concept of conformal region that are discussed in detail in later sections, particularly in Sec. VII. Analyzing the vacuum structure in terms of the Polyakov loops in spatial directions and the specific behavior of the temporal propagators of meson, we show that there exists the conformal region in addition to the confining region and the deconfining region, as shown in Fig. 1. On a finite lattice, both in the cases $1 \leq N_f \leq N_f^c - 1$ and $N_f^c \leq N_f \leq 16$, when the bare coupling constant g_0 is small enough and when the quark mass m_q is larger than the

critical mass, the system is in the deconfining region. On the other hand, when g_0 is larger, it is in the confining region.

In the continuum limit, we argue that in the case $N_f^c \leq N_f \leq 16$ only the confining region outside of the conformal region remains, as shown in Fig. 2: (right panel) when the infrared cutoff Λ_{IR} is finite and (left panel) when $\Lambda_{\text{IR}} = 0$. In the case $1 \leq N_f \leq N_f^c - 1$, only the deconfining region outside of the conformal region remains, as shown in Fig. 3.

F. Phase transition on a finite lattice

As mentioned above, our final goal is to investigate conformal theories in the continuum limit. However, we have to restrict ourselves to the calculations on a lattice with a fixed size in this article.

The phase transition occurs only in the system with infinite degrees of freedom. On a finite lattice, when physical quantities exhibit a “discontinuous gap” (or more precisely a sharp transition) at some point and when theoretical argument supports the existence of the phase transition, we identify the transition as a first-order transition in the continuum limit. Strictly speaking, all of the discontinuities we discuss only exist in the continuum limit, and our numerical simulation on a fixed lattice gives only an indication of the discontinuity as a sharp transition. In

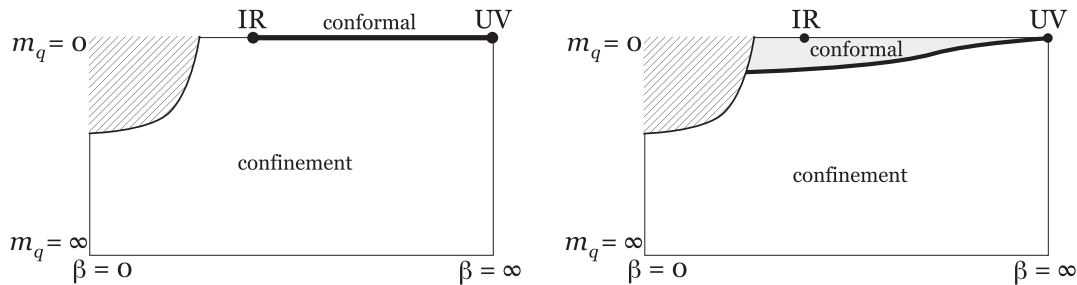


FIG. 2. The phase diagram for the case $N_f^c \leq N_f \leq 16$ predicted from the RG argument: (left) for $\Lambda_{\text{IR}} = 0$ and (right) for $\Lambda_{\text{IR}} = \text{finite}$. The shaded strong coupling region for small quark masses does not exist in the $\beta - m_q$ plane [57] because the region corresponds to Wilson doublers when mapped in terms of $\beta - K$.

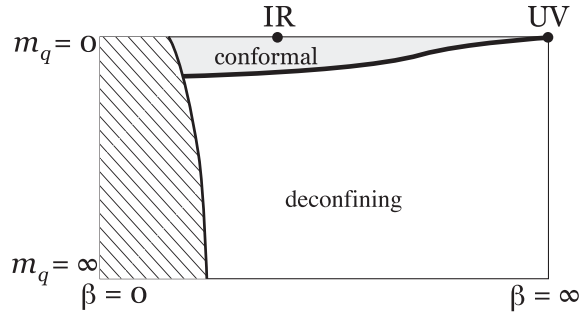


FIG. 3. The phase diagram predicted from the RG argument for fixed temperature T with $T/T_c > 1$ in the case $1 \leq N_f \leq N_f^c - 1$: The shaded strong coupling region does not correspond to the temperature $T/T_c > 1$.

this respect, without taking the continuum limit, we cannot exclude the possibility that the phase transition we propose may result in the crossover.

For a second-order transition, we have to carefully apply a scaling law in order to judge the existence of the phase transition. The same remark for the discontinuity applies here as well.

III. CONFORMAL THEORIES WITH AN IR CUTOFF

We have recently investigated field theories that possess an IR fixed point with an IR cutoff and introduced the nomenclature “conformal field theories with an IR cutoff” reported in short reports (Refs. [64] and [56]).

A. Definition and examples

We first define the conformal field theories with an IR cutoff. The first assumption is that the beta function (either zero temperature or finite temperature) vanishes. Of course, if there were no other dimensionful quantities, this would imply that the theory is scale invariant, and all of the correlation functions show a strict power behavior. In (perturbative) QCD at zero temperature, they are further conformal invariant due to vanishing of trace anomaly (see Appendix B for more details).

Our new observation is that when such theories have a finite cutoff, then they will show the universal behavior that we call conformal field theories with an IR cutoff. In

particular, we claim that within the suitable parameter region that we call the conformal region, the temporal propagators show a power-law-corrected Yukawa-type decaying form. In the examples we study in this paper, the conformal field theories with an IR cutoff are realized as discussed below.

1. Conformal QCD

When the flavor number N_f is within the conformal window $N_f^c \leq N_f \leq 16$, the beta function possesses the Banks-Zaks IR fixed point. The continuum limit 1, 2, or 3 defines a theory with an IR cutoff.

2. High-temperature QCD

When the flavor number N_f is exclusive with the conformal window, $1 \leq N_f \leq N_f^c - 1$, and $T \geq T_c$ with T_c the chiral phase transition point, the beta function of a running coupling constant $g(\mu; T)$ at temperature T possesses an IR fixed point as shown in Ref [56] (it is recapitulated in Appendix B). The temperature T plays a role in the IR cutoff, together with a possible cutoff due to compact space.

As long as $T < T_c$, the beta function is negative all through g . As the temperature is increased further, the form of the beta function will change as in Fig. 4: (Left) when $T > T_c$ but $T \sim T_c$, the beta function changes the sign from negative to positive at large g ; as the temperature increases the fixed point moves toward smaller g . (Right) when $T \gg T_c$ it changes the sign at small g .

3. Numerical simulations on a finite lattice

All numerical simulations are performed on a finite lattice, which introduces an IR cutoff. Therefore, any lattice conformal QCD (N_f is within the conformal window $N_f^c \leq N_f \leq 16$) and lattice high-temperature QCD (N_f is $1 \leq N_f \leq N_f^c - 1$ and $T \geq T_c$) are conformal field theories with an IR cutoff.

B. Phase transition from an RG argument

We have shown two examples of conformal field theories with an IR cutoff: conformal QCD and high-temperature QCD. One of the main claims of the paper is that within the conformal region, there is a correspondence between a set of

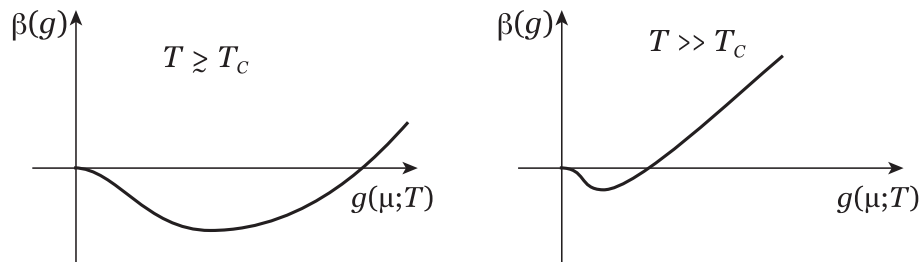


FIG. 4. The beta function $\beta(g(\mu; T))$ at finite temperature T .

theories in each class. We now argue that when we increase the quark mass in each theory with the other parameters fixed (e.g., N , β_0 , and N_f), they show the first-order phase transition and leave the conformal region. Depending on the parameters, the region outside of the conformal region can be either the confining region or the deconfining region for a finite lattice simulation, as shown in Fig. 1.

1. From conformal to confining

Let us discuss the mechanism of the phase transition from the conformal region to the confining region from the argument based on the RG flow. For this purpose, we quickly remind ourselves of the properties of the RG flow of the quark mass and the gauge-coupling constant when the beta function possesses an IR fixed point.

Suppose the IR cutoff is zero. When quarks have tiny masses, the RG trajectory would stay close to the critical line, approaching the IR fixed point, and finally would pass away from the IR fixed point to infinity. Therefore, the IR behavior is governed by the confining region. Only on the massless quark line is the scale invariance realized at the IR fixed point (see the left panel of Fig. 2).

When the cutoff Λ_{IR} is finite, the RG flow from UV to IR does stop evolving at the scale Λ_{IR} . When the typical mass scale (e.g., that of a meson) m_H is smaller than Λ_{IR} , it is in the conformal region. On the other hand, when m_H is larger than Λ_{IR} , the flow passes away from the IR fixed point to infinity with relevant variables integrated out, thus being in the confining region (see the right panel of Fig. 2).

This scenario implies that when physical quantities in the IR limit (e.g., hadron masses) are mapped into a diagram in terms of physical parameters at UV (e.g., the bare coupling constant and the bare quark mass), there will be gaps in the physical quantities along the boundary between the two phases. Thus, the phase transition will be a first-order transition.

2. From conformal to deconfining

A similar argument for the RG flow applies for the phase transition into the deconfining region. Let us consider the case where the bare-coupling constant g_0 is sufficiently small on a finite lattice (see Fig. 1). When the typical mass scale m_H is smaller than Λ_{IR} , it is in the conformal region as before. However, when m_H is larger than Λ_{IR} , the RG flow passes away from the IR fixed point to a point in the deconfining region.

The transition from the conformal region to the deconfining region is a first order when the lattice size is finite, as in the case of the conformal region to the confining region.

Since the deconfining region and the conformal region are supposed to be in the same universality class in the infinite volume limit (see, e.g., [65]), the phase transition between the two will become weaker in the same limit.

3. Confining or deconfining in conformal QCD?

With the finite lattice size, whether the theory is confining or deconfining by increasing the quark mass depends on the bare-coupling β_0 and the lattice size as well as the number of flavor N_f .

In Secs. V–VII, after presenting our numerical simulations, we argue that these two different possibilities realized in finite lattice simulations may be a potential source of the controversy of the conformal behavior of the intermediate ranges of the conformal window such as $N_f = 12$, when one tried to study the mass spectrum by including the mass values outside of the conformal region.

4. Continuum limit

When the lattice size is finite, the large t behavior of the meson propagator $G(t)$ is the exponential type both in the confining region and the deconfining region. More strictly, in the deconfining region, the exponential decay form is an approximate form due to the finiteness of the t range.

In the continuum limit, in the case of the confining region with $T = 0$, the asymptotic behavior is exactly exponential with the mass of the ground state, while in the case of the deconfining region with T finite, the spectral decomposition of $G(t)$ is necessary to accommodate the exact asymptotic behavior.

When the continuum limit is taken in the case where the N_f is within conformal region $N_f^c \leq N_f \leq 16$, the confining region for larger quark masses enlarges, and the deconfining region finally disappears with $N \rightarrow \infty$ (see Fig. 2).

In the case $1 \leq N_f \leq N_f^c - 1$, when g_0 is larger than the critical coupling constant, there is no conformal region, and only the confining region dominates in the continuum limit. On the other hand, when g_0 is smaller (that is, T/T_c kept larger than unity), only the deconfining region remains for larger quark masses (see Fig. 3).

In our discussions, we have considered the simplified RG flow in which only the gauge coupling constant and the quark mass are the relevant parameters. As long as we are in the perturbative regime, this is completely justified. In the nonperturbative regime, there is a theoretical possibility that perturbatively irrelevant operators become relevant in the IR, changing the RG flow. If this were the case, the lattice simulations of conformal window would become much harder because we have to tune these extra parameters [e.g., $O(a)$ lattice action] to reach the fixed point. As far as our numerical analysis with the fixed lattice size suggests, this does not seem to happen (see also the functional RG group analysis of the extended RG flow at zero temperature and at finite temperature in [66,67]). Up to nonuniversal scheme dependence, our RG argument in relation to how the confinement/deconfinement occurs does not contradict with their analysis.

C. In relation to mass-deformed CFT

As we have already emphasized, in the continuum limit without an IR cutoff, the conformal region only exists on the strict massless line $m_q = 0$. Once we have any nonzero quark mass, the theory is in the confining phase. The first-order phase transition line that we have proposed between the confining region and the conformal region becomes coincident with the massless line. The phase transition clearly occurs at $m_q = 0$ for the conformal QCD in the continuum limit without an IR cutoff. While the free energy becomes continuous there because the energy gap behaves as $1/L$, some other physical observables may become discontinuous.

In this continuum limit, the confining region with the tiny quark mass has been known as the mass-deformed conformal field theory and has been studied intensively in the literature (see, e.g., [35,37]). As long as the RG flow stays for a sufficiently long time close to the fixed point, which requires that the mass is significantly smaller compared with the UV cutoff or any other energy scale, various physical observables in the mass-deformed conformal field theory will show the scaling behavior. Here the quark mass serves as the effective IR cutoff in the fermion sector [51,52], and the competition with the intrinsic IR cutoff from the finite lattice size is our main focus. Approaching the massless line makes the correlation length divergent, and the critical exponent is determined from the properties of the conformal fixed point. However, it is not obvious if this criterion has been really achieved in the finite lattice simulations.

The fate of the mass-deformed conformal field theory under the presence of a finite cutoff is twofold. It could be either our conformal region (when the mass is small enough) or confining region (when the mass is larger). In the literature, guided by the expected scaling behavior without the IR cutoff in the mass-deformed conformal field theory, the simulations have been mainly aimed at the confining region. In contrast, our main focus in the following is the conformal region, which is directly connected to the conformal field theory in the continuum limit on the massless line. Note again that the conformal region with nonzero mass exists whenever the IR cutoff is nonzero. As we discuss in the following sections, this enables us to continuously connect the propagators, in principle, to the massless and continuum limit without encountering the phase transition. Indeed, we see the remnant of the power-law behavior in the propagators in the finite lattice simulations in the conformal region, which is not visible in the confining region.

One important remark is in order. In the above paragraphs, we have started with the mass-deformed conformal field theory defined in the continuum limit with no IR cutoff. With the finite IR cutoff, which we have already discussed in Secs. II and III, there exists yet another possible phase, the deconfining region. The properties of

this region are remotely distinguished from the mass-deformed conformal field theory, and we should not be able to test the prediction of the mass-deformed conformal field theory in the deconfining region. The region remains in the continuum limit if we keep the temperature finite, but as we have already mentioned, it should go away in the conformal QCD at zero temperature.

We see that in the finite-size lattice simulations, it depends on the details of the simulation parameters, i.e., the coupling constant or the lattice size whether the confining region or deconfining region will appear above the phase transition line from the conformal region. This is elaborated in Sec. VIIC in the example of $N_f = 12$. A further remark on the finite-size scaling appears in Sec. VIIH.

IV. ANALYSIS OF PROPAGATORS

A. Long-distance behavior of propagators

Based on the above RG argument, we conjecture that the long-distance behavior for the propagator of the local meson operator

$$G_H(t) = \sum_x \langle \bar{\psi} \gamma_H \psi(x, t) \bar{\psi} \gamma_H \psi(0) \rangle$$

qualitatively differs depending on whether the quark mass is smaller than the critical mass or not.

When the theory is in the relatively heavy quark region, it decays exponentially at large t as

$$G_H(t) = c_H \exp(-m_H t). \quad (7)$$

In contrast, in the conformal region defined by

$$m_H \leq c \Lambda_{\text{IR}}, \quad (8)$$

where c is a constant of order 1, the propagator $G(t)$ behaves at large t as

$$G_H(t) = \tilde{c}_H \frac{\exp(-\tilde{m}_H t)}{t^{\alpha_H}}, \quad (9)$$

which is a power-law-corrected Yukawa-type decaying form instead of the exponential decaying form [Eq. (7)].

In the continuum limit, we have to discuss conformal QCD and high-temperature QCD separately.

When the theory is in the confining region in conformal QCD, m_H in Eq. (7) is the mass of the ground state hadron in the channel H . In the continuum limit with $L = \infty$ (i.e., $\Lambda_{\text{IR}} = 0$), the propagator on the massless quark line takes the form

$$G_H(t) = \tilde{c} \frac{1}{t^{\alpha_H}}. \quad (10)$$

If we take the coupling constant $g_0 = g^*$ at the UV cutoff, α_H takes a constant value, and the RG equation demands

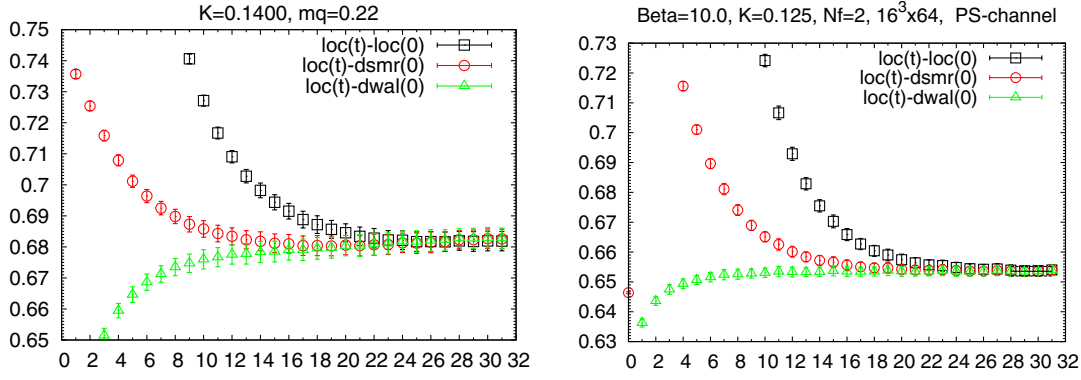


FIG. 5 (color online). The effective mass: (left) $N_f = 7$ at $\beta = 6.0$ and $K = 0.1400$ and (right) $N_f = 2$ at $\beta = 10.0$ and $K = 0.125$ (see the text for the three types of sources).

$$\alpha_H = 3 - 2\gamma^*, \quad (11)$$

for the PS channel with γ^* being the anomalous mass dimension γ at $g = g^*$. The theory is scale invariant and is shown to be conformal invariant within the perturbation theory [68] (see, e.g., [69,70] and the references therein from the AdS/CFT approach). The distinction between scale invariance and conformal invariance in lattice QCD was addressed in [71]. When $0 \leq g_0 < g^*$, α_H depends slowly on t as a solution of the RG equation. In the IR limit $t \rightarrow \infty$, we must retain $\alpha_H(t) \rightarrow 3 - 2\gamma^*$.

In the thermodynamical limit at finite temperature, Eqs. (7) and (9) are valid only approximately due to the finiteness of the t range. A more rigorous way to obtain a physical implication would be to make the spectral decomposition of $G_H(t)$.

However, our objective in this article is to verify the existence of the conformal region and the power-law-corrected Yukawa-type decaying form on a finite lattice in the case of conformal theories with an IR cutoff. It is beyond the scope of our objective to obtain the thermodynamical physical quantities.

The conjecture should be satisfied in (1) large N_f QCD within the conformal window with an IR cutoff and (2) small N_f QCD at high-temperature $T/T_c > 1$ with T_c being the chiral transition temperature.

In order to investigate the large t behavior of a propagator, we define the effective mass $m_H(t)$ by

$$\frac{\cosh(m_H(t)(t - N_t/2))}{\cosh(m_H(t)(t + 1 - N_t/2))} = \frac{G_H(t)}{G_H(t+1)}.$$

In the case of exponential-type decay, the effective mass approaches a constant in the large t region, which is called a plateau.

We show the t dependence of the effective mass in the PS channel with three types of sources for the four examples (light-quark mass and relatively heavy-quark mass cases in each categories):

- (1)
 - (a) $N_f = 7, \beta = 6.0, K = 0.1400$ ($m_q = 0.25$).
 - (b) $N_f = 7, \beta = 6.0, K = 0.1459$ ($m_q = 0.045$).
- (2)
 - (a) $N_f = 2, \beta = 10.0, K = 0.125$ ($m_q = 0.30$).
 - (b) $N_f = 2, \beta = 10.0, K = 0.135$ ($m_q = 0.028$).

Three types of symbols represent three types of source-sink: the local-sink local-source (squares), local-sink (quark-antiquark) doubly exponentially smeared source of a radius 5 lattice units (circles), and local-sink doubly wall source (triangles).

We show in Fig. 5 typical examples of exponential decay in two cases of relatively heavy quark mass cases: $N_f = 7, \beta = 6.0, K = 0.1400$ ($m_q = 0.25$), and $N_f = 2, \beta = 10.0, K = 0.125$ ($m_q = 0.30$).

We see the clear plateau of the effective mass at $t = 24 \sim 31$ in both cases.

Next we show the scattered plot of the Polyakov loop in the complex plane in Fig. 6 in these cases. (The difference for the scales should be noted.) Apparently the former is a disordered state, which implies the confining region, while the latter is an ordered state, which implies the deconfining region. These results can be better understood when we consider the phase structure. We discuss this point in Sec. VII.

Now we show in Fig. 7 typical examples of the Yukawa-type decay in two cases of the very light-quark masses: $N_f = 7, \beta = 6.0, K = 0.1459$ ($m_q = 0.045$), and $N_f = 2, \beta = 10.0, K = 0.135$ ($m_q = 0.028$).

We see in both cases that the effective mass is slowly decreasing without plateau up to $t = 31$, suggesting the power-law correction. We show the power-law-corrected fit for the local-local data with the fitting range $t = [15:31]$ in Fig. 8. The fits with $\alpha_H = 0.8(1)$ and $\alpha_H = 1.1(1)$ reproduce the data very well.

The $\chi^2/\text{dof} = 0.2166 \times 10^{-2} (\pm 0.3352 \times 10^{-2})/14$ and $0.1375 \times 10^{-1} (\pm 0.7847 \times 10^{-2})/14$ are very small. This does not mean that the fits are excellent, but it reflects that the correlation in the t direction is not taken into account. It

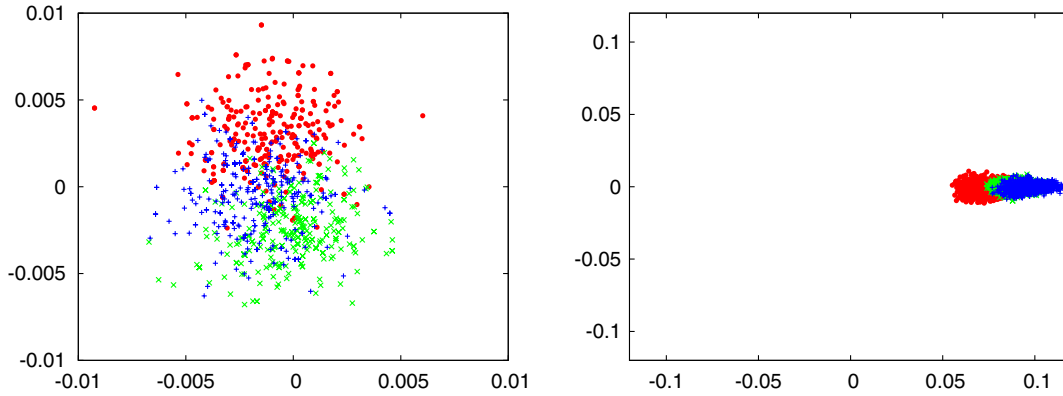


FIG. 6 (color online). The scattered plots of Polyakov loops in the x , y , and z directions overlaid: (left) $N_f = 7$ at $\beta = 6.0$ and $K = 0.1400$ and (right) $N_f = 2$ at $\beta = 10.0$ and $K = 0.125$.

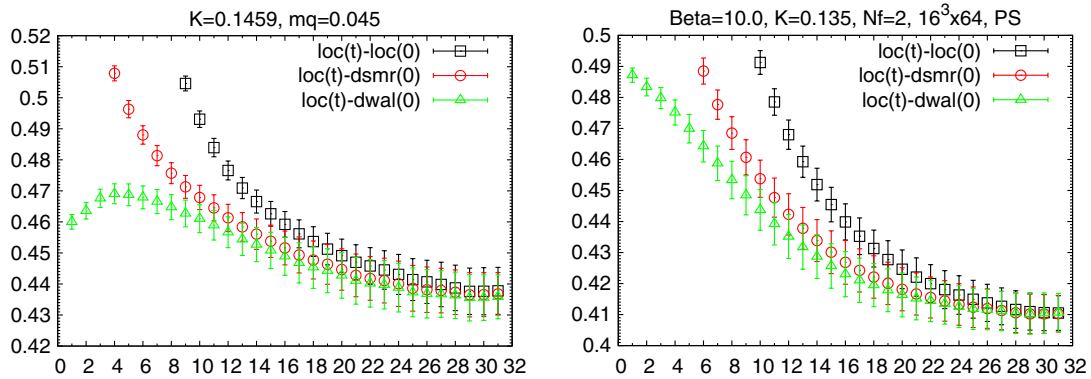


FIG. 7 (color online). The effective mass. (Left) $N_f = 7$ at $\beta = 6.0$ and $K = 0.1459$, and (right) $N_f = 2$ at $\beta = 10.0$ and $K = 0.135$. See the text for the three types of sources.

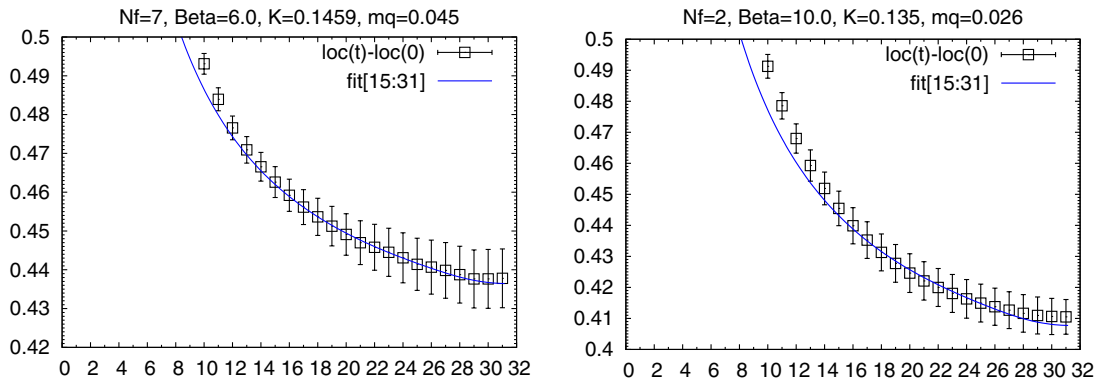


FIG. 8 (color online). The effective mass plots for local-sink local-source case and fits by power-law-corrected Yukawa-type decay. (Left) $N_f = 7$ at $\beta = 6.0$ and $K = 0.1459$ and (right) $N_f = 2$ at $\beta = 10.0$ and $K = 0.135$.

is well known that it requires data in high statistics to take into account the correlation. Furthermore, it is a notorious problem to fit data with power terms. Therefore, it is hard to estimate the error including the correlation. We have estimated the errors by a jackknife method.

We have confirmed in all cases with $m_q \leq 0.4$ that the propagator of a meson $G_H(t)$ behaves at large t as a power-law-corrected Yukawa-type decaying form $G_H(t) =$

$\tilde{c}_H \exp(-\tilde{m}_H t) / t^{\alpha_H}$ instead of the exponentially decaying form $c_H \exp(-m_H t)$.

We show in Fig. 9 the scattered plot of the Polyakov loop in spatial directions. The patterns are apparently different from those in the confining region and the deconfining region. They exhibit the characteristics in the conformal region.

We defer the detailed discussion on the Polyakov loop and the boundary of the conformal region after the

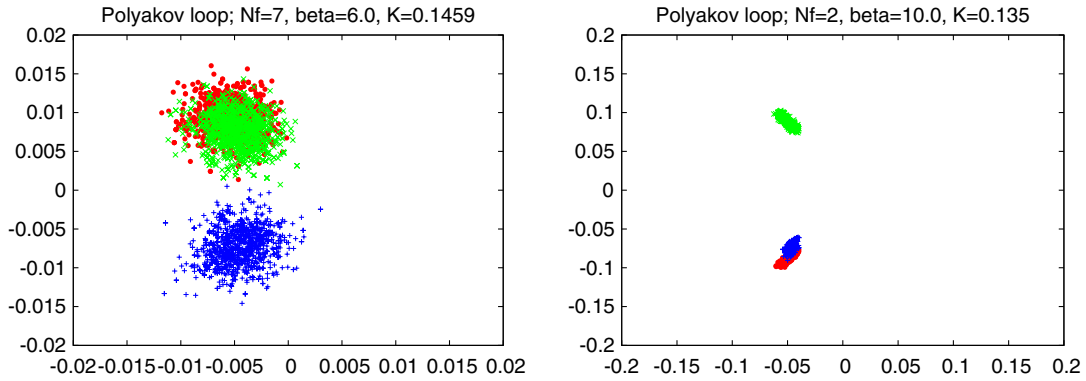


FIG. 9 (color online). The scattered plots of Polyakov loops in the x , y , and z directions overlaid. (Left) $N_f = 7$ at $\beta = 6.0$ and $K = 0.1459$ and (right) $N_f = 2$ at $\beta = 10.0$ and $K = 0.135$.

discussion of the structure of the vacuum in Sec. VII. We show that the boundary between the conformal region and the confining region is a first-order transition in the $N_f = 7, 12$, and 16 cases.

B. Local analysis of propagators

We are able to extract the properties of a quark and antiquark system in the IR region from the long-distance behavior of temporal propagators. However, the propagators contain more information for the properties of a quark and antiquark system. For example, from the short-distance behavior, we may extract the properties in the UV region.

In order to investigate the dynamics of the theory, we make a detailed analysis of temporal propagators that we call the local analysis of propagators [56]. We restrict ourselves to the case of the local-sink local-source for the local analysis. We parametrize the propagator $G(t)$ as

$$G(t) = c \frac{\exp(-m(t)t)}{t^{\alpha(t)}}. \quad (12)$$

It is possible to determine $c, m(t_0), \alpha(t_0)$ locally, using three-point data $G(t_0), G(t_0 + 1), G(t_0 + 2)$. This is not a fit. One important point is that $m(t)$ and $\alpha(t)$ are smooth functions in t . In spirit, this is analogous to the Callan-Symanzik RG approach where we interpret $m(t)$ as the scale-dependent mass and $\alpha(t)$ as the wave-function renormalization factor. We have also made fits to the form Eq. (12) using five-point data. The fit gives generally similar results with the three-point determination. It implies that the three-point determination will represent the dynamics of the system.

The $m(t)$ and $\alpha(t)$ at short distance are governed by the UV fixed point and take the value of a free quark and an antiquark: $m(t) = 2m_q$ and $\alpha(t) = 3.0$ in the limit $t \rightarrow 0$ of the continuum theory. While in the limit $t \rightarrow \infty$, $m(t)$ and $\alpha(t)$ are governed by the IR fixed point. First, the $m(t)$ should approach a hadronic mass m_H . The exponent α_H in $t \rightarrow \infty$ with $t\tilde{m}_H \ll 1$ takes the universal formula $3 - 2\gamma^*$, while with $t\tilde{m}_H \gg 1$ it takes a value depending on the dynamics.

The $m(t)$ and $\alpha(t)$ evolve with t from UV to IR and thereby contain useful information on the dynamics, which we discuss below.

We show the $m(t)$ and $\alpha(t)$ for the four examples discussed above:

- (1) Fig. 10, exponential decay
 - (a) $N_f = 7, \beta = 6.0, K = 0.1400$ ($m_q = 0.25$)
 - (b) $N_f = 2, \beta = 10.0, K = 0.125$ ($m_q = 0.30$)
- (2) Fig. 11, power-corrected Yukawa-type decay
 - (a) $N_f = 7, \beta = 6.0, K = 0.1459$ ($m_q = 0.045$)
 - (b) $N_f = 2, \beta = 10.0, K = 0.135$ ($m_q = 0.028$)

In Fig. 10, where the propagators decay exponentially, the exponents $\alpha(t)$ take values close to 3.0 at $t = 3$ (we disregard the data at $t = 1$ and 2, as they are affected by the boundary) and decrease monotonously down to 0.0. In the confining region (left), it decays without a particular pattern, while in the deconfining region (right), it stays around 3.0, which means a free quark and antiquark pair, at $t = 4 \sim 8$. The $m(t)$ take values close to $2m_q$ at $t = 3$ and increase to the values of a meson state m_H , which are around $0.6 \sim 0.7$.

In Fig. 11, both of the exponents $\alpha(t)$ exhibit characteristic t dependence. However, they are quite different from each other. On the left panel, it shows a plateau at $t = 14 \sim 31$. On the other hand, it shows a shoulder $t = 10 \sim 16$ on the right panel of the figure. The difference arises from the difference of the dynamics.

The four examples exhibit the usefulness of the local analysis of propagators. We are able to learn not only the phase structure of the theories but also the detailed dynamics. We fully utilize the technique in the following.

V. STRUCTURE OF THE VACUUM AND POLYAKOV LOOPS

A. The $Z(3)$ twisted vacuum

To understand the phase structure in relation to the expectation values of the Polyakov loops, we discuss the

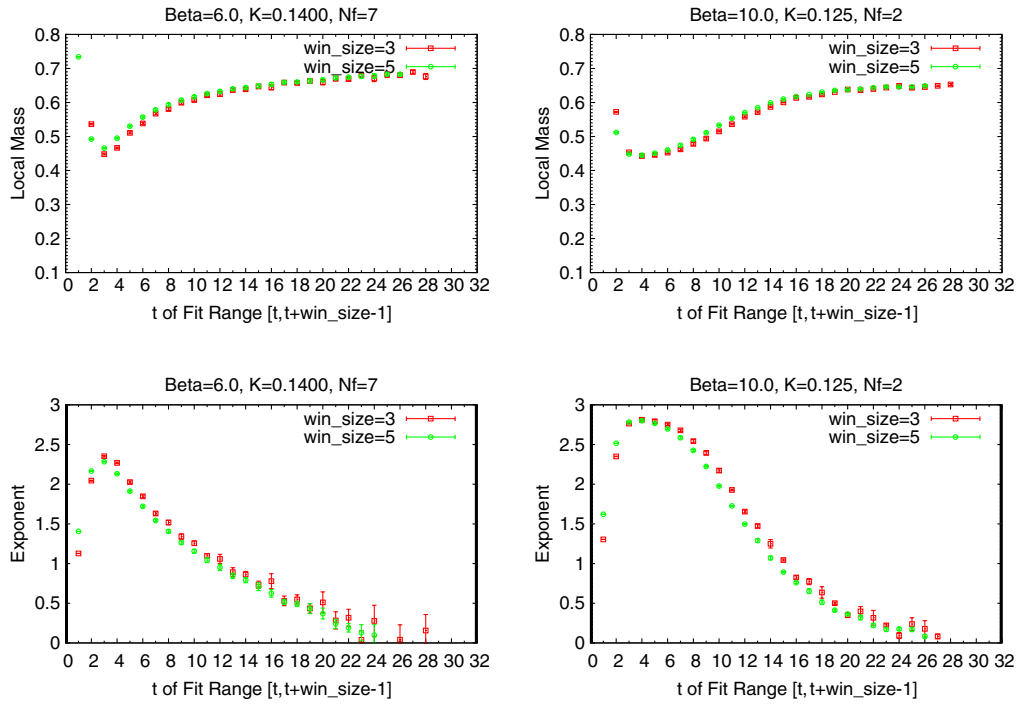


FIG. 10 (color online). The local mass $m(t)$ and local exponent $\alpha(t)$. (Left) $N_f = 7$ at $\beta = 6.0$ and $K = 0.1400$ and (right) $N_f = 2$ at $\beta = 10.0$ and $K = 0.125$.

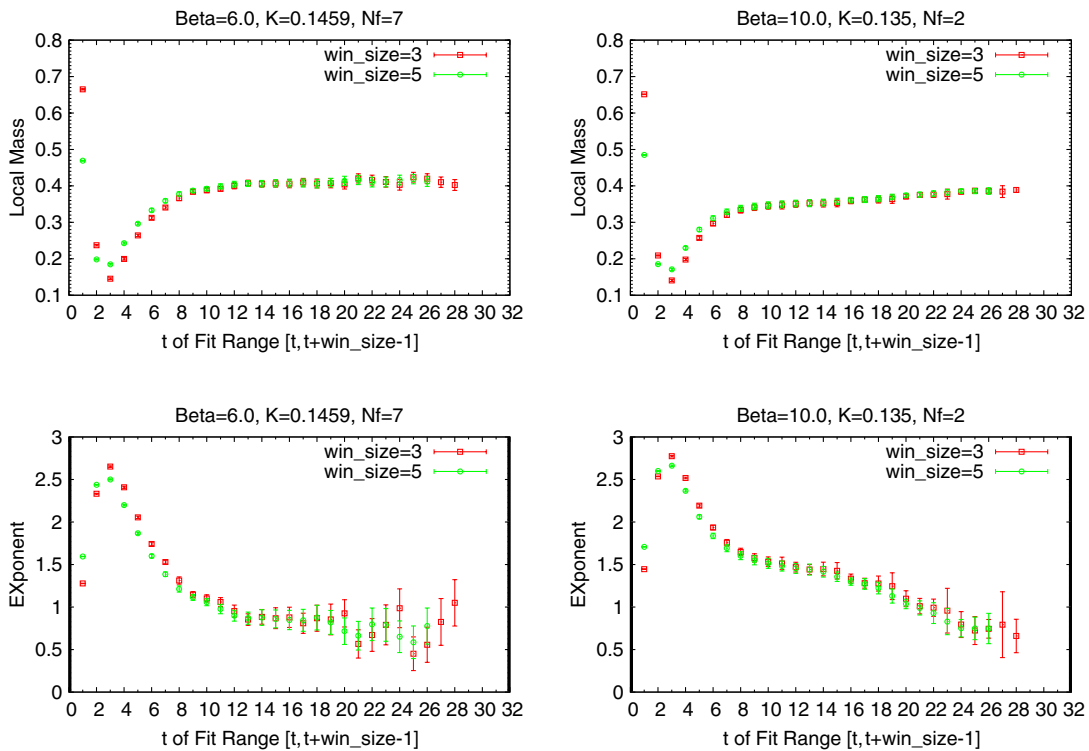


FIG. 11 (color online). The local mass $m(t)$ and local exponent $\alpha(t)$. (Left) $N_f = 7$ at $\beta = 6.0$ and $K = 0.1459$ and (right) $N_f = 2$ at $\beta = 10.0$ and $K = 0.135$.

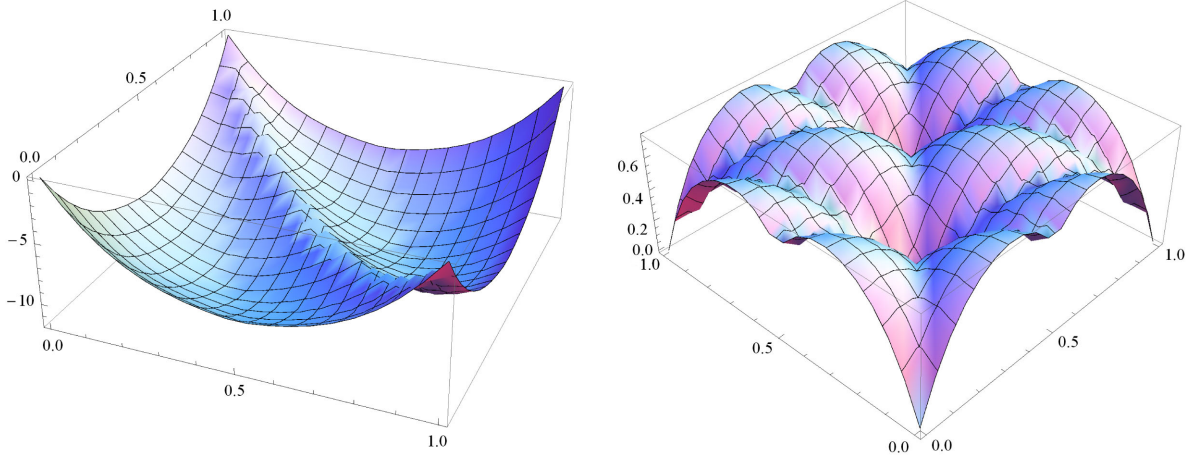


FIG. 12 (color online). The effective potential $V_{\text{eff}}(a, b)$ in terms of a and b : $m = 0.0$ (left) and $m = 1.0$ (right).

vacuum structure of the perturbative QCD on the lattice in the one-loop approximation by computing the zero-temperature vacuum energy.

In the perturbative QCD in the finite volume, the classical vacua are characterized by the flat connection. In the case of our torus lattice, the flat connection is given by the Polyakov loop in x, y, z directions [in fundamental representation of $SU(3)$]:

$$\begin{aligned}
 U_x &= \exp\left(i \int A_x dx\right) = \text{diag}(e^{i2\pi a_x}, e^{i2\pi b_x}, e^{i2\pi c_x}) \\
 U_y &= \exp\left(i \int A_y dy\right) = \text{diag}(e^{i2\pi a_y}, e^{i2\pi b_y}, e^{i2\pi c_y}) \\
 U_z &= \exp\left(i \int A_z dz\right) = \text{diag}(e^{i2\pi a_z}, e^{i2\pi b_z}, e^{i2\pi c_z}), \quad (13)
 \end{aligned}$$

with $a_i + b_i + c_i \in \mathbb{Z}$ for $(i = x, y, z)$ from the unitary condition. Note that $a_i = b_i = c_i = \frac{1}{3}, \frac{2}{3}$ gives a nontrivial center of the gauge group.

When the space is compact, we expect that a nontrivial potential for the flat direction is quantum mechanically generated similarly to the Hosotani mechanism [72]. The one-loop effective energy, including both fermion loops and gauge field loops for the $N_f = 16$ case with $m_q = 0.0$ on a 16^3 lattice, is calculated at the zero temperature in the six-parameter space; a_i, b_i in the x, y , and z directions. The details of calculation are given in Appendix D. The effective potential and the contour map in terms of two parameters, a, b in one direction among six parameters, are shown in Figs. 12 and 13.

By denoting the Polyakov loop in the x, y , and z directions by $P_x = \frac{1}{3}\text{Tr}U_x$, $P_y = \frac{1}{3}\text{Tr}U_y$, and $P_z = \frac{1}{3}\text{Tr}U_z$, respectively, and writing

$$(P_x, P_y, P_z) = |P| \exp(2\pi i((P_x, P_y, P_z))),$$

where $|P|$ is the absolute value and $((P_x, P_y, P_z))$ is the argument in units of 2π of Polyakov loops, it turns out that the local extremum of the one-loop energy is given by elements of the $Z(3)$ center:

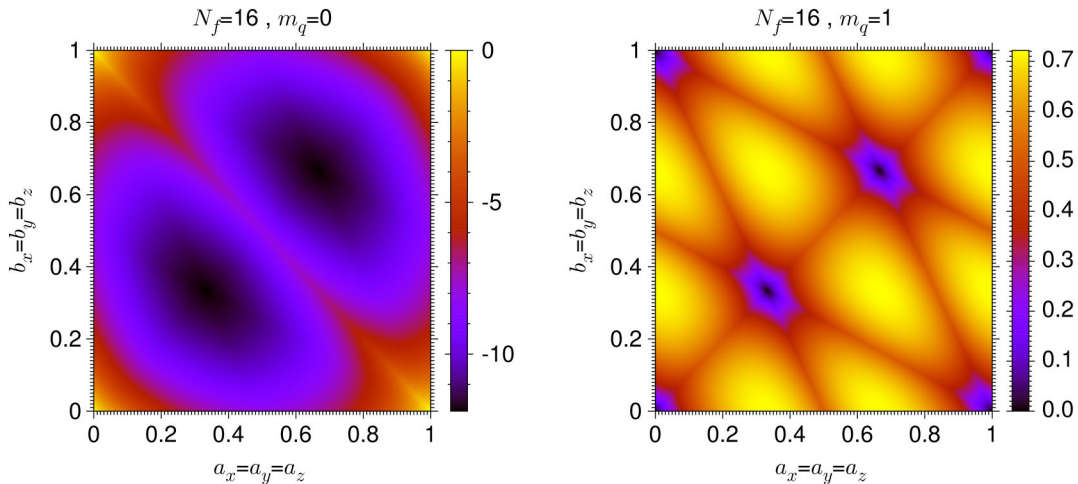


FIG. 13 (color online). The contour of the effective potential $V_{\text{eff}}(a, b)$ in terms of a and b : $m = 0.0$ (left) and $m = 1.0$ (right).

$$\begin{aligned} ((P_x, P_y, P_z)) &= (0, 0, 0), & (0, 0, \pm 1/3), \\ (0, \pm 1/3, \pm 1/3), & & (\pm 1/3, \pm 1/3, \pm 1/3), \end{aligned}$$

with $|P| = 1.0$. They are 3^3 fold and become degenerate in the quench limit $m_q \rightarrow \infty$. This is expected because without the matter the theory must be symmetric under the center of the gauge group. In the above, the order of P_x, P_y, P_z is cyclic.

From now on, we present the mean value of the argument of the state without the \pm symbol for simplicity. We use $(0, 0, 0)$, $(0, 0, 1/3)$, $(0, 1/3, 1/3)$, and $(1/3, 1/3, 1/3)$ to denote the phase of the mean values of the Polyakov loops in units of 2π , without mentioning the absolute value. When the state is in a confining region, the mean value of the Polyakov loop as a complex number is zero, and therefore, we denote the state by $(*, *, *)$.

The effective energy depends on the $Z(3)$ value, and we clearly see from Figs. 12 and 13 that the eightfold states $(1/3, 1/3, 1/3)$ are the lowest energy states in periodic boundary conditions in the one-loop approximation. The $(0, 0, 0)$ state is locally unstable when m_q is light, whereas it becomes locally stable as the m_q becomes heavy; $m_q = 0.15 \sim 0.25$. We can also confirm that the $(0, 0, 0)$ state is unstable at $m = 0.0$ but stable at $m = 1.0$ from Figs. 12 and 13 of the effective potential.

In Ref. [53], a similar result is obtained in the case of the twisted boundary conditions in the x and y directions: Assuming a priori that the lowest state is represented by the $Z(3)$ center in the z and t directions, the vacuum takes the nontrivial center in the fermion one-loop approximation.

We have several remarks of the vacuum structure. First, in the one-loop approximation, the global vacuum structure does not depend on the number of fermions very much, while the shape of the potential does depend on the number of fermions. For example, the shape of the potential for $N_f = 2$ and $m_q = 0.0$ is similar to that for $N_f = 16$. Second, the discussion here is done in the zero-temperature limit, and the phase structure at finite temperature does not necessarily follow the vacuum structure here. Finally, we expect that the strong interaction does change the structure of the vacuum, as we see that the Polyakov loop behaves very

differently in the confining region from that in the deconfining region. At the same time, we also see that in the perturbative regime in the deconfining region, the one-loop vacuum structure discussed here more or less survives.

B. The vacuum of conformal QCD

1. $N_f = 16$

We compare the vacuum of $N_f = 16$ obtained by simulations at $\beta = 11.5$ with $K = 0.1315$ ($m_q = 0.055$) with the vacuum in the one-loop approximation obtained above. The history of the Polyakov loop at $\beta = 11.5$ is shown in Fig. 14. The argument is very stable during 1,000 trajectories, taking the value of $\pm 2/3\pi$. However, the magnitude is about ~ 0.2 , clearly smaller than 1.0. This implies that the vacuum of $N_f = 16$ at $\beta = 11.5$ is close to the vacuum in the one-loop approximation but is not well described by the perturbation theory.

2. Smaller N_f

We show in Fig. 15 the Polyakov loop for $N_f = 7, 8, 12$, and 16 in the cases we have observed the Yukawa-type decay.

As N_f decreases, the magnitude decreases, and the fluctuation of magnitude and argument increases. Therefore, the transition among the vacua often occurs in the cases $N_f = 8$ and 7. However, the mean value of the arguments are $(1/3, 1/3, 1/3)$ in units of 2π .

C. The vacuum of high-temperature QCD, $N_f = 2$

1. The $\beta = 10.0 \sim 1000.0$

In Figs. 16 and 38,39 in Appendix F, we show the Polyakov loop for $N_f = 2$ at $\beta = 10.0, 15.0, 100.0, 1000.0$. As the temperature increases, the argument is more stable during simulations, taking the value of $\pm 2/3\pi$. The magnitude increases as the temperature increases, taking the values $\sim 0.1, 0.2, 0.82$, and 0.96, respectively. The approach to the magnitude unity is very slow. That is, at $T/T_c \approx 10^2$ or 10^5 , $|P| \approx 0.1 \sim 0.2$.

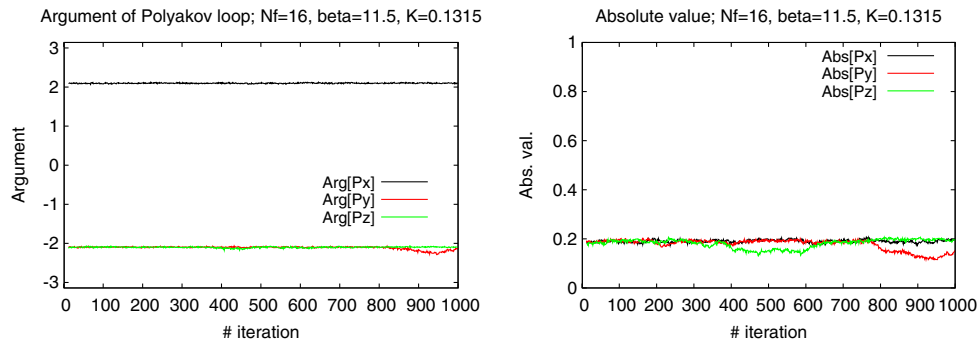


FIG. 14 (color online). The time history of the argument and the absolute value of Polyakov loops for $N_f = 16$ at $\beta = 11.5$ and $K = 0.1315$.

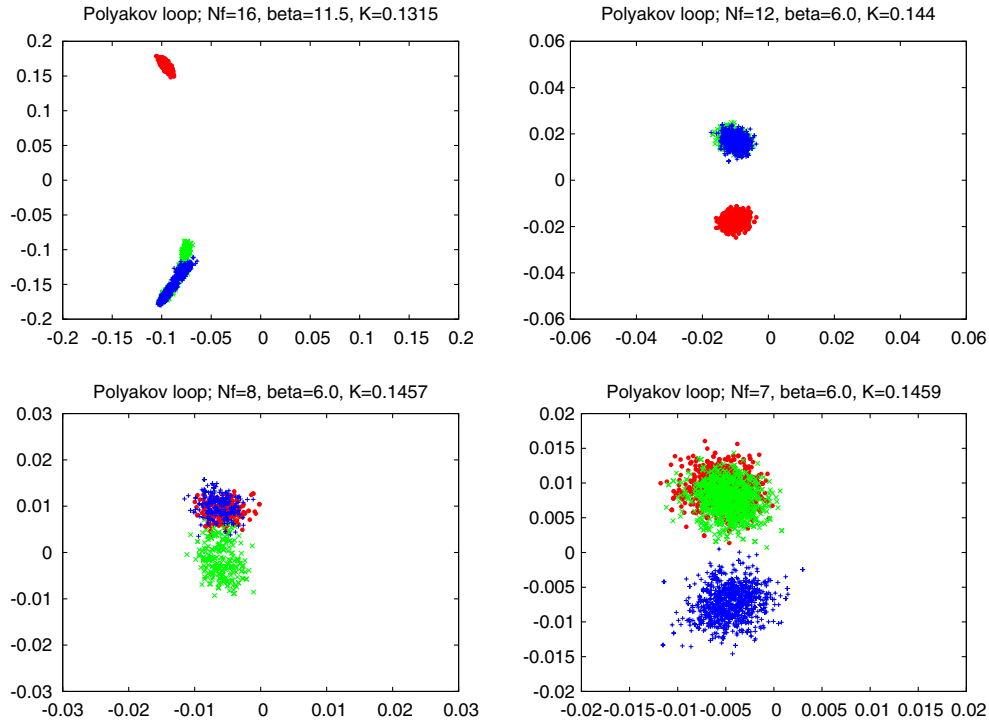


FIG. 15 (color online). The scattered plots of Polyakov loops in the x , y , and z directions overlaid; $N_f = 16$ at $\beta = 11.5$ and $K = 0.1315$, $N_f = 12$ at $\beta = 6.0$ and $K = 0.144$, $N_f = 8$ at $\beta = 6.0$ and $K = 0.1457$, and $N_f = 7$ at $\beta = 6.0$ and $K = 0.1459$.

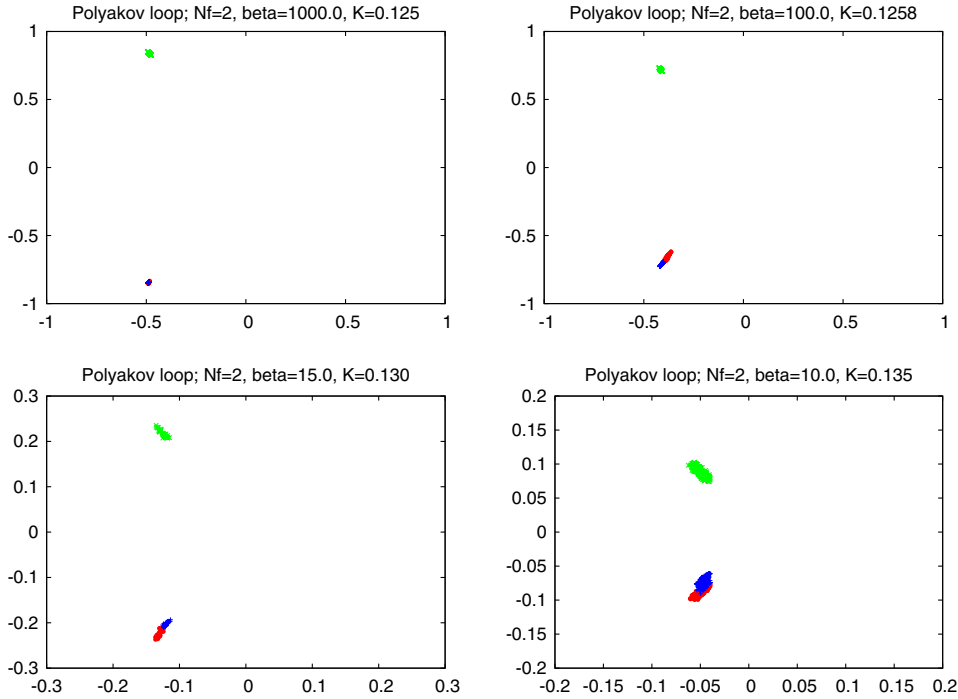


FIG. 16 (color online). The scattered plots of Polyakov loops in the x , y , and z directions overlaid; $N_f = 2$ at $\beta = 1000.0$ and $K = 0.125$, $\beta = 100.0$ and $K = 0.1258$, $\beta = 15.0$ and $K = 0.130$, and $\beta = 10.0$ and $K = 0.135$.

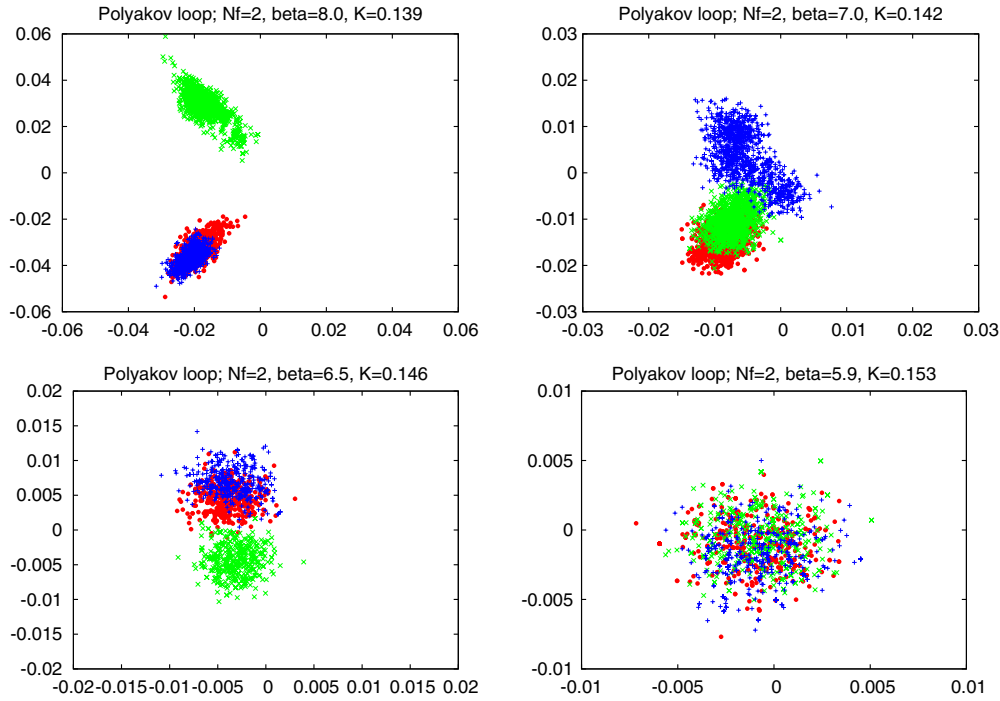


FIG. 17 (color online). The scattered plots of Polyakov loops in the x , y , and z directions overlaid; $N_f = 2$ at $\beta = 8.0$ and $K = 0.139$, $\beta = 7.0$ and $K = 0.142$, $\beta = 6.5$ and $K = 0.146$, and $\beta = 5.9$ and $K = 0.153$.

2. Smaller β

In Fig. 17, we show the Polyakov loop at lower temperatures in the cases where we have observed the Yukawa-type decay for $N_f = 2$ at $\beta = 6.5, 7.0$, and 8.0 .

We clearly see that as β decreases in high-temperature QCD, the magnitude decreases, and the fluctuation of magnitude and argument increases. Therefore, the transition among the vacua often occurs. Nevertheless, the mean value of the arguments is $(1/3, 1/3, 1/3)$ down to $\beta = 6.5$.

However, at $\beta = 5.9$, which is smaller than the chiral transition point, the mean value of the Polyakov loop vanishes as a complex number, which shows that the state is in the confining region.

VI. TEMPORAL PROPAGATORS IN VARIOUS VACUA

A. Free Wilson fermion and $\beta = 100.0$

In the limit $T/T_c \rightarrow \infty$, it is natural to consider that the quark pair becomes a free quark pair. Therefore, we calculate the propagator of the PS channel using the free Wilson quark propagator in the vacuum: in all of the four species of vacua, shown in the previous section.

We also calculate the meson propagators for $N_f = 2$, at $\beta = 100.0$ and $K = 0.1258$, which correspond to $T \sim 10^{56} T_c$ and $m_q = 0.015$

We have performed simulations first at a small value for the temperature $T/T_c \approx 2$ and gradually increased the

temperature. At small values of temperatures, the transition among the four vacua often occurs because the barriers among them are low, and therefore, the lowest energy state is chosen during the simulations. Then the temperature is gradually increased up to $\beta = 100.0$. In this way, the state becomes $(1/3, 1/3, 1/3)$.

Alternatively, by choosing a configuration in the quenched QCD as the initial state and varying the simulation parameters in several ways, we are also able to obtain the state at $\beta = 100.0$ and $K = 0.1258$, with $(0, 1/3, 1/3)$ and $(0, 0, 1/3)$. However, we are unable to obtain the state with $(0, 0, 0)$. This is consistent with the analysis of the vacuum energy that the state $(0, 0, 0)$ is locally unstable, when $m_q \leq 0.15$.

Let us show on the right side of Figs. 18 and 40–42 in Appendix F the $m(t)$ and $\alpha(t)$ of the free fermion state with $m_q = 0.01$ calculated in the four species of the vacuum, together with the results of Monte Carlo calculations at $\beta = 100.0$ with $K = 0.1258$, which corresponds to $m_q = 0.0015$ on the left side. The figures corresponding to the state $(0, 0, 0)$ at $\beta = 100.0$ with $K = 0.1258$ are missing due to the reason given above.

The similarities between the free Wilson quark states and the $\beta = 100.0$ states are excellent. However, if one closely looks at the both, one notices that the exponents $\alpha(t)$ at large t in the case of $\beta = 100.0$ are systematically larger than those of the free Wilson cases. We discuss this point later.

The values of the mass determined by $m(t)$ at $t \rightarrow 31$ are in good tendency with the value estimated by the lowest

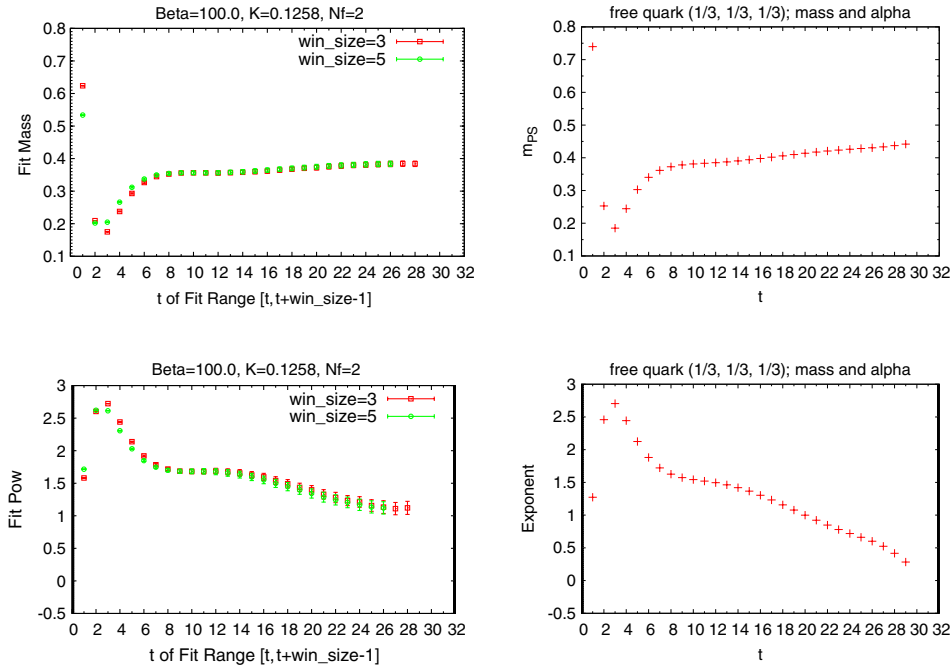


FIG. 18 (color online). The local mass $m(t)$ and the local exponent $\alpha(t)$ at $\beta = 100.0$ and $K = 0.1258$ (left) and a free particle $(1/3, 1/3, 1/3)$ with $m_q = 0.01$ (right).

Matsubara frequency: For $(1/3, 1/3, 1/3)$, $m_{PS} = 0.384(8)$ vs $\sqrt{34}\pi/3L = 0.45345$. For $(0, 1/3, 1/3)$, $m_{PS} = 0.328(3)$ vs $\sqrt{24}\pi/3L = 0.37024$. For $(0, 0, 1/3)$, $m_{PS} = 0.226(3)$ vs $4\pi/3L = 0.2618$.

The differences between the free cases and the simulation results are discussed below.

B. $\beta = 10.0, 15.0, 100.0, 1000.0$

In order to understand the difference for $\alpha(t)$ and $m(t)$ at large t between the free case and the state at $\beta = 100.0$, we calculate the PS propagator in the vacuum mentioned above at $\beta = 10.0, 15.0, 100.0, 1000.0$.

The results of the $\alpha(t)$ are shown in Fig. 43. The $\alpha(t)$ s at four values of β seem almost the same each other at first glance.

However, we know already that the magnitudes $|P|$ are 0.1, 0.2, 0.82, 0.96, respectively, for $\beta = 10.0, 15.0, 100.0, 1000.0$.

We see that as the temperature increases up to $\beta = 1000.0$, which corresponds formally to $T/T_c \approx 10^{598}$, the exponent $\alpha(t)$ at large t becomes smaller and approaches to the free case.

This implies that even at $\beta = 1000.0$ nonperturbative effects still work to reduce the magnitude of the Polyakov loop and the temporal propagators differ slightly from the free case. Therefore, the perturbation around the vacuum may not give a quantitatively good result at $T/T_c = 10^2 \sim 10^5$.

In a similar way, the discrepancy of the observed value of the mass and the one estimated by the lowest Matsubara

frequency with the twisted boundary condition of the free quarks tends to be resolved at a higher temperature. At $\beta = 1000.0$ with $K = 0.125$, we obtain $m_{PS} = 0.4254(16)$, which is significantly closer to the prediction $m_{PS} = 0.45345$ than at $\beta = 100.0$ with $m_{PS} = 0.384(8)$.

We think that this is closely related to the slow approach of the free energy to the Stefan-Boltzmann ideal gas limit. To conclude that, we must perform simulations toward the thermodynamical limit.

VII. CONFORMAL REGION AND VACUUM STRUCTURE

The conformal region is defined by Eq. (8),

$$m_H \leq c\Lambda_{\text{IR}},$$

where the propagator $G(t)$ behaves at large t as a power-law-corrected Yukawa-type decaying form [Eq. (9)]

$$G_H(t) = \tilde{c}_H \frac{\exp(-\tilde{m}_H t)}{t^{\alpha_H}},$$

instead of the exponential decaying form [Eq. (7)] observed in the confining region and deconfining region.

We have shown examples of the Yukawa-type decays in many cases: $N_f = 7, 8, 12$, and 16 in conformal QCD and $N_f = 2$, $\beta = 6.5, 7.0, 8.0, 10.0, 100.0, 1000.0$ in high-temperature QCD.

The RG argument implies that the boundary is a first-order transition. Indeed, in the previous paper [64] we have

shown in the case $N_f = 7$ that the existence of two states at the same parameters and the transition is first order.

In this section, we intensively investigate the conformal region in several cases: $N_f = 16$, $N_f = 12$, $N_f = 7$ in conformal QCD and $N_f = 2, \beta = 10.0$ in high-temperature QCD. In doing so, we clarify that the vacuum of the conformal region is $(1/3, 1/3, 1/3)$ and outside the boundary is either the $(0,0,0)$ vacuum for the deconfining region or the $(*, *, *)$ vacuum for the confining region. Therefore, the transition across the boundary is the transition between different vacua, and we argue that the transition must be first order, being consistent with the gap observed in other physical quantities.

We also make a cautious remark that in order to investigate conformal properties such as the anomalous mass dimension from the spectrum one must be inside the conformal region. Otherwise, one may obtain either the deconfining behavior or the confining behavior depending on the β and lattice size, irrespective of the conformal behavior inside the conformal region. We show examples in the case $N_f = 12$.

In relation to the first-order phase transition, the search of the gap in spectrum is crucial. To systematically address the question, we carefully perform simulations in the following way. We first simulate at small quark mass (large K) where

the propagator $G(t)$ behaves at large t as a power-law-corrected Yukawa-type decaying form. Then we simulate at a smaller K (larger quark mass) using the configuration at the larger K . We gradually decrease K . When the step size of K is small enough, one will find a gap in the PS mass at some K . Further, we decrease K . After reaching some K , we then increase K in the opposite direction to the above. Then we find a gap at the same (or similar) K to the one in the process of decreasing K .

When the step size is large, one may miss the gap since each vacuum is quasistable. In particular, at large β , large N_f and large quark mass, one may obtain the result of a quasistable state. We give such examples also in the case $N_f = 12$.

A. $N_f = 16$

The results in the $N_f = 16$ case for m_q and m_{PS} (or \tilde{m}_{PS}) are shown in Fig. 19. We note that the quark mass m_q denoted by filled circles on the left panel is excellently proportional to $1/K$ in the whole region from 0.00 to 0.4.

For the propagators of the PS meson, we observe a clear transition from the exponentially decaying form to the power-law-corrected Yukawa-type decaying form at

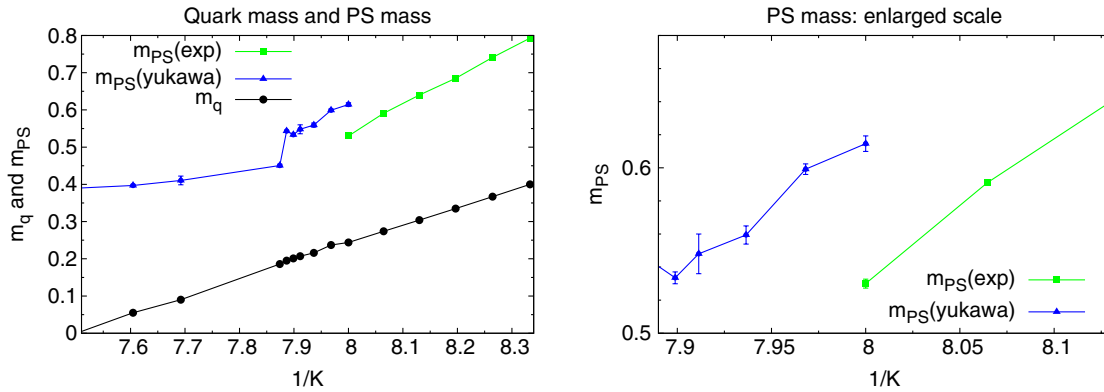


FIG. 19 (color online). m_q and m_{PS} (or \tilde{m}_{PS}) vs $1/K$ in the case $N_f = 16$ for the range $0.130 \leq K \leq 0.1472$. The transition region is enlarged in the right panel.

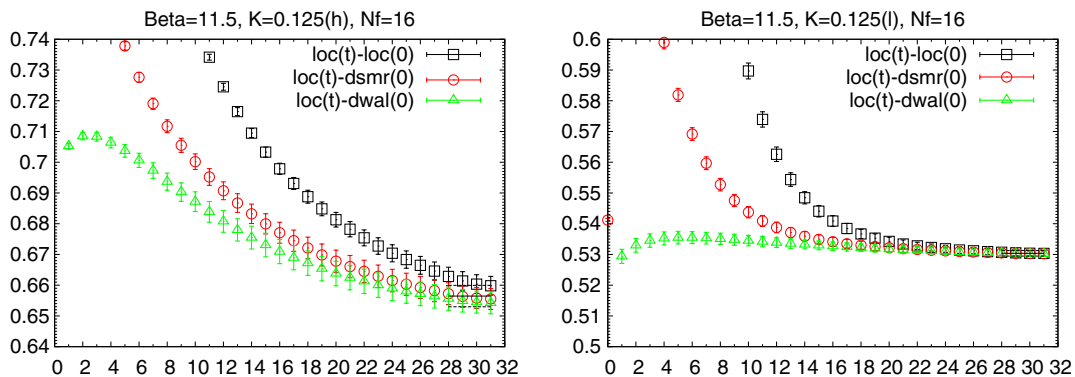


FIG. 20 (color online). The effective mass, both for $N_f = 16$ at $\beta = 11.5$ and $K = 0.125$: (left) from larger K and (right) from smaller K (see the main text for the three types of sources).

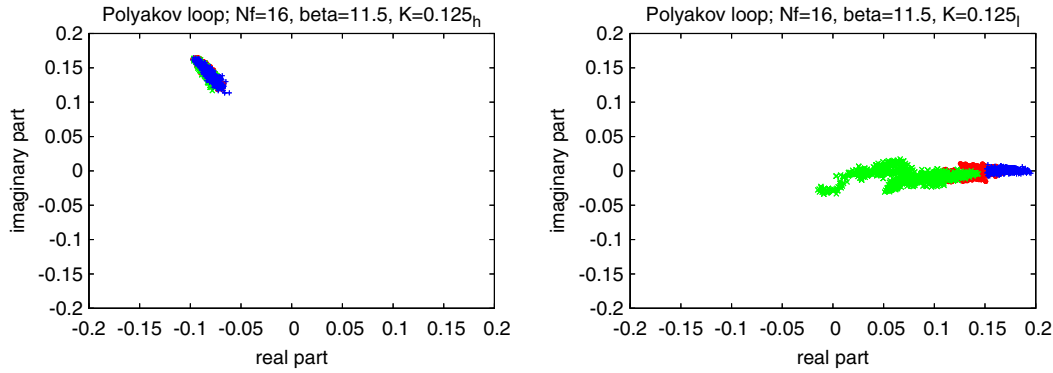


FIG. 21 (color online). The scattered plots of Polyakov loops in the x , y , and z directions overlaid, both for $N_f = 16$ at $\beta = 11.5$ and $K = 0.125$: (left) from larger K and (right) from smaller K .

$K = 0.125$. The transition region is enlarged on the right panel in Fig. 19.

The values of m_{PS} and \tilde{m}_{PS} are different in the limit $K = 0.125$ from smaller K (denoted by $K = 0.125_l$) and from larger K (denoted by $K = 0.125_h$). The effective mass plot at $K = 0.125_h$ and $K = 0.125_l$ on the right and left panels of Fig. 20, respectively, clearly shows not only quite a large difference of the effective mass at large t but also a completely different decaying behavior.

The scattered plots of the Polyakov loops in the complex plane at $K = 0.125_h$ and $K = 0.125_l$ are shown on the right and left panels of Fig. 21, respectively. In the conformal region, the arguments are $\pm 2/3\pi$, and the magnitudes are $|P| \approx 0.18$, while outside the conformal region the arguments are 0 and the magnitudes are $\sim 0.05 \sim 0.2$. It is characteristic in the deconfining region.

The vacuum of all the other states in the conformal region are $(1/3, 1/3, 1/3)$, while all of the states outside the conformal region are $(0, 0, 0)$.

The m_{PS}^2 and m_{PS} are plotted as a function of m_q in Fig. 22 on the right and left panels, respectively. The m_{PS} plotted linearly as a function of m_q outside the conformal region can be smoothly extrapolated to the $m_{PS} = 0$ point in the limit $m_q = 0$ compared with the m_{PS}^2 extrapolation. This behavior is as expected in the deconfining region.

Thus, we conclude that the conformal region is the $(1/3, 1/3, 1/3)$ vacuum, and the deconfining region is the $(0, 0, 0)$ vacuum. The transition across the boundary is a first-order transition between different vacua.

From the analysis we have made, we are able to draw the phase structure as shown on the left panel of Fig. 32. The transition in the quench limit on the lattice $16^3 \times 64$ is estimated to be about $\beta = 6.7$. This value is independent from N_f . Therefore, the $\beta = 11.5$ is in the deconfining region at least for heavy quarks. As the quark mass decreases, the line of $\beta = 11.5$ hits the boundary between the deconfining region and the conformal region.

The m_q dependence of \tilde{m}_{PS} inside the conformal region is rather complicated around $m_q \approx 0.2$. Apparently the small \tilde{m}_{PS} region suffers from finite size effects. To verify the scaling relation [35,71,73] for \tilde{m}_{PS} as a function of m_q , we have to control finite size effects.

The transition occurs at $m_{PS} \approx 0.539$ with $m_q \approx 0.244$ ($K \approx 0.125$) from which we estimate $c \approx 1.94$ with our working definition of $\Lambda_{IR} = 2\pi(N^3 \times N_t)^{-1/4}$.

B. $N_f = 7$

We have observed in Ref. [56] a transition from the exponentially decaying form to the power-law-corrected Yukawa-type decaying form around $K = 0.1413$: the

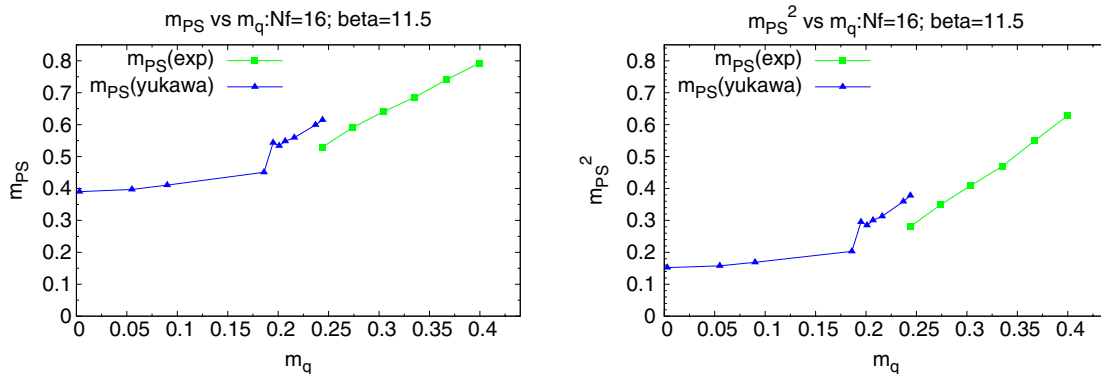


FIG. 22 (color online). The m_{PS} (or \tilde{m}_{PS}) vs m_q for $N_f = 16$: (left) linear m_{PS} and (right) squared m_{PS} .

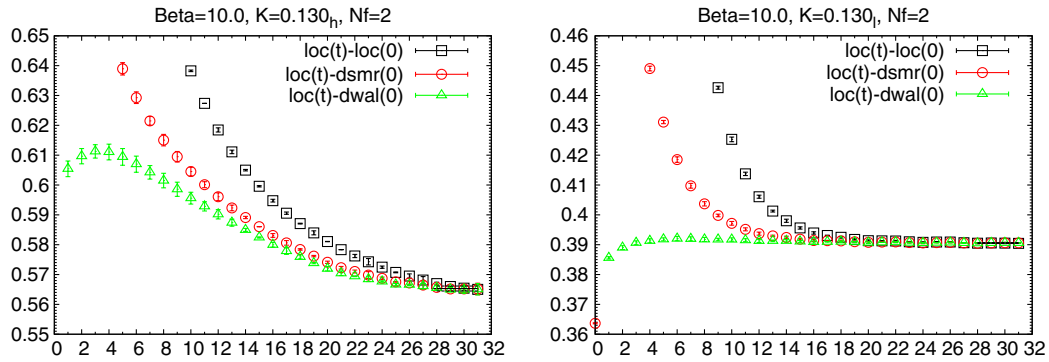


FIG. 23 (color online). The effective mass both for $N_f = 2$ at $\beta = 10.0$ and $K = 0.130$: (left) from larger K and (right) from smaller K .

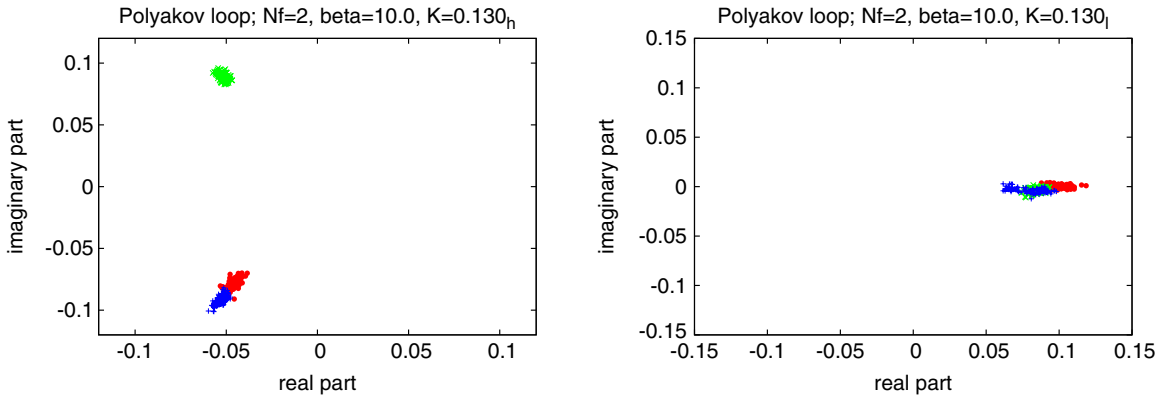


FIG. 24 (color online). The scattered plots of Polyakov loops in the x , y , and z directions overlaid, both for $N_f = 2$ at $\beta = 10.0$ and $K = 0.130$: (left) from larger K and (right) from smaller K .

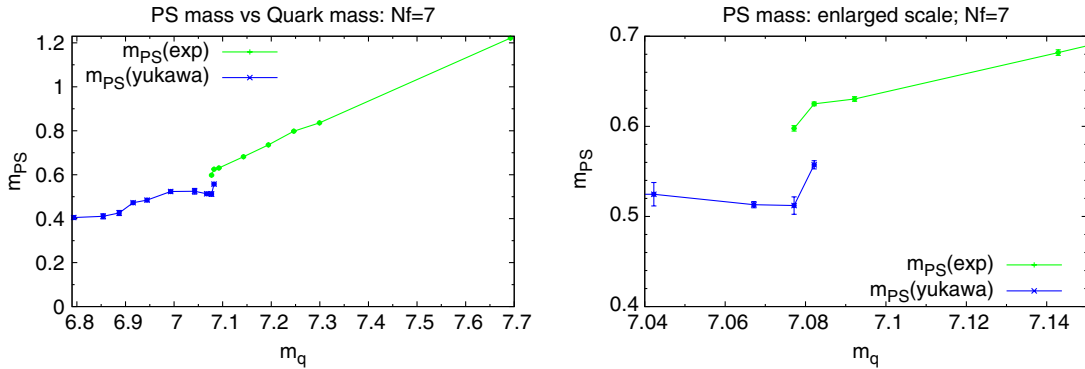


FIG. 25 (color online). m_q and m_{PS} (or \tilde{m}_{PS}) vs $1/K$ in the case $N_f = 7$ for the range $0.130 \leq K \leq 0.1472$. The transition region is enlarged in the right panel.

results of new simulations measuring the Polyakov loop on the fly are shown in Fig. 25, which are the same as the previous results within errors. The effective mass plots for $K = 0.1413_h$ and $K = 0.1413_l$ shown on the right and left panels of Fig. 26 clearly indicate a gap of the mass cross the transition.

The vacuum structure in terms of the Polyakov loops becomes less clear as N_f decreases, as shown in Sec. VIII.

First we show the scattered plot of the Polyakov loops in the complex plane for two states in Fig. 44: One is an example state outside of the conformal region, $K = 0.1400$, and the other in the conformal region, $K = 0.1459$. The state $K = 0.1459$ on the left panel indicates that the state is $(1/3, 1/3, 1/3)$, while the state $K = 0.1400$ on the right panel implies that the state is in the confining state $(*, *, *)$.

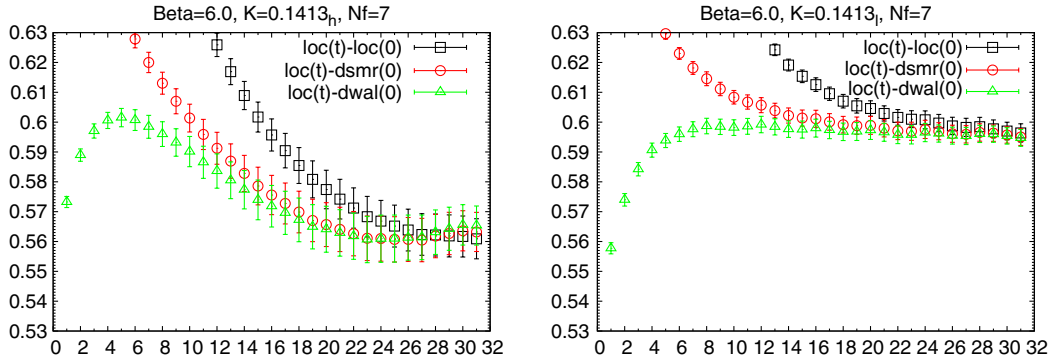


FIG. 26 (color online). The effective mass both for $N_f = 7$ at $\beta = 6.0$ and $K = 0.1413$: (left) from larger K and (right) from smaller K .

As these two states approach to the boundary $K = 1.413$ from the both sides, the difference between the two states becomes less clear, as shown in Fig. 45.

As discussed in Sec. II C, the order parameters, the chiral condensate in the massless limit, and the Polyakov loop in the time direction in the quenched limit are not well defined far from the massless limit and the quenched limit, respectively. The $Z(3)$ center values are good indicators for the structure of the vacuum, when β is large or N_f is large. However, they are not good indicators when N_f becomes small in conformal QCD or small β in high-temperature QCD due to nonperturbative effects. This is similar to the behavior of the chiral condensate and the Polyakov loop in the time direction, as discussed above.

Irrespective of the existence of a good indicator in terms of the $Z(3)$ center values, the transition across the boundary is a strong first-order transition, manifesting it in terms of the temporal propagators.

All of the states outside the conformal region are the confining region, from the Polyakov loop analysis. In accordance with this, the m_{PS} quadric plotted as a function of m_q in Fig. 27 on the right panel can be smoothly extrapolated to the $m_{PS} = 0$ point in the limit $m_q = 0$ compared with the linear plot on the left panel.

From the analysis we have made, we also are able to draw the phase structure for $N_f = 7$, as on the right

panel of Fig. 32. The point $\beta = 6.0$ is in the confining region.

The m_q dependence of \tilde{m}_{PS} is rather complicated around $m_q \approx 0.2$. Apparently the small \tilde{m}_{PS} region suffers from finite size effects. To verify the scaling relation [35,71,73] for \tilde{m}_{PS} as a function of m_q , we have to control the finite size effects. We have more to say about the finite size scaling in section VII H.

The transition occurs at $m_{PS} \approx 0.601$ with $m_q \approx 0.216$ ($K \approx 0.1413$) from which we estimate $c \approx 2.16$ with our working definition of $\Lambda_{IR} = 2\pi(N^3 \times N_t)^{-1/4}$.

C. $N_f = 12$

The m_q dependences of m_{PS} outside of the conformal region are different in the cases $N_f = 16$ and $N_f = 7$: In the $N_f = 16$ case, the linear m_{PS} is proportional to m_q , which is the relation expected in the deconfining (chiral symmetric) region, while in the case of $N_f = 7$ the square of m_{PS} is proportional to m_q , which is the relation expected in the confining (chiral symmetry broken) region. This difference is not originated from the difference of N_f , but from the β value. To make this point clear, we make simulations for $N_f = 12$ at $\beta = 6.0$ and $\beta = 8.0$.

We show two typical examples of scattered plot of the Polyakov loops in each case: Fig. 28 shows the examples in the case $\beta = 6.0$. They are consistent with the fact that the

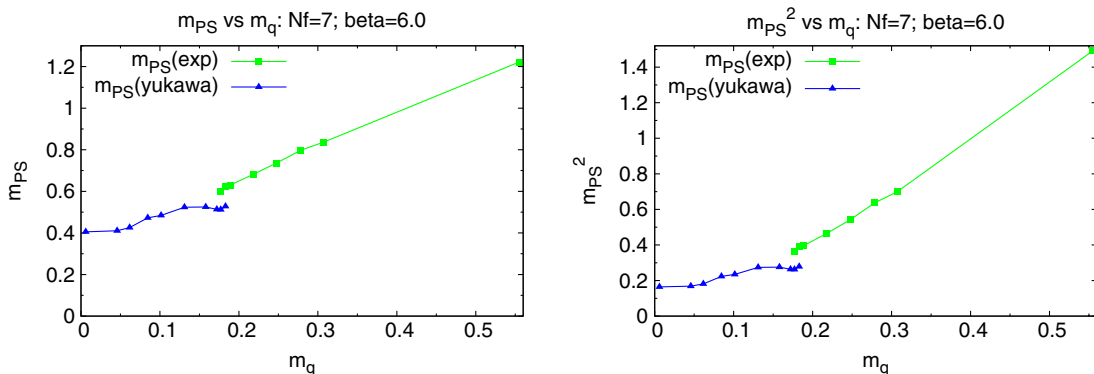


FIG. 27 (color online). The m_{PS} (or \tilde{m}_{PS}) vs m_q for $N_f = 7$: (left) linear m_{PS} and (right) squared m_{PS} .

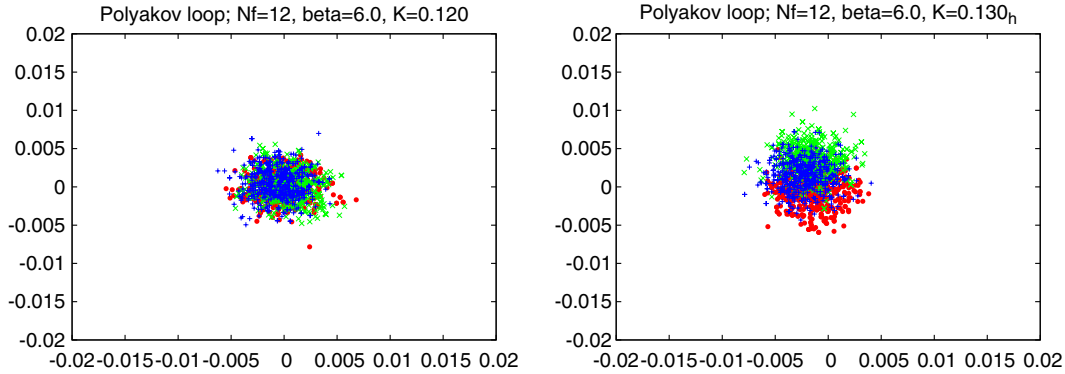


FIG. 28 (color online). The scattered plots of Polyakov loops in the x , y , and z directions overlaid, both for $N_f = 12$ at $\beta = 6.0$: (left) $K = 0.120$ and (right) $K = 0.130$.

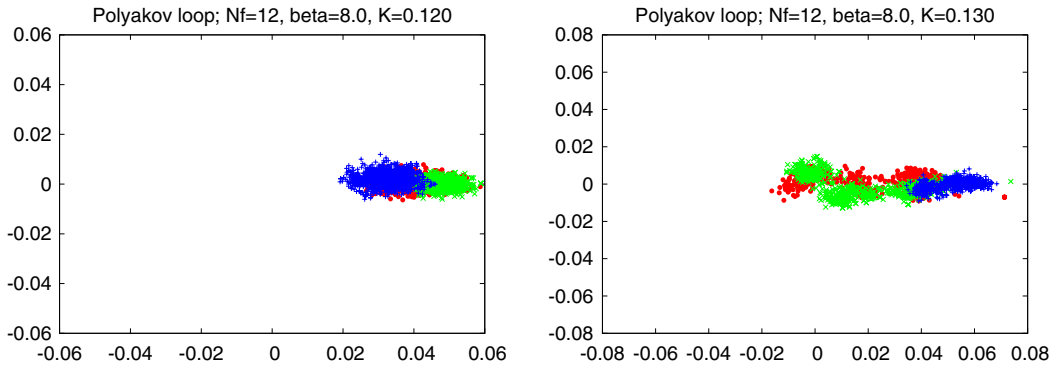


FIG. 29 (color online). The scattered plots of Polyakov loops in the x , y , and z directions overlaid, both for $N_f = 12$ at $\beta = 8.0$: (left) $K = 0.120$ and (right) $K = 0.130$.

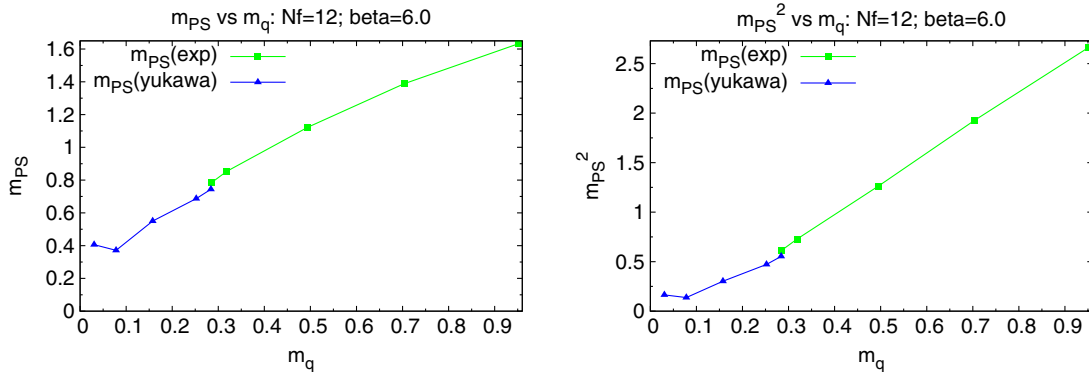


FIG. 30 (color online). The m_{PS} (or \tilde{m}_{PS}) vs m_q for $N_f = 12$ and $\beta = 6.0$: (left) linear m_{PS} and (right) squared m_{PS} .

states are $(*, *, *)$, which is characteristic in the confining region. On the other hand, the plots of Fig. 29 are for $\beta = 8.0$. The Polyakov loops are on the real axis. This implies that the states are $(0,0,0)$, which is characteristic in the deconfining region.

The m_{PS}^2 and m_{PS} are plotted as a function of m_q for $\beta = 6.0$ and $\beta = 8.0$, respectively, in Figs. 30 and 31. The m_{PS} quadratically plotted as a function of m_q at $\beta = 6.0$ can be more smoothly extrapolated to the $m_{PS} = 0$ point in the

limit $m_q = 0$ compared with the linear plot on the left panel. On the other hand, at $\beta = 8.0$, the m_{PS} linearly plotted in m_q can be more smoothly extrapolated to the $m_{PS} = 0$ point in the limit $m_q = 0$ compared with the quadric plot on the right panel.

From all results, we are able to draw the phase structure for $N_f = 12$: on the right panel of Fig. 32 for $\beta = 6.0$ (confining region) and on the left panel for $\beta = 8.0$ (deconfining region).

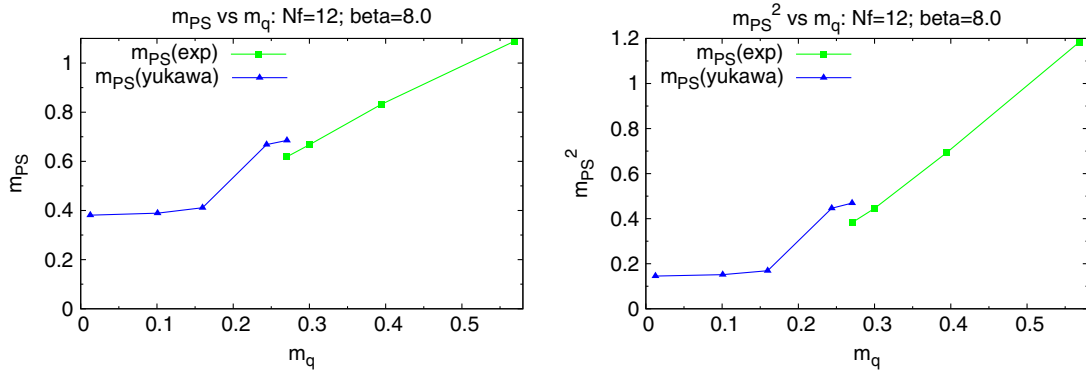


FIG. 31 (color online). The m_{PS} (or \tilde{m}_{PS}) vs m_q for $N_f = 12$ and $\beta = 8.0$: (left) linear m_{PS} and (right) squared m_{PS} .

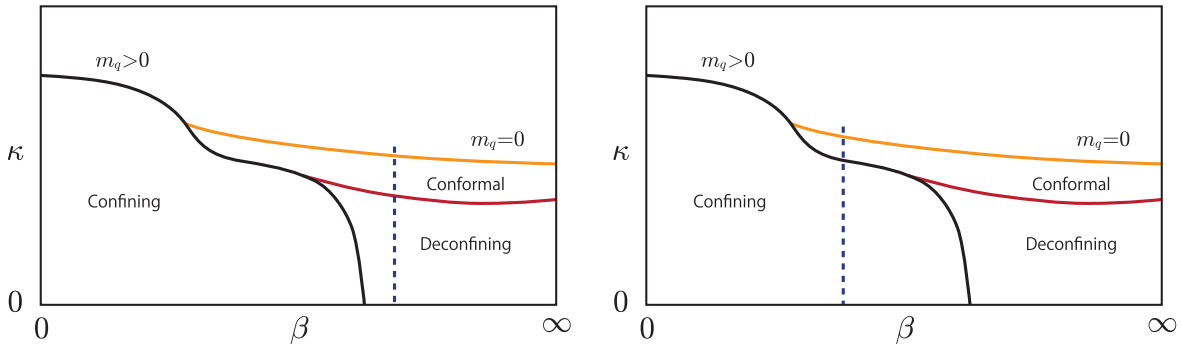


FIG. 32 (color online). The phase diagram on a finite lattice for $N_f^c \leq N_f \leq 16$: the solid line toward the quench QCD $K = 0$ is the boundary between the deconfining and confining regions. The dashed line represents the simulation line. The massless line hits the bulk transition point at finite β .

Here is a cautionary remark. The m_q dependence of m_{PS} outside of the conformal region is determined by the lattice size and the beta. It is irrelevant to the conformal behavior. In order to obtain conformal properties, one should be inside the conformal region.

Another comment concerns quasistable states. Doing the simulation by decreasing K in a small step and taking a state $(1/3, 1/3, 1/3)$ as the initial state, one find a transition at some K to a state $(0,0,0)$ or $(*, *, *)$. This implies that the potential energy of the states $(0,0,0)$ or $(*, *, *)$ is smaller than that of the state $(1/3, 1/3, 1/3)$ for $K \leq K^c$. It should be stressed that this is different from the perturbation theory where the state $(1/3, 1/3, 1/3)$ is the lowest state for all K . Because of this fact, the first-order transition occurs.

As mentioned above, each vacuum is quasistable, in particular, at large β , large N_f , and large quark mass. Instead of the process in small steps of K , when one jumps from $K > K^c$ to some smaller K , the state may stay at a state $(1/3, 1/3, 1/3)$. We have checked in the $N_f = 12$ case that at $\beta = 6.0$, $m_q^c = 0.284$ ($K^c = 0.136$) and the allowed region for the next step from a state $(1/3, 1/3, 1/3)$ is $0.285 \leq m_q \leq 0.704$. On the other hand, at $\beta = 8.0$, $m_q^c = 0.271$ ($K^c = 0.129$), and the allowed

region is $0.271 \leq m_q \leq 0.394$. If we would take a next step wider than this allowed region, the state will be a state $(1/3, 1/3, 1/3)$. The state is quasistable for order of 1,000 trajectories. The allowed region becomes smaller for increasing β as expected.

Furthermore, if one would not systematically decrease or increase K but would use a bisectionlike method to choose K , one would obtain a complicated phase structure with quasistable vacua.

D. $N_f = 2$ at $\beta = 10.0$

Now we investigate a case in high-temperature QCD. It was shown in Sec. IV A for $N_f = 2$ at $\beta = 10.0$ that the propagator behaves at large t exponential decay at $K = 0.125$ ($m_q = 0.30$), while Yukawa-type decay is at $K = 0.135$ ($m_q = 0.028$).

Here we further investigate the state at $K = 0.130$. We observe two states: one at $K = 0.130_h$ continued from $K = 0.135$ and the other at $K = 0.130_l$ from $K = 0.125$. Effective mass plots are shown in Fig. 23, and the scattered plots of the Polyakov loops in the complex plane are in Fig. 24. Thus, we see that the difference between the two

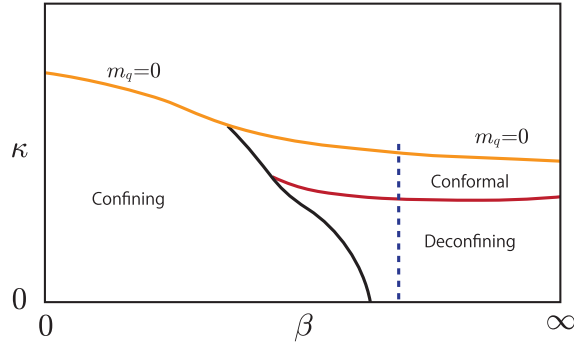


FIG. 33 (color online). The phase diagram on a finite lattice for $1 \leq N_f \leq -1$: the solid line toward the quench QCD $K = 0$ is the boundary between the deconfining and confining region. The dashed line represents the simulation line. The massless line runs through from $\beta = \infty$ to $\beta = 0$.

sates is exactly the same as in the $n_f = 16$ case: The conformal region can be identified with the vacuum $(1/3, 1/3, 1/3)$, while the deconfining region with $(0, 0, 0)$. The transition across the boundary is a first-order transition between different vacua in this case also.

We are able to draw the phase structure as shown in Fig. 33, which is similar to the left panel of Fig. 32. However, in Fig. 32 there is no $m_q = 0$ in the confining phase, which is quite different from Fig. 33.

E. Phase structure on a lattice

From the above detailed analyses for $N_f = 16$, $N_f = 12$, $N_f = 7$, and $N_f = 2$, $\beta = 10.0$, we make one of the main conclusions in this article, announced in Sec. II E that the phase structures on a finite lattice are as shown in Fig. 1. Thus, there exists on a finite lattice the conformal region in addition to the confining region and the deconfining region both in conformal QCD and high-temperature QCD.

F. The vector channel

We have mainly discussed the temporal propagators in the PS channel so far. We have also measured the propagator in the vector channel, the results being listed in the tables. In general, the signal is worse in the vector channel, in particular, at the very small quark mass. This is common to the usual QCD.

In the confining region, the pion mass in the chiral limit satisfies $m_\pi^2 \sim m_q$ as a softly broken Goldstone particle. Therefore, m_V deviates from m_π and takes a nonzero value in the chiral limit. In the case $N_f = 2$, we are able to take a very small quark mass $m_q = 0.0332(1)$ at $\beta = 5.9$, which is lower than the chiral transition at $\beta = 6.0$. We see clearly that the vector meson deviates from the PS meson: $m_\pi = 0.328(6)$ and $m_V = 0.449(6)$. At $\beta = 6.0$ for $N_f = 12$ and $N_f = 7$, there is a tendency for m_V to be slightly larger than m_π . However, the quark mass is heavy to conclude the deviation.

In the deconfining region at $\beta = 11.5$ for $N_f = 16$, at $\beta = 6.0$ for $N_f = 12$, and at $\beta \geq 6.5$ for $N_f = 2$, m_π agrees with m_V within errors. This is consistent with the fact that the chiral symmetry is not spontaneously broken. However, the quark mass is relatively heavy, and we have to measure the scalar meson to conclude that the chiral symmetry is conserved.

In the conformal region, we measure both the mass \tilde{m} and the exponent of power-modified Yukawa-type decay. From the tables, we see that the \tilde{m}_V agrees with \tilde{m}_π with almost one standard deviation, while α_V is in general systematically larger than α_{PS} , albeit errors are large. Theoretically, it is possible that the anomalous dimension in the vector channel is different from the PS channel. To conclude the difference, we need many more high-statistics data.

G. $N_f = 18$

It is believed that when $N_f \geq 17$ the theory is a free theory in the continuum limit since the point $g_0 = 0$ and $m_0 = 0$ is an IR fixed point in this case. The simulations are performed both at heavy quarks, $K = 0.100$ ($m_q = 1.00$), and light quarks, $K = 0.125$ ($m_q = 0.027$). The result for heavy quarks is in complete agreement with the free case with $m_q = 1.00$, as shown in Fig. 47. The result for light quarks is also in good agreement with the free case. However, the behavior in the IR limit is slightly different.

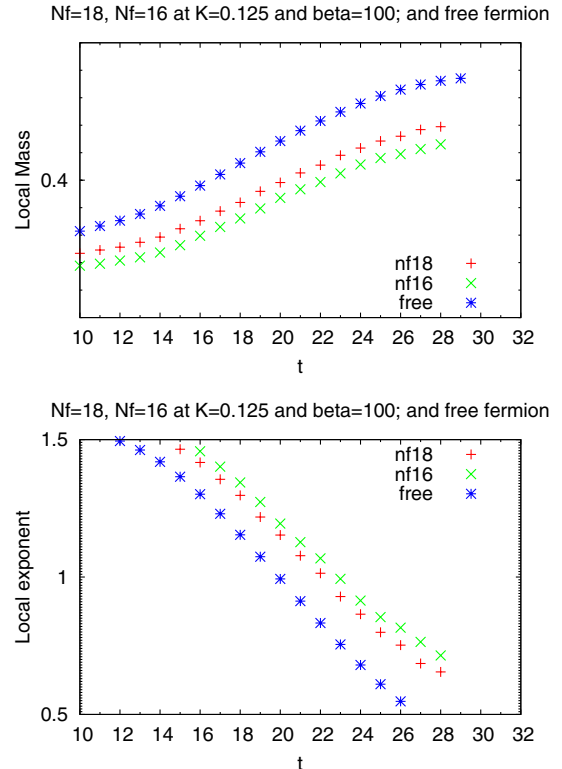


FIG. 34 (color online). The local mass $m(t)$ and the exponent $\alpha(t)$ in the large t region for $N_f = 16, 18$ and the free case.

In Fig. 34, the local mass $m(t)$ and the local exponent $\alpha(t)$ enlarged at large t for $N_f = 18$ and $N_f = 16$ (at $K = 0.125$ and $\beta = 10.0$) together with the free fermion $m_q = 0.01$ are shown. The $N_f = 18$ case is closer to the free case, but there is still a gap between the $N_f = 18$ case and the free case. Although it would be intriguing to take the continuum limit of the $N_f = 18$ case, since the direction of the RG flow is opposite to the $N_f \leq 16$, it is out of the scope of this article. The results obtained so far are consistent with the common lore that the theory must become a free theory in the continuum limit.

H. Finite-size scaling

Since our discussions on the conformal field theory with an IR cutoff crucially depend on the existence of the finite lattice, in particular at zero temperature, it would be important to ask if our theoretical as well as numerical results are consistent with the finite-size scaling argument based on the RG analysis. We would like to stress that the finite-size scaling is based on very general properties of the RG, and it is applicable to any vacua irrespective of if the theory is in the conformal region or in the confining region. Some of the implicit assumptions, however, may be valid only when the theory stays for a sufficiently long time close to the fixed point. Such an assumption does not necessarily hold in the confining region, as we discuss in the following.

Let us consider the conformal QCD in a finite box with the size L . The simple scaling argument (see, e.g., [32,33,35–38] and the references therein for the argument as well as attempts for its verification in numerical simulations) tells that any dimensionful quantity such as m_{PS} (or \tilde{m}_{PS}) is a function of the scaling variable $x = L^{1+\gamma^*} m_q$ as

$$L \cdot m_{PS} = f(x). \quad (14)$$

In the thermodynamics limit $x \rightarrow \infty$, it was claimed [35] that the scaling function should behave as $f(x) \sim x^{\frac{1}{1+\gamma^*}}$ under the assumption that the RG flow stays for a sufficiently long time close to the fixed point. Note that this assumption is not valid if we take $m_q \rightarrow \infty$ with a fixed L , so the naive limit in the confining region may not be used to determine the mass anomalous dimension. This scaling relation also assumes that the continuum limit $a \rightarrow 0$ is implicitly taken. Indeed, we have seen that m_q dependence on m_{PS} in the confining region in the large m_q limit (for any N_f) does not satisfy this scaling behavior with nontrivial γ^* corresponding to the fixed point. We stress that this is not in contradiction with the underlying IR fixed point in any means. It is rather due to the fact that the large m_q limit is not ideal to probe the underlying IR fixed point from the scaling behavior of $f(x)$ with the fixed lattice size.

On the other hand, our numerical results in the conformal region predict the behavior of the scaling function in the opposite limit ($x \sim 0$):

$$f(x) = c_0 + g(x), \quad (15)$$

where $g(0) = 0$. The power ansatz $g(x) \sim x^\alpha$ is typically employed in the literature (e.g., [51,52]). The function $f(x)$ from our numerical simulations can be read from Figs. 22, 27, 30, and 31, where we have also discussed some qualitative features of the shape of $f(x)$ in the main text. One remark here is that the contribution from the constant c_0 dominates in the conformal region (as also noted in [51,52] for the small x region in $N_f = 12$). A theoretical explanation of this constant is given by studying the effective potential for the Polyakov loops, where we have shown that when $\beta \rightarrow \infty$, the constant c_0 is determined by the nontrivial condensation of the Polyakov loops. In addition, the presence of the first-order transition tells us that $f(x)$ is discontinuous as a function of x . Indeed, we have shown that the value of c_0 is affected by the choice of the vacuum. Apart from this, our results have no discrepancy with the existing finite-size scaling argument as they should. This is because the finite-size scaling is just a consequence of the RG with the fixed point. Note that the crucial assumption that the RG flow stays close to the fixed point is much more reliable in the conformal region than in the confining region. It remains an open problem to determine the large x behavior within the conformal region to see the scaling behavior of $f(x)$.

While our results give a prediction of the scaling function $f(x)$ for small x as long as our assumption that the RG flow stays for a sufficiently long time close to the fixed point is valid, we have not directly checked the L (in)dependence of the scaling function numerically except for the trivial limit of $\beta \rightarrow \infty$ because our numerical analysis is done with the fixed lattice size. It would be interesting to study the finite-size scaling function $f(x)$ systematically under the change of the lattice size to see if further evidence for the fixed point may be obtained.

As we have already mentioned at the end of Sec. II C, the continuum limit is subtle in the conformal QCD. We would like to propose to take the limit while keeping the condition

$$L \cdot m_{PS} < c \quad (16)$$

in order to be within the conformal region, as we have demonstrated for a fixed L . This condition is equivalent to evaluating $f(x)$ below the discontinuity. If we would like to take the limit in the confining region, we have to pay extra care to ensure that the RG flow stays close to the fixed point for a sufficiently long time. It is, however, beyond our scope of this paper to take the continuum limit, and we leave it for the future study.

VIII. BOUNDARY CONDITIONS AND THE STRUCTURE OF THE VACUUM

We have shown that in the case of periodic boundary conditions in spatial directions for fermions, the lowest effective energy states (the vacuum) in the one-loop approximation are the eightfold states $(1/3, 1/3, 1/3)$. On the other hand, the $(0,0,0)$ state is locally unstable when m_q is light, whereas it becomes locally stable as the m_q becomes heavy: $m_q = 0.15 \sim 0.25$.

The lowest energy state depends on the boundary conditions. We discuss the other relevant cases here.

In the case of antiperiodic boundary conditions in spatial directions, we are able to show that the $(0,0,0)$ state is the lowest energy state by performing the one-loop computation of the vacuum energy at zero temperature, as in the case of periodic boundary conditions.

We compare, in the cases of antiperiodic boundary conditions in spatial directions, analytic results for free Wilson fermions with $m_q = 0.01$ on the left panel of Fig. 46 with the results of simulations shown on the right panel for $N_f = 2$ at $\beta = 100.0$ with $K = 0.125$ ($m_q = 0.03$). Both of them show the characteristic pattern for the vacuum $(0,0,0)$, and they are in good agreement with each other. However, when one closely looks at the details, one notices that the exponent of the free case is smaller and the mass is larger than those of $N_f = 2$ case at large t . The situation is similar to the periodic case. The difference is due to nonperturbative effects.

The value of the mass $m(t)$ at large t should be compared with the lowest Matsubara frequency $2\sqrt{3}\pi/L = 0.680115$, which is larger than that of the periodic boundary conditions with twisted vacuum $2\sqrt{3}2\pi/(3L) = 0.45345$. The result for the $N_f = 2$ case $m(t)$ at large t is $m(t) = 0.634(2)$, which is close to 0.680.

We make short runs of simulations for other cases such as $N_f = 7, 8, 12, 16$ and $N_f = 2$ at $\beta = 6.5, 7.0, 8.0$. The most characteristic shared feature for them is that $m(t)$ becomes larger than those for periodic boundary conditions. Therefore, it is more difficult to investigate the conformal properties.

We perform a long run for $N_f = 7$ at $K = 0.1446$ and 0.1459. We obtain $m_{PS} = 0.5462(41)$ at $K = 0.1446$ and $m_{PS} = 0.5479(19)$ at $K = 0.1459$, with the fit range [28:31]. We do not see the power-law-corrected Yukawa-type decay since we think $m_{PS} = 0.5462(41)$ and 0.5479(19) are larger than the critical mass.

When antiperiodic and periodic boundary conditions are mixed, the Polyakov loop in the lowest energy state takes either $\exp(\pm i2\pi/3)$ or 1 depending on the boundary conditions in that direction.

In the limit $L \rightarrow \infty$, physical quantities will not depend on boundary conditions. Therefore, it is natural to conjecture that the true vacuum in the limit $L \rightarrow \infty$ is a weighted superposition of 27-fold local minima with four different species.

When β is large on a finite lattice with a medium size, the transition between two different local minima is hard to occur. However, as the lattice size is increased, the barrier between the vacua is decreased as $O(1/L)$. Therefore, although it takes time, it will eventually reach an equilibrium state.

In order to obtain a physical quantity in the continuum limit, we first perform simulations on a large lattice for a long period in such a way that the transition among different vacua occurs with a nonnegligible probability. We repeat the same computation by changing the lattice size. Finally, we fit the data with a constant plus a $1/L$ term and extract the physical quantity in the continuum limit.

Ideally, we would like to repeat a similar procedure with antiperiodic boundary conditions and get the physical quantity in the continuum limit. Then we should be able to check that the result does not depend on the boundary conditions. Probably this requires a lot of CPU times.

We need certainly more works to investigate the vacuum and conformal properties in the limit $L \rightarrow \infty$.

IX. UNPARTICLE MODELS

In order to understand the relation between the power exponent obtained in the Yukawa-type power-decaying form of the propagators and the mass anomalous dimensions, we need a concrete theoretical model that realizes the effects of an IR cutoff in (strongly coupled) conformal field theories. For this purpose, let us discuss a meson unparticle model, which is motivated by the soft-wall model in AdS/CFT correspondence [74] (for details, see Appendix C). We regard the unparticle models as effective descriptions of the conformal field theory with an IR cutoff in the continuum limit.

The soft-wall model predicts the form of the propagator in the momentum space as

$$\langle O(p)O(-p) \rangle = \frac{1}{(p^2 + m^2)^{1-\alpha}}. \quad (17)$$

The spectrum in the momentum representation has a cut instead of a pole. As we see in Appendix C, this ansatz of the propagator explains the power-law-corrected Yukawa-type form of the propagator in position space.

When $mt \ll 1$, the mass anomalous dimension and the power are related by $\alpha(t) = 3 - 2\gamma^*$. This is model independent and universal. On the other hand, when $mt \gg 1$, the computation in Appendix C shows that $\alpha(t) = 2 - \gamma^*$ for $t \gg \Lambda_{\text{CFT}}^{-1}$. Here Λ_{CFT} is the scale under which the coupling constant does not effectively run. When β_0 is sufficiently close to the fixed-point value, it is very close to the UV cutoff.

A possible scenario for $T/T_c \gg 1$ is to treat $\bar{\psi}\gamma_5\psi(x)$ as the nonbound state of unfermions. The soft-wall model

predicts the form of the propagator with scale dimension Δ_f in the momentum space as

$$\langle \Psi(p) \bar{\Psi}(-p) \rangle = (p^\mu \gamma_\mu + m) \frac{1}{(p^2 + m^2)^{\frac{3}{2} - \Delta_f}}. \quad (18)$$

As shown in Appendix C, one can compute the power corrections for the meson operators out of the fermion unparticle model. When $mt \ll 1$, $\alpha(t) = 3 - 2\gamma^*$. On the other hand, when $mt \gg 1$, $\alpha(t) = 1.5 - \gamma^*$ for $t \gg \Lambda_{\text{CFT}}^{-1}$.

X. CORRESPONDENCE BETWEEN CONFORMAL QCD AND HIGH-TEMPERATURE QCD

As a highlight of our discussions on the conformal field theories with an IR cutoff, we propose the direct correspondence between conformal QCD and high-temperature QCD in the conformal region. This enables us to understand the boundary of the conformal region and the computation of the mass anomalous dimension.

A. Similarity of the beta function

We first observe the similarity of the beta functions on the N_f dependence of the conformal QCD and the T/T_c dependence of high-temperature QCD, as shown in Fig. 35: When $N_f = N_f^c$ and $T/T_c \sim 1$, the beta function changes the sign at large g , as N_f and T/T_c increase, and the point of the sign change moves toward smaller g . When $N_f = 16$ and $T/T_c \gg 1$, it changes signs at very small g .

This fact is only suggestive for the similarity on the dynamics of the two sets of conformal theories with an IR cutoff. We argue that the similarity is more than that.

B. Correspondence on the t dependence of propagators

Now let us compare the exponent $\alpha(t)$ and the local mass $m(t)$ between conformal QCD and high-temperature QCD. The form of $\alpha(t)$ changes with the temperature T/T_c in high-temperature QCD or the number of flavor N_f in conformal QCD. On the other hand, the t dependence of $m(t)$ does not depend very much on them.

We show the two sets of $\alpha(t)$ side by side in Fig. 36, the conformal QCD data on the right panel and the high-temperature QCD data on the left panel in order to compare them directly. We take a quark mass that is not close to the boundaries of the conformal region in order to avoid boundary effects. We also check in several cases that the quark mass dependence is weak in the case that the quark mass is well between the boundaries. We do not make a fine tuning to state the correspondence.

We observe that the correspondence on the t dependence of $\alpha(t)$ between the two sets of data is excellent with each of the following pairs: $T \sim 2T_c$ and $N_f = 7$, $T \sim 4T_c$ and $N_f = 8$, $T \sim 16T_c$ and $N_f = 12$, and $T \sim 256T_c$ and $N_f = 16$.

Thus we plot schematically the correspondence between conformal QCD and high-temperature QCD, as in Fig. 35. The correspondence is a powerful tool to investigate the properties of conformal theories. The T/T_c is a continuous variable, while the N_f is a discrete variable. Therefore, we are able to use the information in high-temperature QCD to understand the properties of conformal QCD.

On the other hand, for conformal QCD, we are able to extend the region to $N_f \geq 17$ out of the conformal window. This extension is useful to investigate the limiting behavior of high-temperature QCD in the limit $T/T_c \rightarrow \infty$ since there is no state for $T/T_c > \infty$.

The correspondence we propose can be supported by the following RG argument. When the quark mass m_q is sufficiently small, the RG equation for our propagator is governed by just one number, the mass anomalous dimension γ^* , so whenever the mass anomalous dimension is the same, they must satisfy the same equation (e.g., [35]), which gives a heuristic support to how the correspondence works. The implicit assumption here is that they are in the same vacuum. Due to this, the correspondence does not necessarily work outside of the conformal region because the confining vacuum and the deconfining vacuum are different.

While this agreement of the RG equation is a necessary kinematical condition for the correspondence, we would

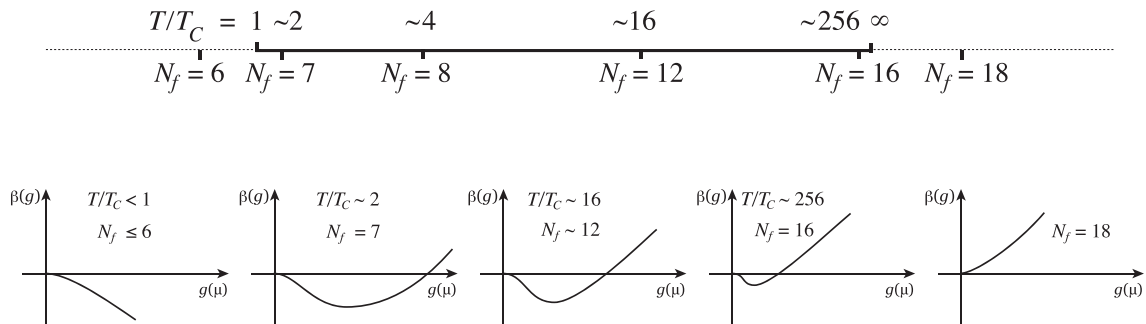


FIG. 35. The correspondence between conformal QCD and high-temperature QCD in terms of the beta function. The horizontal line on the top represents the correspondence between the number of flavor N_f and the temperature T/T_c .

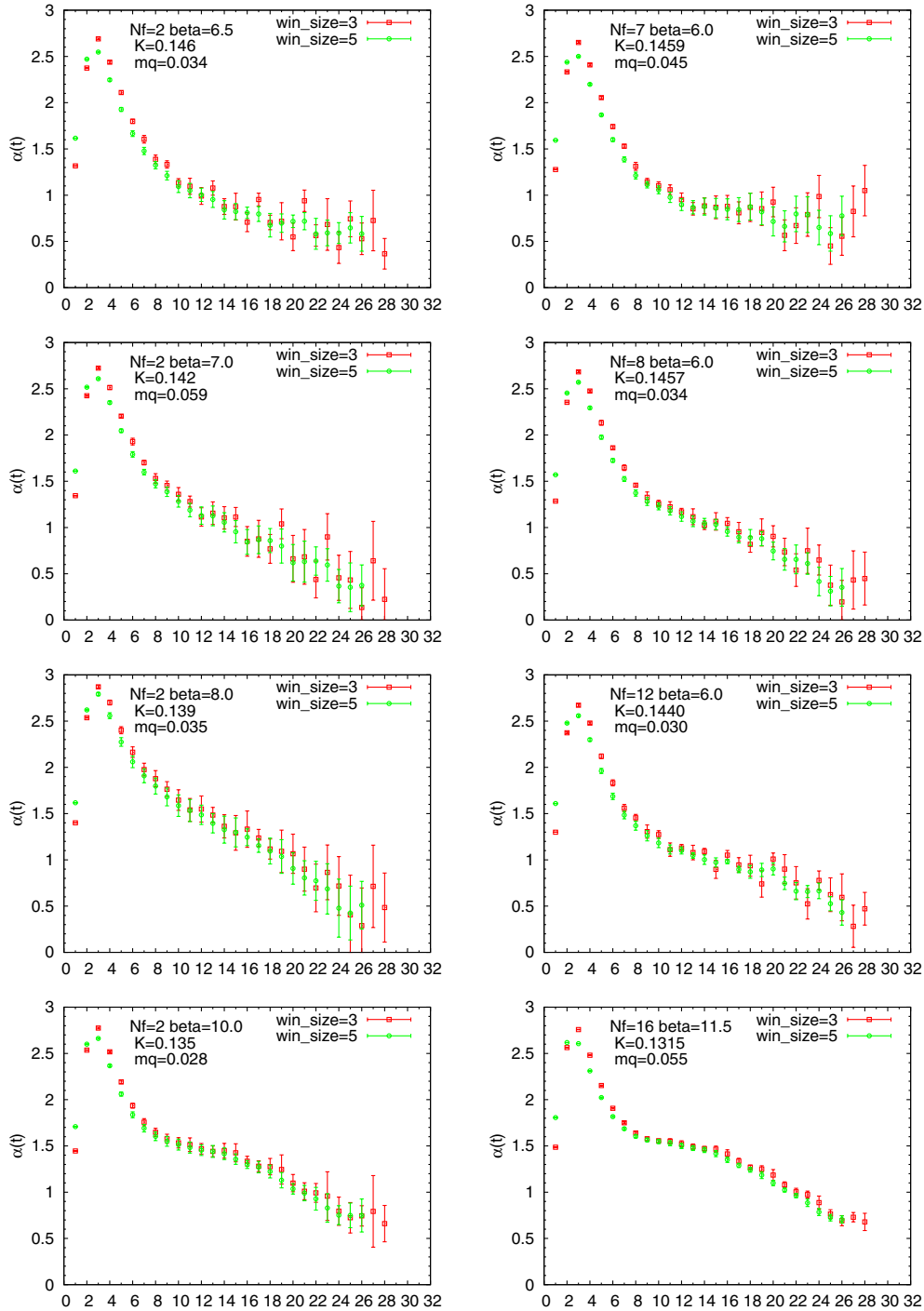


FIG. 36 (color online). The correspondence of the local exponent $\alpha(t)$ for high-temperature QCD (left) and for conformal QCD (right).

like to stress that our correspondence tells us more than that. The agreement of the detailed form of the propagator (even with the finite size corrections) suggests the underlying universal dynamics beyond what conformal invariance dictates.

In order to make the underlying dynamics clear, in addition to the vacuum structure, we need a comparison with the unparticle models we proposed in Sec. IX.

C. $N_f = 7$ and $T/T_c \simeq 2$

We note that both in the $N_f = 7$ case of conformal QCD and at $T \sim 2T_c$ in high-temperature QCD, we have a plateau in the $\alpha(t)$ at large t ($15 \leq t \leq 31$).

This behavior of the propagator at large t implies Eq. (17) in the momentum representation. Thus, in both cases, the IR behavior of the state is well described by the meson unparticle model.

The value of $\alpha(t)$ at plateau ($t = 15 \sim 31$) is 0.8(1) for $K = 0.1452$ and $K = 0.1459$ in the $N_f = 7$ case. We have taken, to avoid boundary effects, the quark masses middle among those within the conformal region.

Applying the formula $\alpha(t) = 2 - \gamma^*$, we have $\gamma^* = 1.2(1)$. Although this value should be refined in the future by taking the continuum limit, this value implies that the anomalous mass dimension is of order unity.

D. $N_f = 16$ and $T/T_c \simeq 256$

As discussed in Sec. V, the vacuum of $N_f = 16$ at $\beta = 11.5$ (and $N_f = 2$ at $T/T_c \simeq 100.0$) is close to the twisted $Z(3)$ vacuum, but is different in the magnitude of the Polyakov loop taking $|P| \simeq 0.2$. It is tempting to identify the corresponding effective theory as the fermion unparticle model in the continuum limit. The smallness of the deviation from the free fermion certainly suggests that the model cannot be a meson unparticle.

It is important to note that the unparticle models are effective descriptions and do not directly encode the vacuum structure nor boundary conditions. It is interesting to question whether the fermion unparticle model with twisted boundary condition might explain this difference. However, it turns out to be hard to resolve the difference by the fermion unparticle model within the lattice size that we have studied.

Comparing the previous subsection with this subsection, we note the effect of the finite lattice size is smaller for the meson unparticle models due to the pointlike nature of the bound states, so we expect that the meson unparticle models near $N_f = N_f^c$ are more trustworthy in comparison with the lattice simulation.

XI. TWO SETS OF CONFORMAL THEORIES WITH AN IR CUTOFF

Now we have two sets of conformal theories with an IR cutoff: (1) $7 \leq N_f \leq 16$ in conformal QCD and (2) $1 \leq T/T_c \leq \infty$ in high-temperature QCD.

We have verified on a finite lattice $16^3 \times 64$ that the two sets satisfy the properties of conformal theories with an IR cutoff.

We have pointed out from our theoretical analysis based on the RG flow and our numerical simulations that there is a precise correspondence between conformal QCD and high-temperature QCD. The correspondence between the two sets is realized between a continuous parameter T/T_c and a discrete parameter N_f as depicted in Fig. 35:

- (i) $T \sim 2T_c$ and $N_f = 7$,
- (ii) $T \sim 4T_c$ and $N_f = 8$,
- (iii) $T \sim 16T_c$ and $N_f = 12$,
- (iv) $T \sim 64T_c$ and $N_f = 16$.

One boundary is close to meson states, and the other is close to free quark states.

Now, we have systematic understanding of high-temperature QCD for $1 \leq T/T_c \leq \infty$. In the limit $T \rightarrow T_c$, the ground state becomes a meson state. As the T/T_c increases, a meson becomes a meson unparticle. The meson unparticle with α in Eq. (17) smoothly changes the state with α . When $N_f = 2$, the transition at $T = T_c$ is second order (or weak first order), and therefore, it is expected that the α changes smoothly at $T \rightarrow T_c$. As $T \rightarrow T_c$, $\alpha \rightarrow 0$. Note that $\alpha = 0$ means $\gamma^* = 2$, from the formula $\alpha = 2 - \gamma^*$ (see Appendix C for a debate on the critical value for confinement). We check in the future the smoothness for other cases $N_f = 3 \sim 6$.

The state gradually changes following T/T_c through nonmeson unparticle states toward a free fermion anti-fermion pair state in the twisted $Z(3)$ vacuum. Here, of course, $\gamma^* = 0.0$.

Therefore, at $T/T_c \rightarrow \infty$, $\gamma^* = 0.0$, and at $T/T_c = 1$, $\gamma^* = 2.0$. It is natural to assume that γ^* is a monotonous function of T/T_c . We may regard the set of high-temperature QCD for $1 \leq T/T_c \leq \infty$ as a conformal window. The window from $T/T_c = 1$ to $T/T_c \rightarrow \infty$ is complete in the sense that it covers $0.0 \leq \gamma^* \leq 2.0$.

Corresponding to this viewpoint, we also have reached systematic understanding of the range of conformal windows $7 \leq N_f \leq 16$ in conformal QCD. Similarly, a meson at $N_f = 6$ becomes an unparticle at $N_f = 7$, changes through nonmeson unparticle states, and finally reaches close to a free fermion state at $N_f = 16$. When $N_f \geq 17$, it is a free quark state due to the loss of the asymptotic freedom.

It is natural to assume that the mass anomalous dimension γ^* takes a monotonously increasing discrete value between 0.0 and 2.0 from $N_f = 16$ and $N_f = 7$.

Since high-temperature QCD covers $0.0 \leq \gamma^* \leq 2.0$ and conformal QCD takes discrete values of γ^* between 0.0 and 2.0, the correspondence is realized between a continuous parameter T/T_c and a discrete parameter N_f . This is the precise origin of the correspondence between the two observed in the local analysis of propagators.

The plateau at $15 \leq t \leq 31$ in $\alpha(t)$ for $T \sim 2T_c$ disappears as the temperature increases to $T \sim 4T_c$. Translating this fact into conformal QCD is that the plateau in $\alpha(t)$ at $15 \leq t \leq 31$ observed as the IR behavior of $N_f = 7$ disappears for $N_f = 8$.

We stress that the IR behavior of the $N_f = 7$ reported in this paper is numerically verified independently from the assumption of the conformal window. However, solely from this fact we are not able to conclude that $N_f = 7$ is within the conformal window. It implies the $N_f = 7$ is either in the conformal window or in high-temperature QCD. If the $N_f = 7$ would be in high-temperature QCD, there should be a chiral phase transition point, and there should be a confining region below the critical point β^c . Nevertheless, since there is no confining region on the massless line for actions composed of the Wilson fermion

action and any type of gauge actions, it is unlikely that $N_f = 7$ belongs to high-temperature QCD. This is the same logic as in Ref. [4].

Another viewpoint is this: If the case $N_f = 7$ were outside of the conformal window, it would imply that there is no corresponding state to $T \sim 2T_c$, which is closest state to a meson in our proposed correspondence. Logically, this possibility cannot be excluded. However, we believe that the physical picture for the case where $N_f = 7$ is within the conformal window is more appealing.

Thus, our analyses presented in this article are consistent with our conjecture $N_f^c = 7$. We would like to conclude the conjecture $N_f^c = 7$ by investigating directly the existence of the IR point in the future study.

XII. SUMMARY AND DISCUSSION

Motivated by RG argument, we theoretically conjectured that conformal QCD with an IR cutoff and high-temperature QCD show the common feature as the conformal theories with an IR cutoff: In the conformal region, where the quark mass is smaller than the critical value, a propagator $G(t)$ of a meson behaves at large t as a power-law corrected Yukawa-type decaying form [Eq. (9)] instead of the exponential decaying form observed in the confining region and deconfining region:

$$G_H(t) = \tilde{c}_H \frac{\exp(-\tilde{m}_H t)}{t^{\alpha_H}}.$$

We note that the behavior Eq. (9) is proposed based on the AdS/CFT correspondence with a soft-wall cutoff in the literature [74]. The meson propagator in the momentum space has a cut instead of a pole: $G_H(p) = 1/(p^2 + \tilde{m}_H^2)^{1-\alpha_H}$. The propagator in the position space (after space integration) takes the form Eq. (9) in the limit $t\tilde{m}_H \gg 1$.

In the continuum limit with $L = \infty$ (i.e., $\Lambda_{\text{IR}} = 0$), the propagator on the massless quark line takes the form [Eq. (10)]:

$$G_H(t) = \tilde{c} \frac{1}{t^{\alpha_H}}.$$

If we take the coupling constant $g_0 = g^*$ at the UV cutoff, α_H takes a constant value, and the RG equation demands [Eq. (11)]:

$$\alpha_H = 3 - 2\gamma^*,$$

for the PS channel with γ^* being the anomalous mass dimension γ at $g = g^*$. The theory is scale invariant (and shown to be conformal invariant within perturbation theory [68]; see also, e.g., [70] and the references therein from the AdS/CFT approach). When $0 \leq g_0 < g^*$, α_H depends slowly on t as a solution of the RG equation. In the IR limit $t \rightarrow \infty$, we must retain $\alpha_H(t) \rightarrow 3 - 2\gamma^*$.

Clarifying the vacuum structure and properties of temporal propagators in QCD with N_f flavors in fundamental representation, we have verified numerically on a lattice $16^3 \times 64$ the following: The conformal region exists together with the confining region and the deconfining region in the phase structure parametrized by β and K both in conformal QCD and in high-temperature QCD. The structure of the vacuum of the conformal region is characterized by the Polyakov loops in spatial directions, and the vacuum is the nontrivial $Z(3)$ twisted vacuum modified by nonperturbative effects. On the other hand, the vacua of the confining region and the deconfining region are the vacuum characterized by the zero-expectation values and the untwisted vacuum, respectively.

We find the transition from the conformal region to the deconfining region or the confining region is a transition between different vacua in our finite lattice simulations, and therefore, we conjecture that the transition is a first-order transition both in conformal QCD and in high-temperature QCD. However, we do not exclude the possibility that the phase transition becomes weaker or the discontinuities vanish as crossovers in the continuum/thermodynamic limit, whose confirmation need further studies.

The results for the existence of the conformal region mean that when the quark mass decreases from a heavy mass with fixed β , there is a first-order transition at the critical quark mass m_q^c , and after the critical mass, there is no singular point up to the zero mass. In particular, the hadronic mass smoothly changes from very small quark mass to the zero quark mass. This is realized indeed in the fact that Eq. (10) is consistent with the $\tilde{m}_H = 0$ limit of Eq. (9). Conversely, we can say that the smoothness from massive quark to the $m_q = 0$ limit and Eq. (10) at $m_q = 0$ requires the behavior Eq. (9) or a similar one. The exponential form is expected from the view point of physics. The form also corresponds to a cut in the momentum representation, as mentioned above. Furthermore, all numerical results are beautifully fitted with Eq. (9). From all of these, we conclude that the ansatz based on the RG argument is to the point.

It should be noted that when Λ_{IR} is finite, even at the massless quark, m_H is not zero in general. Therefore, the propagator behaves as Eq. (9) at large t . In the weakly coupled region (i.e., high temperature or $N_f \sim 16$), we have shown that the main source of the m_H is due to the nontrivial Polyakov loop condensate with some nonperturbative contributions.

We argue from our theoretical analysis based on the RG flow and our numerical simulations that there is a precise correspondence between conformal QCD and high-temperature QCD in the temporal propagators under the change of the parameters N_f and T/T_c with the same anomalous mass dimension.

Thereby we clarify the global structure of conformal theories with an IR cutoff on the finite lattice. The

conformal window from $T/T_c = 1$ to $T/T_c \rightarrow \infty$ is complete in the sense that it covers $0.0 \leq \gamma^* \leq 2.0$, while the conformal window from $N_f = 16$ to $N_f = 7$ takes a discrete value of γ^* between 0.0 and 2.0. The one boundary of the two sets is close to meson states, and the other is close to free quark states. This observation turns out to be very useful to reveal the characteristics of each theory.

In particular, we find the correspondence between conformal QCD with $N_f = 7$ and high-temperature QCD with $N_f = 2$ at $T \sim 2T_c$ being in close relation to a meson unparticle model. From this, we estimate the anomalous mass dimension $\gamma^* = 1.2(1)$ for $N_f = 7$. We also show that the asymptotic state in the limit $T/T_c \rightarrow \infty$ is a free quark state in the $Z(3)$ twisted vacuum. The approach to a free quark state is very slow; even at $T/T_c \sim 10^5$, the state is affected by nonperturbative effects.

We have verified our conjectures on the finite lattice $16^3 \times 64$. Since our conjectures are based on the general RG argument, we expect that the conjectures are also satisfied on a larger lattice. This will be studied in future research.

For now, let us theoretically speculate about what will happen in the continuum limit of the conformal QCD and the high-temperature QCD separately. In the case of conformal QCD, the vacuum structure of the conformal region is the nontrivial $Z(3)$ twisted vacuum modified by nonperturbative effects, as far as the lattice size is not very large and the periodic boundary conditions are imposed for fermions in spatial directions. As lattice size N increases, the transition to other vacua occurs since the energy difference decreases as $1/N$. Finally, in the limit $N \rightarrow \infty$, we are able to obtain physical quantities in the continuum theory.

The phase diagrams that we expect in the continuum limit are shown in Fig. 2 (left, for $\Lambda_{\text{IR}} = 0$, and right, for $\Lambda_{\text{IR}} = \text{finite}$). The shaded strong coupling region for small quark masses does not exist in the $\beta - m_q$ plane [57]. When the phase structure is described in terms of $\beta - K$, the corresponding phase belongs to a region for Wilson doubles. Therefore, when it is mapped to the $\beta - m_q$ planes, the region corresponding to the shaded one does not exist.

In high-temperature QCD, our conjecture is applicable to any QCD with compact space, even for the case $L < 1/T$. However, the thermodynamical limit where $L = \infty$ is most relevant to our Universe.

In the thermodynamical limit at finite temperature, the exponential type decay Eq. (7) and the power-law-corrected Yukawa-type decay Eq. (9) are valid only approximately due to the finiteness of the t range. In order to obtain physical quantities in the thermodynamical limit, a more rigorous way would be to make the spectral decomposition of $G_H(t)$ by using, e.g., the maximal entropy method [75].

Let us consider what can be conjectured in the thermodynamical limit. The existence of an IR fixed point is

deduced from general argument. In addition, the temperature plays as an IR cutoff. Thus, we safely conjecture the conformal behavior in the conformal region in the continuum limit. However, as mentioned earlier, the vacuum structure is not necessarily the nontrivial $Z(3)$ twisted vacuum.

As one application of the conformal field theory with an IR cutoff in the thermodynamical limit, we have recently pointed out that the hyperscaling relation of physical observables may modify the existing argument about the order of the chiral phase transition in the $N_f = 2$ case. We recapitulate our argument in Appendix E.

We also believe that the very slow approach to a free quark state in the limit $T/T_c \rightarrow \infty$ on the $16^3 \times 64$ lattice is closely connected with the slow approach of the free energy to the Stefan-Boltzmann ideal gas limit. We would like to investigate the case where the aspect ratio N_t/N is small like $N_t/N = 1/4$ to conclude it in the future.

Based on the global structure of conformal theories with an IR cutoff on the finite lattice we have established in this article, we would like to investigate further the global structure of conformal theories in the continuum limit. In parallel, we would like to confront the nature from the viewpoint of the conformal theories. In particular, we believe in the scenario in which the model for the beyond standard model and the thermodynamics in the early Universe are described by the conformal theories (with an IR cutoff). In addition to these phenomenological applications, it is of our utmost priority to unambiguously establish the lower critical flavor number for the conformal window.

ACKNOWLEDGMENTS

We express our gratitude to T. Yanagida for providing an opportunity to start this collaboration. We also thank S. Aoki, H. Fukaya, E. Itou, K. Kanaya, T. Hatsuda, Y. Taniguchi, A. Ukawa, and N. Yamada for useful discussion. The calculations were performed on a Hitachi SR16000 at KEK under its Large-Scale Simulation Program and HA-PACS computer at CCS, University of Tsukuba under the HA-PACS Project for advanced interdisciplinary computational sciences by exascale computing technology. The work by Y. N. is supported by the World Premier International Research Center Initiative (WPI Initiative), MEXT, Japan.

APPENDIX A: OUR PREVIOUS WORKS

We started our projects at an early stage. In 1992 [76] we pointed out, employing the Wilson fermion, that for $N_f \geq 7$ there is a bulk transition in the strong coupling limit when the quark mass decreases from the large value and there is no massless state in the confining region.

To investigate the continuum limit of the theory, we then started the analysis of the phase structure. In particular, in

order to understand the phase for the region that corresponds to the small quark mass, we made the analysis of the phase structure for very large N_f up to 300. When N_f is very large, there is no bulk transition, and the massless quark line from $\beta = \infty$ smoothly moves to the point at $\beta = 0$. Decreasing N_f gradually, we conclude that the region that corresponds to the small quark mass corresponds to the region of doublers; that is, $K \geq 1/8$ at $\beta = \infty$ [77,78].

We further applied an MCRG method to investigate the RG flow (the last in [77]) in the $N_f = 12$ case. However, we noticed the well-known subtlety of MCRG method: Without very precise calculations, it depends on the observable to match and the number of RG transformation. Furthermore, because of the fact that the massless line for m_q hits a bulk transition around $\beta = 4.0$, it is difficult to determine the location of the IR fixed point. We only stated that the lower limit of the IR fixed point is $\beta \leq 5.0$.

In 2004, we published the results obtained so far in [4]. The salient facts that we found are the following: In the case $7 \leq N_f \leq 16$, the massless line originating from the UV fixed point hits a bulk transition at finite β . The massless line belongs to a deconfining region all through the line. In contrast, in the confining region at the strong coupling region there is no massless line. Thus, this confining region is irrelevant to the continuum theory.

On the other hand, in the case $N_f \leq 6$, there is a chiral transition on the massless quark line originating from the UV fixed point [63]. In the strong coupling region $\beta < \beta^c$ the massless line exists in the confining region. As the lattice size increases, the confining region enlarges, and finally, the confining region occupies the phase space as far as the coupling constant is kept larger than the chiral transition value.

From this analysis, we conjectured that the conformal window is $7 \leq N_F \leq 16$ for the $SU(3)$ and similarly $3 \leq N_F \leq 10$ for the $SU(2)$.

We make a side remark. For $N_f \leq 6$ at a strong coupling constant, the system is in the confining region even in the chiral limit. In particular, at $\beta = 0$ in the chiral limit, the pion mass should vanish within order a correction. We had assumed that the chiral point at $\beta = 0$ is $K = 0.25$, which is the quenched value. In fact, the chiral point K_c decreases as N_f increases, as pointed out in Ref. [79]. However, as stated clearly on the fourth page (right column, 17th line) in Ref. [79], ‘‘This fact is sufficient to leave the conclusions of Ref. [1] intact.’’

Here Ref. [1] corresponds to Ref. [4]. That is, the conclusions in Ref. [4] that there is a bulk transition and that there is no massless state in the strong region for $7 \leq N_F \leq 16$ are intact. All of the results and statements in Ref. [79] are consistent with our results. We just have to refine the results with the correct value for K_c .

Actually, new simulations at $\beta = 0$ for $N_f = 6$ QCD with Wilson fermions have been carried out in order to reinforce our conclusion [4,76] that the chiral limit is in the

confining region with the chiral symmetry spontaneously broken. The results are given below.

Please do not confuse the unrefereed conference report [80] with the refereed paper (Ref. [79]). In the unrefereed paper, there are some statements that are difficult for us to understand, such as the $N_f = 6$ case in the $SU(3)$ gauge theory with Wilson fermions is not in the confinement region because the pion mass at $K_c = 0.25$ is not zero. However, we believe that this is logically incorrect. Of course, one must measure the pion mass at the correct $K = 0.243(2)$. We have updated the calculation at $\beta = 0$ for $N_f = 6$ with the corrected value. The result clearly shows that the $N_f = 6$ case in the $SU(3)$ gauge theory with Wilson fermions is in the confining region, as usually expected.

They said that they do not support the claim that the critical flavor of the conformal window is 7, since we only made simulations on the lattice with $N_t = 4$. This is not correct. In fact, we made simulations on lattice with $N_t = 4, 6, 8$, and 18, as written in the paper [4].

1. Results at $\beta = 0$ for $N_f = 6$ QCD

The simulations are performed as similarly as possible to those in Ref. [79]. Configurations are generated on $8^3 \times 16$ lattices with periodic boundary conditions for both gauge and fermion fields in all directions (different from the boundary conditions in the other parts of this article) for $K = 0.2, 0.21, 0.22, 0.23, 0.235$, and 0.239. We employ the HMC algorithm. The run parameters are chosen in such a way that the acceptance is about 70%

Chiral extrapolations of m_π^2 and m_q are made with quadratic polynomial functions of $1/K$ (Fig. 37). Fits to m_π^2 and m_q with lightest four data points reproduce data well with reasonable χ^2/dof of 0.20 and 0.84, respectively. We find that m_π^2 and m_q vanish at almost the same K_c :

$$K_c(m_\pi^2) = 0.24326(7), \quad K_c(m_q) = 0.24301(13). \quad (\text{A1})$$

This strongly supports that the chiral symmetry is spontaneously broken in the critical limit.

In addition, we measure the number of iterations N_{inv} of the solver (BiCGStab-L2) necessary to invert the Dirac operator. As K increases, N_{inv} diverges toward K_c , as shown in Fig. 37. This implies that zero eigenvalues appear in the Dirac operator around K_c . We also have tried to simulate at $K = K_c(m_\pi^2)$ and found that the BiCGStab solver fails to converge. These observations are consistent with fact that the system is in the confining region at K_c .

We also estimate the chiral condensate using the Banks-Casher relation [81]. Following Ref. [82], we first calculate the effective chiral condensate

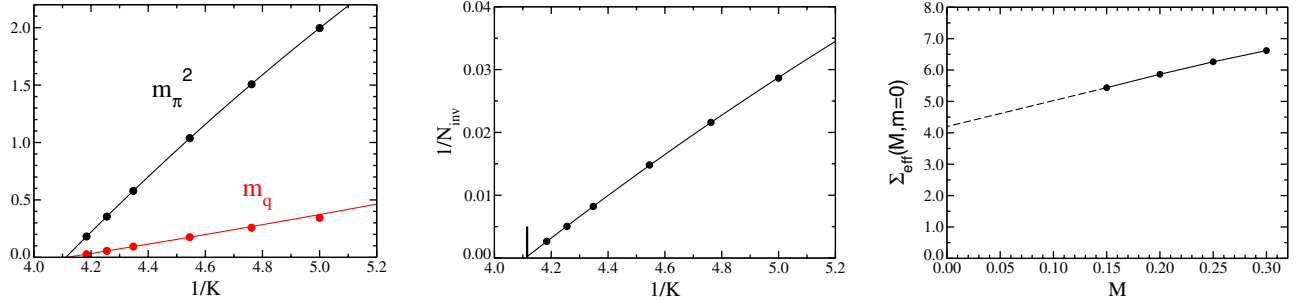


FIG. 37 (color online). (Left) m_π^2 and m_q vs $1/K$ and their chiral extrapolations. (Center) $1/N_{\text{inv}}$ vs $1/K$. The vertical line indicates $1/K_c(m_q)$. (Right) Effective chiral condensate at $m = 0$. Solid and dashed lines are a guide for the eye.

$$\Sigma_{\text{eff}}(M, m) = \frac{\pi}{2V} \sqrt{1 - \left(\frac{m}{M}\right)^2} \frac{\partial \nu(M, m)}{\partial M}, \quad (\text{A2})$$

where $\nu(M, m)$ is the average number of eigenmodes of the Hermitian Dirac operator $\gamma_5 D(m)$ with eigenvalues α in the range $-M < \alpha < M$, $m = (1/K - 1/K_c)/2$ and V is the lattice volume. We extrapolate $\Sigma_{\text{eff}}(M, m)$ to $m = 0$ and then to $M = 0$. As Fig. 37 shows, the chiral condensate takes a finite value in the limits of $m = 0$ and $M = 0$. This implies that chiral symmetry is spontaneously broken.

APPENDIX B: THE RUNNING COUPLING CONSTANT, THE BETA FUNCTION, AND THE TRACE ANOMALY AT FINITE TEMPERATURE

Let us consider the case where the renormalized quark mass is zero. Then the renormalized coupling constant is the only relevant variable in the theory. A running coupling constant $g(\mu; T)$ at temperature T can be defined as in the case of $T = 0$. The following discussion can be applied to any definition of the running coupling constant $g(\mu; T)$. Several ways to define the running coupling constant $g(\mu; T)$ are proposed in the literature (see, e.g., Ref. [83]). For example, in [83], a running coupling constant $g(r; T)$ is defined in terms of the quark antiquark free energy [Eq. (8) in [83]], where r , the distance between the static quark and antiquark, plays the running scale. An alternative way is the Wilson MCRG method to investigate the running coupling, fixing the temperature $T = 1/N_t a$ at the block transformation.

In the UV regime, since the theory is asymptotically free, the running coupling constant at finite T can be expressed as a power series of the running coupling constant at $T = 0$ as long as g is small [55]. The leading term is universal in the limit $g \rightarrow 0$.

However, in the IR region, $g(\mu; T)$ is quite different from $g(\mu; T = 0)$ since the IR cutoff Λ_{IR} in the time direction is T while the IR cutoff is zero at zero temperature. Furthermore, when $T/T_c > 1$, where the quark is not confined, the running coupling constant $g(\mu; T)$ cannot be arbitrarily large. This means that there is an IR fixed

point with nontrivial zero of the beta function when $T/T_c > 1$. This is the key observation in this article.

As long as $T < T_c$, the beta function is negative all through g . As the temperature is increased further, the form of the beta function will change, as in Fig. 4: (Left) When $T > T_c$ but $T \sim T_c$, the beta function changes the sign from negative to positive at large g ; as the temperature increases, the fixed point moves toward smaller g . (Right) When $T \gg T_c$, it changes the sign at small g .

Numerical results of the running coupling constant $g(r; T)$ shown in Fig. 2 in [83] are consistent with the above statement: The running coupling constant $g(r; T)$ increases as r increases up to some value and does not further increase more than that, and the maximum value decrease as T/T_c increases.

To avoid a possible confusion about the implication of vanishing of the beta function at finite temperature we have just introduced, we recall the relation between the trace anomaly of energy momentum tensor and the beta function with massless quarks:

$$\langle T_\mu^\mu \rangle_T = \mathcal{B}(g^{-2}(\mu)) \langle \text{Tr}(F_{\mu\nu}(\mu))^2 \rangle_T,$$

where $\mathcal{B}(g^{-2}(\mu))$ is the zero temperature beta function evaluated at $g = g(\mu)$ and $\langle \text{Tr}(F_{\mu\nu}(\mu))^2 \rangle_T$ is the field strength squared at temperature T renormalized at scale μ .

The derivation of the relation is a standard method that is probably well known. For the reader who is not familiar with it, a simple note is attached as a subsection below.

In Lorentz invariant zero-temperature field theories, the vanishing beta function means that the theory is scale invariant. In general, scale invariance and conformal invariance are two distinct concepts [68] because the requirement of scale invariance alone is weaker. In (perturbative) QCD, we can further show from Eq. (B8) that the trace anomaly vanishes and that the theory is conformal invariant in the chiral limit $m_q = 0$ (see, e.g., [70] for a review). In our situation, however, we claim that the beta function at finite temperatures vanishes, which does not imply vanishing of the trace of the energy-momentum tensor. Thus, the vanishing beta function at $T > T_c$ does not contradict with the nonvanishing of the difference of energy density and three times the pressure.

1. Note on the trace anomaly at finite temperature

The trace of the energy-momentum tensor $\epsilon - 3p$ is given by

$$\langle T_\mu^\mu \rangle_T = \epsilon - 3p = -T^5 \frac{\partial}{\partial T} (T^{-4} f), \quad (\text{B1})$$

where f is the free energy density given by $f = -\frac{T}{Z} \log Z$.

In massless QCD, the free energy density is given by

$$f = T^4 \bar{f}(T, \Lambda_0, g_0), \quad (\text{B2})$$

where \bar{f} is dimensionless. Λ_0 is the cutoff, and g_0 is the bare QCD coupling constant. (In lattice QCD, g_0 appears in the action, and Λ_0 and T are defined implicitly through $N_t/\Lambda_0 = T$, where N_t is the lattice size in the t direction.) Since \bar{f} is dimensionless, the dependence on T is only through T/Λ_0 , and we have the trivial identity

$$\Lambda_0 \frac{\partial}{\partial \Lambda_0} \bar{f} = -T \frac{\partial}{\partial T} \bar{f}. \quad (\text{B3})$$

On the other hand, renormalizability of QCD means that the cutoff Λ_0 and the bare coupling constant g_0 must be correlated so that the QCD scale Λ is fixed (irrespective of the temperature). This is governed by the RG equation

$$\Lambda_0 \frac{\partial}{\partial \Lambda_0} \bar{f} = \mathcal{B}(g_0^{-2}) \frac{\partial}{\partial g_0^{-2}} \bar{f}, \quad (\text{B4})$$

where $\mathcal{B}(g_0^{-2})$ is the zero-temperature QCD beta function at the cutoff scale. This is nothing but the statement that \bar{f} is a function of T/Λ . For this to hold, $\mathcal{B}(g_0^{-2})$ must be the zero-temperature QCD beta function.

Combining (B3) and (B4), we can rewrite the thermodynamic trace identity (B1) in QCD as

$$\langle T_\mu^\mu \rangle_T = \epsilon - 3p = -T^5 \frac{\partial}{\partial T} (T^{-4} f) = T^4 \mathcal{B}(g_0^{-2}) \frac{\partial}{\partial g_0^{-2}} \bar{f}. \quad (\text{B5})$$

At this point, we recall the (bare) Schwinger action principle

$$\begin{aligned} \frac{\partial}{\partial g_0^{-2}} \bar{f} &= -\frac{1}{T^3 V} \frac{\partial}{\partial g_0^{-2}} \log Z = \frac{1}{T^3 V} \left\langle \int d^4 x \text{Tr}(F_{\mu\nu}^0)^2 \right\rangle_T \\ &\sim T^{-4} \langle \text{Tr}(F_{\mu\nu}^0)^2 \rangle_T, \end{aligned} \quad (\text{B6})$$

where $\text{Tr}(F_{\mu\nu}^0)^2$ is the bare field strength squared defined at the cutoff scale. In the third line, the translational invariance was assumed. Thus, indeed, we arrive at the anomalous trace identity

$$\langle T_\mu^\mu \rangle_T = \mathcal{B}(g_0^{-2}) \langle \text{Tr}(F_{\mu\nu}^0)^2 \rangle_T. \quad (\text{B7})$$

We again emphasize that $\mathcal{B}(g_0^{-2})$ is the zero-temperature beta function.

The right-hand side of (B7) is RG invariant. Therefore, we may change the renormalization scale as we wish:

$$\langle T_\mu^\mu \rangle_T = \mathcal{B}(g^{-2}(\mu)) \langle \text{Tr}(F_{\mu\nu}(\mu))^2 \rangle_T, \quad (\text{B8})$$

where $\mathcal{B}(g^{-2}(\mu))$ is the zero-temperature beta function evaluated at $g = g(\mu)$ and $\langle \text{Tr}(F_{\mu\nu}(\mu))^2 \rangle_T$ is thermal expectation value of the field strength squared at temperature T , renormalized at scale μ . In particular, we may put $\mu = T$ in (B8). However, the $\mathcal{B}(g^{-2}(\mu = T))$ is different from the beta function at fixed temperature T ; $\mathcal{B}(g^{-2}(\mu; T))$ we have defined in this appendix and used for the fixed point for the high-temperature QCD.

APPENDIX C: MASSIVE UNPARTICLE CORRELATOR

In general, there is no universal way to construct the temporal propagators of mass-deformed conformal field theories. Some particular proposals are made in the literature of unparticles. They are motivated by the soft-wall model in AdS/CFT correspondence [74].

1. Mass-deformed scalar unparticle correlator

Let us discuss the mass-deformed scalar unparticle correlator $\langle O(x)O(0) \rangle$ with scale dimension Δ . The soft-wall model predicts the form in the momentum space as

$$\langle O(p)O(-p) \rangle = \frac{1}{(p^2 + m^2)^{2-\Delta}}. \quad (\text{C1})$$

In position space, the Fourier transform gives (up to constant)

$$\langle O(x)O(0) \rangle = \frac{K_\Delta(m|x|)}{|x|^\Delta}, \quad (\text{C2})$$

where $K_\Delta(z)$ is the modified Bessel function.

We would like to study the temporal propagator $\int d^3 \vec{x} \langle O(x)O(0) \rangle$. In the $mt \ll 1$ limit, we can approximate $K_\Delta(m|x|) \sim \frac{1}{(m|x|)^\Delta}$, so the integral gives

$$\int d^3 \vec{x} \langle O(x)O(0) \rangle \sim \int d^3 \vec{x} \frac{1}{(\sqrt{t^2 + \vec{x}^2})^{2\Delta}} \sim \frac{1}{t^{-3+2\Delta}}. \quad (\text{C3})$$

In terms of the anomalous dimension $\Delta = 3 - \gamma_m$, we have $\sim \frac{1}{t^{3-2\gamma_m}}$.

On the other hand, in the other extreme limit $mt \gg 1$, one can approximate $K_\Delta(m|x|) \sim \frac{e^{-m|x|}}{\sqrt{m|x|}}$ and integrate over \vec{x} by Gaussian integral by expanding $\sqrt{t^2 + \vec{x}^2} \sim t + \frac{\vec{x}^2}{2t}$. The result is

$$\int d^3\vec{x} \langle O(x)O(0) \rangle \sim \int d^3\vec{x} \frac{e^{-m\sqrt{t^2+\vec{x}^2}}}{(\sqrt{t^2+\vec{x}^2})^{\Delta+\frac{1}{2}}} \sim \frac{e^{-mt}}{t^{\Delta-1}}. \quad (\text{C4})$$

With the anomalous dimension $\Delta = 3 - \gamma_m$, we have $\frac{e^{-mt}}{t^{\Delta-\frac{1}{2}}}$. For a free scalar (= confined free hadrons), $\Delta = 1$, so the temporal propagator is $\sim e^{-mt}$ with no power as expected.

There is a debate whether $\gamma_m = 1$ [84] or $\gamma_m = 2$ [85] would be the critical value for confinement. The CFT unitarity argument suggests $\gamma_m = 2$, and it is realized here in the naive application of AdS/CFT. On the other hand, the ‘‘conformality lost’’ scenario cited above suggests $\gamma_m = 1$. It is possible that AdS/CFT accommodates the latter possibility because when $\Delta < 2$ we observe the ambiguities in the boundary condition in the soft-wall model.

2. Mass-deformed unfermion correlator

Another plausible scenario is to treat $\bar{\psi}\gamma_5\psi(x)$ as the nonbound state of unfermions. We see that it has a different $mt \gg 1$ asymptotic.

Let us discuss the mass-deformed unfermion correlator $\langle \bar{\Psi}(x)\bar{\Psi}(0) \rangle$ with scale dimension Δ_f . The soft-wall model predicts the form in the momentum space as

$$\langle \bar{\Psi}(p)\bar{\Psi}(-p) \rangle = (p^\mu\gamma_\mu + m) \frac{1}{(p^2 + m^2)^{\frac{3}{2}-\Delta_f}}. \quad (\text{C5})$$

In position space, we have

$$\langle \bar{\Psi}(x)\bar{\Psi}(0) \rangle = (\partial^\mu\gamma_\mu + m) \frac{K_{\Delta_f-\frac{1}{2}}(m|x|)}{|x|^{\Delta_f-\frac{1}{2}}}. \quad (\text{C6})$$

We would like to study $\int d^3\vec{x} \langle \bar{\Psi}\gamma_5\Psi(x)\bar{\Psi}\gamma_5\Psi(0) \rangle$. When $mt \ll 1$, we can neglect mass and obtain

$$\int d^3\vec{x} \langle \bar{\Psi}\gamma_5\Psi(x)\bar{\Psi}\gamma_5\Psi(0) \rangle \sim \int d^3\vec{x} \frac{1}{(\sqrt{t^2+\vec{x}^2})^{4\Delta_f}} \sim \frac{1}{t^{-3+4\Delta_f}}. \quad (\text{C7})$$

For free fermion, we have $\Delta_f = \frac{3}{2}$, and we obtain $\sim \frac{1}{t^3}$. If $\Delta_f = \frac{3}{2} - \frac{\gamma_m}{2}$ (so that $\bar{\Psi}\Psi$ has dimension $\Delta = 3 - \gamma_m$), we obtain $\sim \frac{1}{t^{3-2\gamma_m}}$, as in the scalar unparticle scenario. This is uniquely determined from the scale invariance.

On the other hand, in the other extreme limit $mt \gg 1$, one can approximate $K_{\Delta_f-\frac{1}{2}}(m|x|) \sim \frac{e^{-m|x|}}{\sqrt{m|x|}}$ and integrate over \vec{x} by the Gaussian integral by expanding $\sqrt{t^2+\vec{x}^2} \sim t + \frac{\vec{x}^2}{2t}$. The result is

$$\int d^3\vec{x} \langle \bar{\Psi}\gamma_5\Psi(x)\bar{\Psi}\gamma_5\Psi(0) \rangle \sim \int d^3\vec{x} \frac{e^{-m\sqrt{t^2+\vec{x}^2}}}{(\sqrt{t^2+\vec{x}^2})^{2\Delta_f}} \sim \frac{e^{-2mt}}{t^{2\Delta_f-\frac{3}{2}}}. \quad (\text{C8})$$

For free fermion, we have $\Delta_f = \frac{3}{2}$, and we obtain $\sim \frac{e^{-2mt}}{t^{\frac{3}{2}}}$ as expected. If $\Delta_f = \frac{3}{2} - \frac{\gamma_m}{2}$ due to the anomalous dimension (so that $\bar{\Psi}\Psi$ has dimension $\Delta = 3 - \gamma_m$), we obtain $\sim \frac{e^{-2mt}}{t^{\frac{3}{2}-\gamma_m}}$.

APPENDIX D: VACUUM

1. Periodic boundary condition

In general quantum field theories, the one-loop corrections to the zero-temperature vacuum energy are obtained by the sum over the (tree-level) on-shell energy

$$E = \sum_{\text{boson}} \frac{E_B}{2} - \sum_{\text{fermion}} \frac{E_F}{2}, \quad (\text{D1})$$

which is the same as computing the one-loop determinant $\pm \text{Tr} \log(D)$ in the path integral formulation. In the perturbative QCD at zero temperature on the lattice, tree-level degenerate vacua are characterized by the flat connection. On \mathbb{T}^3 , the most generic Polyakov loop [in fundamental rep of $SU(3)$] with a flat connection would be

$$\begin{aligned} U_x &= \exp\left(i \int A_x dx\right) = \text{diag}(e^{i2\pi a_x}, e^{i2\pi b_x}, e^{i2\pi c_x}) \\ U_y &= \exp\left(i \int A_y dy\right) = \text{diag}(e^{i2\pi a_y}, e^{i2\pi b_y}, e^{i2\pi c_y}) \\ U_z &= \exp\left(i \int A_z dz\right) = \text{diag}(e^{i2\pi a_z}, e^{i2\pi b_z}, e^{i2\pi c_z}), \end{aligned} \quad (\text{D2})$$

with $a_i + b_i + c_i \in \mathbb{Z}$ for $i = x, y, z$ up to gauge transformation. Note that $a_i = b_i = c_i = \frac{1}{3}, \frac{2}{3}$ gives a nontrivial center of the gauge group. Due to the one-loop corrections (D1), we obtain a nontrivial potential for (a_i, b_i, c_i) , which will determine the one-loop vacua.

For free Wilson fermion, the on-shell energy used in (D1) can be obtained by

$$\begin{aligned} k^2[k_x, k_y, k_z] &= (\sin^2(k_x) + \sin^2(k_y) \\ &\quad + \sin^2(k_z))m^2[k_x, k_y, k_z] \\ &= (m_q + 3 - \cos(k_x) - \cos(k_y) - \cos(k_z))^2, \end{aligned} \quad (\text{D3})$$

where m_q is the quark mass in the action, with the implicit form

$$\cosh(E[k_x, k_y, k_z]) = 1 + \frac{k^2 + m^2}{2(1+m)}. \quad (\text{D4})$$

The mode number k_i is determined from the boundary condition for the quarks.

If we do the singular gauge transformation, the Wilson line can be encoded in the twisted boundary condition for the quark field, which in turn changes momentum quantization in the summation. Therefore, the one-loop potential is obtained by

$$\begin{aligned}
 -V_F(a_i, b_i, c_i) = & \sum_{n_i=a_i}^{N-1+a_i} E[2\pi n_x/N, 2\pi n_y/N, 2\pi n_z/N] \\
 & + \sum_{n_i=b_i}^{N-1+b_i} E[2\pi n_x/N, 2\pi n_y/N, 2\pi n_z/N] \\
 & + \sum_{n_i=c_i}^{N-1+c_i} E[2\pi n_x/N, 2\pi n_y/N, 2\pi n_z/N].
 \end{aligned} \tag{D5}$$

The summation is taken for $n_i = a_i, a_i + 1, a_i + 2, \dots$. In the figure, we subtracted $V(0, 0, 0)$ since the absolute value is unphysical and thereby cancels the singular behavior in the massless quark limit.

One can compute the one-loop shift of energy (vacuum energy) of the gauge field by using the similar formula to the above by the momentum shift for the adjoint representation. For $SU(3)$, the adjoint representation (octet) of the gauge group obtains the shift of momentum in $(a-b), (b-a), (c-a), (a-c), (b-c), (c-b), 0, 0$:

$$\begin{aligned}
 +V_B(a_i, b_i, c_i) = & \sum_{n_i=a_i-b_i}^{N-1+a_i-b_i} E_G[2\pi n_x/N, 2\pi n_y/N, 2\pi n_z/N] \\
 & + (\text{seven other shifts in the momentum}).
 \end{aligned} \tag{D6}$$

Here $E_G(\vec{k})$ is determined from the pole of the propagator of the gauge fields:

$$\begin{aligned}
 & \sinh(E_G[k_x, k_y, k_z]/2) \\
 & = \sqrt{\sin^2(k_x/2) + \sin^2(k_y/2) + \sin^2(k_z/2)}.
 \end{aligned} \tag{D7}$$

Note that the one-loop energy is typically divergent both in IR and UV, but since we are only interested in the energy difference, if we subtract the energy by $V(0, 0, 0)$, the result is finite. The total effective energy in terms of (a_x, a_y) is shown in Fig. 12, and the contour of the effective energy is shown in Fig. 13. The minimums are at $(a_x = 1/3, a_y = 1/3)$ and $(a_x = 2/3, a_y = 2/3)$.

2. Antiperiodic boundary condition

We could instead use the antiperiodic boundary condition for the quarks. With the above Wilson line

introduced, the one-loop potential for quark fields becomes

$$\begin{aligned}
 -V_F(a_i, b_i, c_i) = & \sum_{n_i=a_i+1/2}^{N-1+a_i+1/2} E[2\pi n_x/N, 2\pi n_y/N, 2\pi n_z/N] \\
 & + \sum_{n_i=b_i+1/2}^{N-1+b_i+1/2} E[2\pi n_x/N, 2\pi n_y/N, 2\pi n_z/N] \\
 & + \sum_{n_i=c_i+1/2}^{N-1+c_i+1/2} E[2\pi n_x/N, 2\pi n_y/N, 2\pi n_z/N].
 \end{aligned} \tag{D8}$$

The one-loop potential from gauge field does not change. We realize that $a_i = b_i = c_i = 0$ is the minimum of the total potential.

APPENDIX E: THE ORDER OF THE CHIRAL PHASE TRANSITION IN $N_f = 2$ CASE

Here we discuss an implication of the existence of the IR fixed point in high-temperature QCD for the issue of the order of the chiral phase transition in the $N_f = 2$ case. Our key observation is the existence of an IR fixed point at $T > T_c$. We stress that the reasoning for the existence can be justified even in the thermodynamic limit.

Pisarski and Wilczek [86] mapped $N_f = 2$ QCD at high temperature to the three-dimensional sigma model and pointed out that if $U_A(1)$ symmetry is not recovered at the chiral transition temperature, the chiral phase transition of QCD in the $N_f = 2$ case is second order with exponents of the three-dimensional $O(4)$ sigma model.

For the Wilson quarks, it was shown that the chiral condensate satisfies remarkably the $O(4)$ scaling relation, with the RG improved gauge action and the Wilson quark action [87] and with the same gauge action and the clover-improved Wilson quark action [88] (see, for example, Fig. 6 in Ref. [87]). It was also shown for staggered quarks that the scaling relation is satisfied in the $N_f = 2 + 1$ case [89], extending the region from $T/T_c > 1$ adopted in [87] and [88] to the region including $T/T_c < 1$. These results imply that the transition is second order.

However, recently, it was shown that the expectation value of the chiral susceptibility $\chi_\pi - \chi_\sigma$ is zero [90] in thermodynamic limit when the $SU(2)$ chiral symmetry is recovered under the assumptions we discuss below. This is consistent with that fact that the $U_A(1)$ symmetry is recovered, which implies that the transition is first order according to [86]. Apparently the two conclusions are in contradiction.

Here we revisit this issue with the new insight of conformal field theories with an IR cutoff. It is assumed in Ref. [90] that the vacuum expectation value of mass-independent observable is an analytic function of m_q^2 , if the chiral symmetry is restored. However, in the conformal

region, the propagator of a meson behaves as Eq. (3), and the relation between the m_H and the m_q is given by the hyperscaling relation [35,73]

$$m_H = cm_q^{1/(1+\gamma)},$$

with γ^* the anomalous mass dimension. This anomalous scaling implies that m_H is not analytic in terms of m_q^2 and that the analyticity assumption does not hold. It should be

noted that the Ward-Takahashi identities in [90] are proved in the thermodynamic limit, and therefore, the numerical verification of the hyperscaling in the limit will be decisive. We stress, however, that the hyperscaling is theoretically derived with the condition of the existence of the IR fixed point and multiplicative renormalization of m_q . We believe that this violation of the analyticity assumption resolves the apparent discrepancy, as also mentioned in [90] as a viable possibility.

APPENDIX F: SUPPLEMENTARY FIGURES

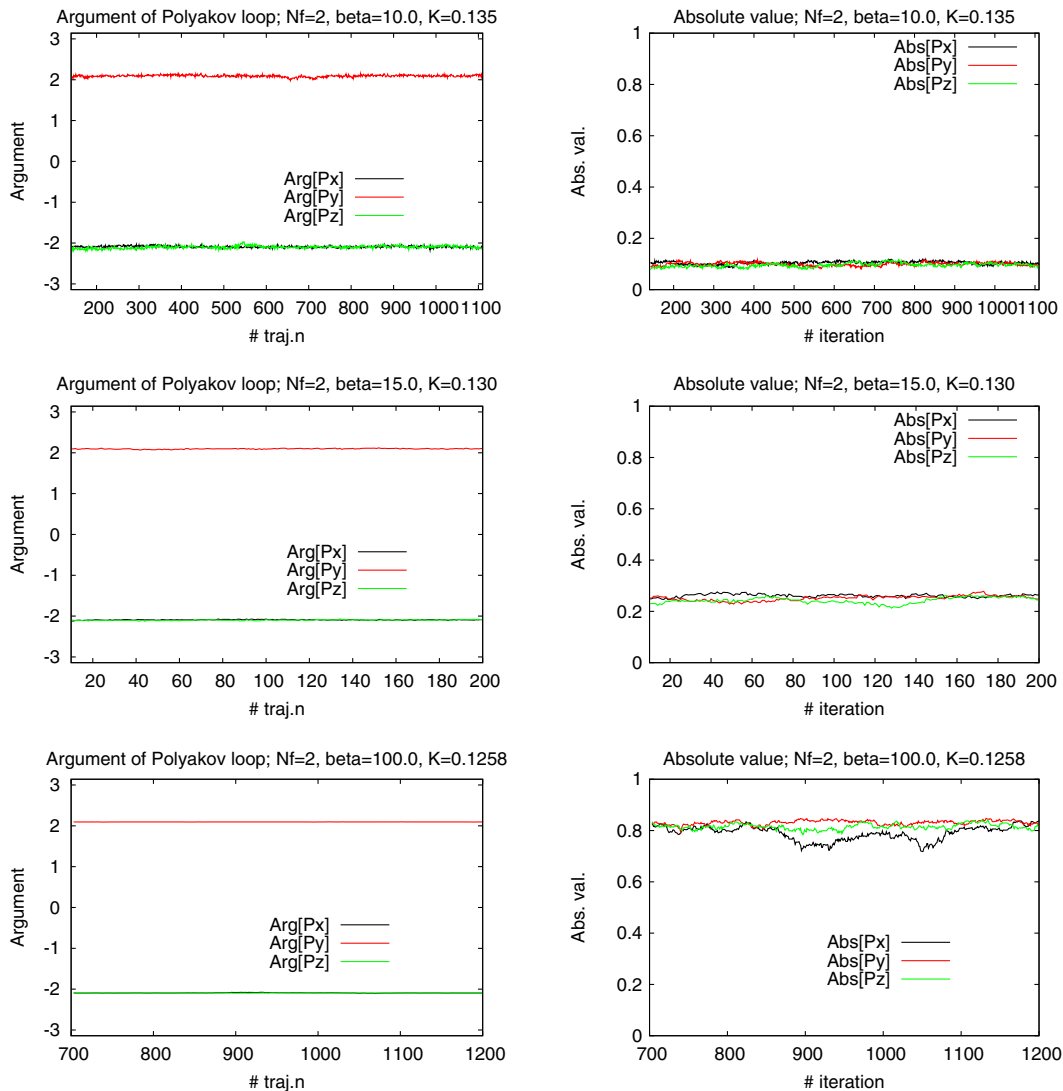


FIG. 38 (color online). The time history of the argument and the absolute value of Polyakov loops for $N_f = 2$ at $\beta = 10.0$ and $K = 0.135$, $\beta = 15.0$ and $K = 0.130$, and $\beta = 100.0$ and $K = 0.1258$.

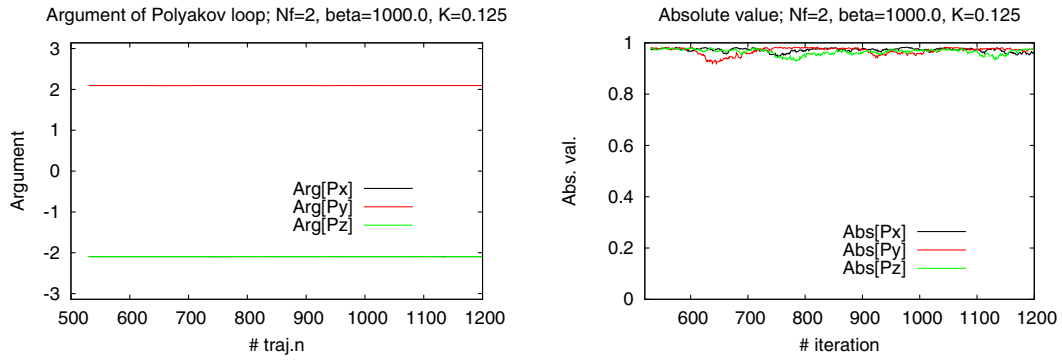


FIG. 39 (color online). The time history of the argument and the absolute value of Polyakov loops for $N_f = 2$ at $\beta = 1000.0$ and $K = 0.125$.

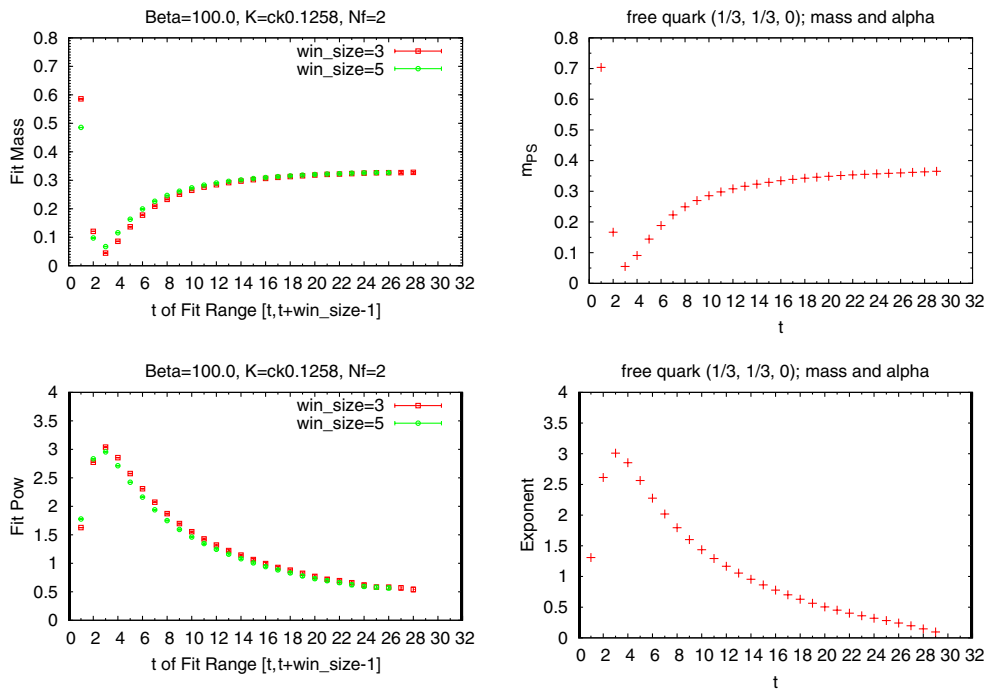


FIG. 40 (color online). The local mass $m(t)$ and the local exponent $\alpha(t)$ for $N_f = 2$ at $\beta = 100.0$ and $K = 0.1258$ (left) and for a free particle $(1/3, 1/3, 0)$ with $m_q = 0.01$ (right).

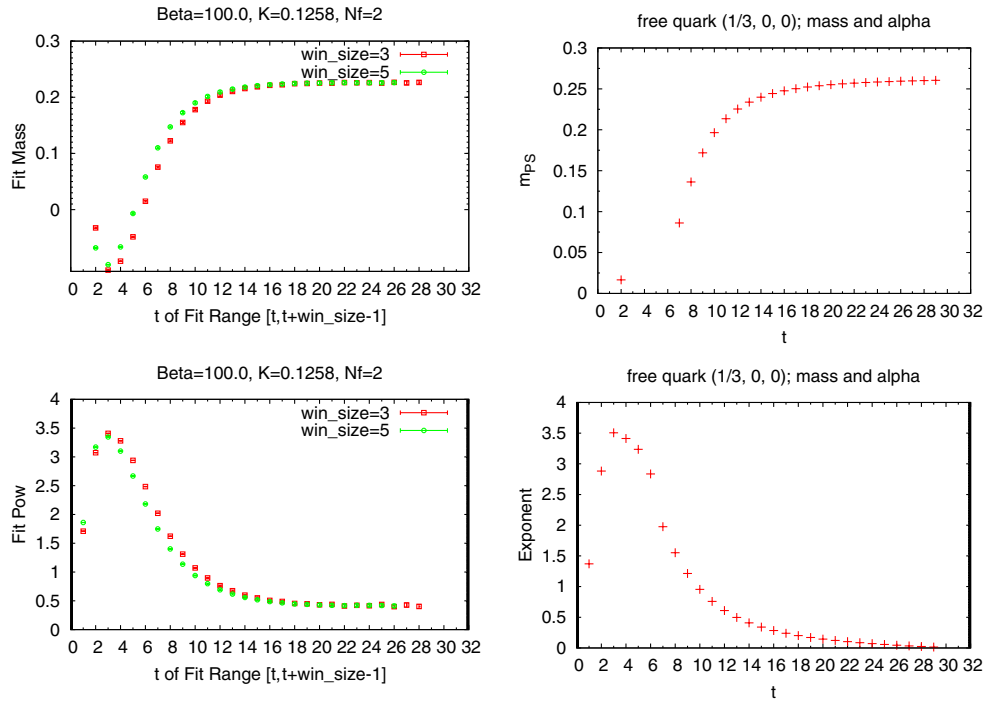


FIG. 41 (color online). The local mass $m(t)$ and the local exponent $\alpha(t)$ for $N_f = 2$ at $\beta = 100.0$ and $K = 0.1258$ (left) and for a free particle $(1/3, 0, 0)$ with $m_q = 0.01$ (right).

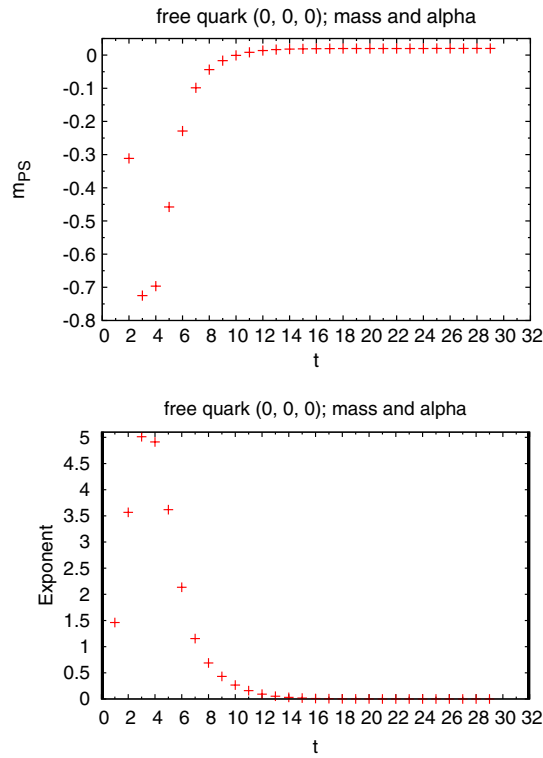


FIG. 42 (color online). The local mass $m(t)$ and the local exponent $\alpha(t)$ for a free particle $(0,0,0)$ with $m_q = 0.01$.

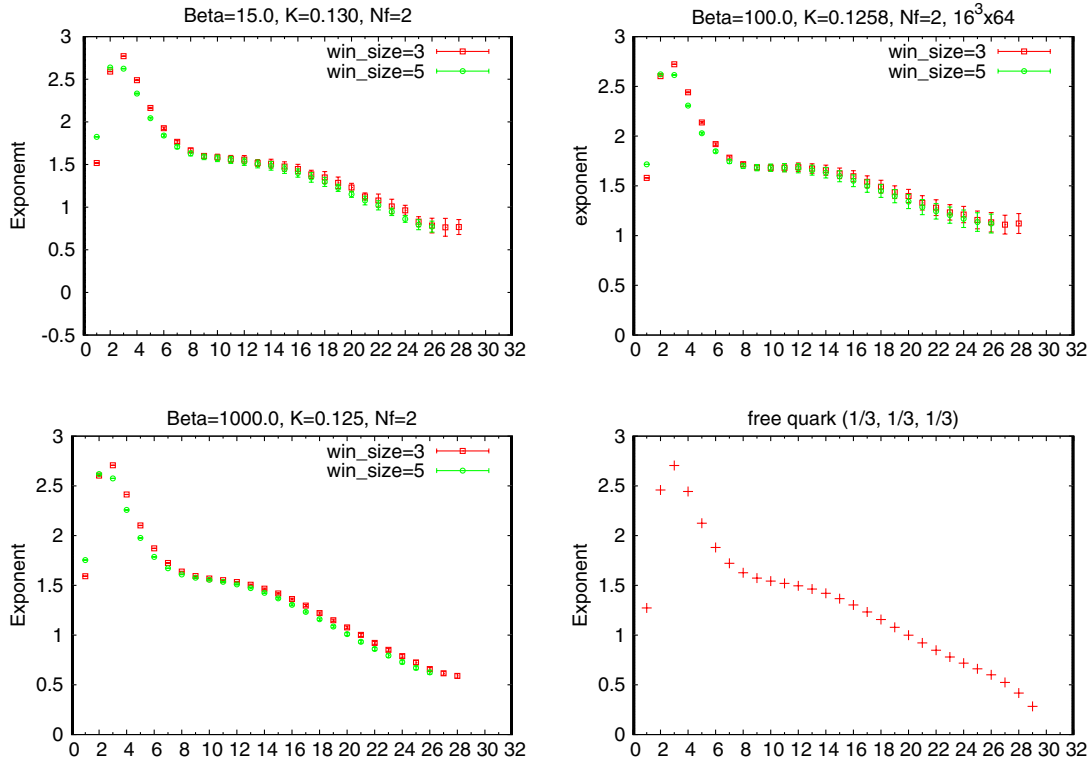


FIG. 43 (color online). The local exponent $\alpha(t)$: $N_f = 2$ at $\beta = 15.0$ and $K = 0.130$, $\beta = 100.0$ and $K = 0.1258$, and $\beta = 1000.0$ and $K = 0.125$, and for a free particle $(1/3, 1/3, 1/3)$ with $m_q = 0.01$.

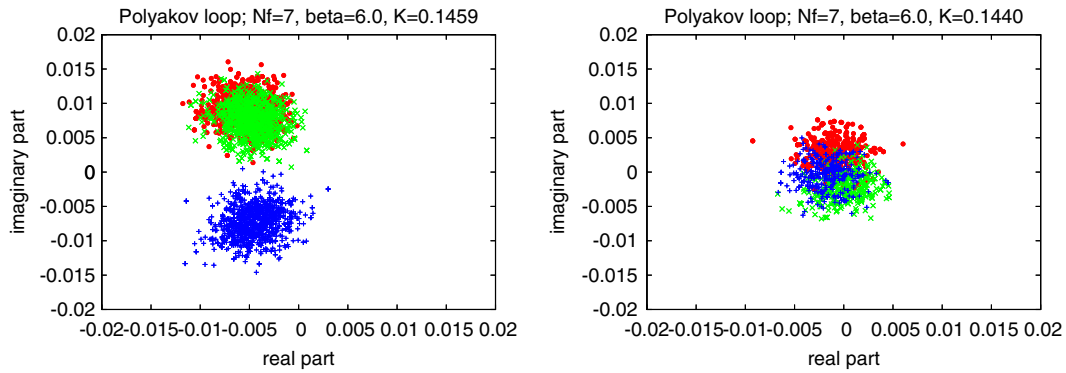


FIG. 44 (color online). The scattered plots of Polyakov loops in the x , y , and z directions overlaid, both for $N_f = 7$ at $\beta = 6.0$. (Left) $K = 0.1459$ and (right) $K = 0.1440$.

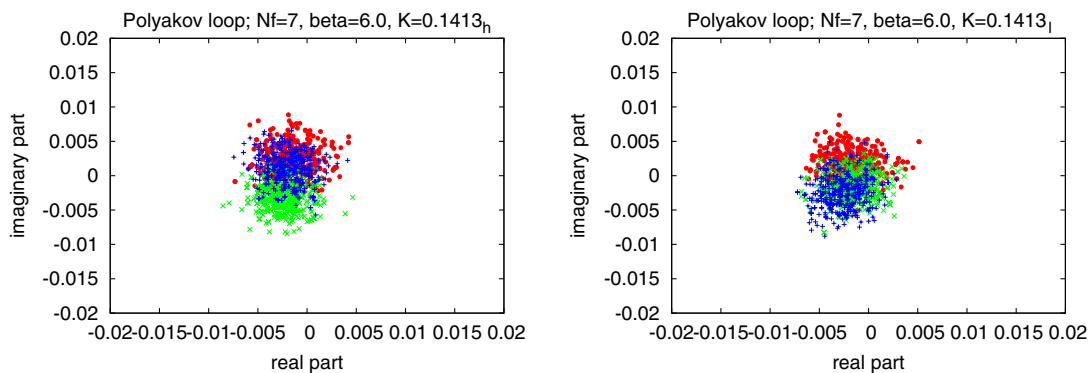


FIG. 45 (color online). The scattered plots of Polyakov loops in the x , y , and z directions overlaid, both for $N_f = 7$ at $\beta = 6.0$ and $K = 0.1413$. (Left) from larger K and (right) from smaller K .

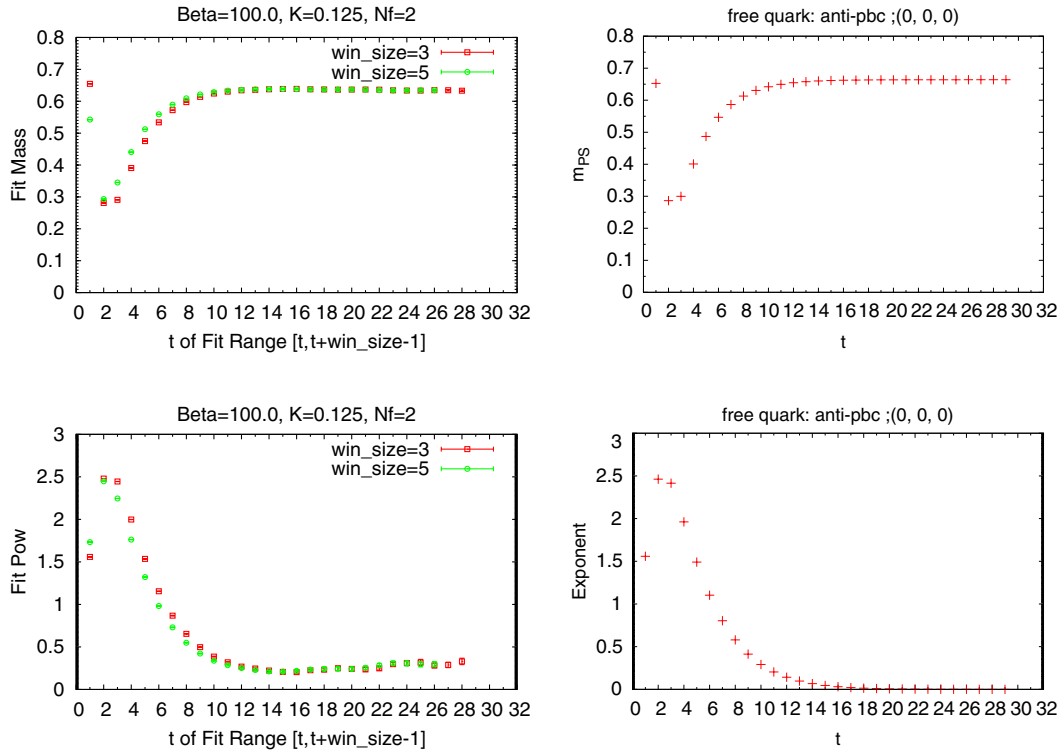


FIG. 46 (color online). The antiperiodic boundary conditions for fermion in the spatial directions; The local mass $m(t)$ and the local exponent $\alpha(t)$ for a free particle (0,0,0) (right) with $m_q = 0.01$ and for $N_f = 2$ at $\beta = 100.0$ and $K = 0.125$ (left).

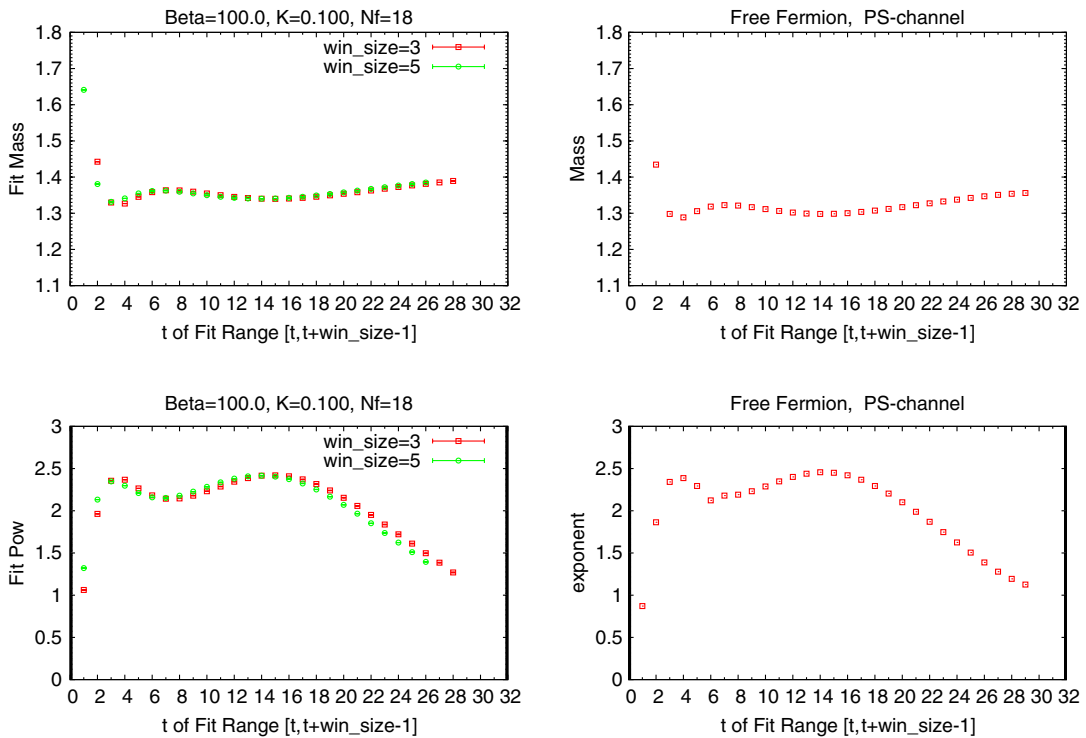


FIG. 47 (color online). The local mass $m(t)$ and the local exponent $\alpha(t)$ for $N_f = 18$ at $\beta = 100.0$ and $K = 0.100$ (left) and for a free particle (0,0,0) with $m_q = 1.0$ (right).

- [1] J. Giedt, *Proc. Sci.*, LATTICE2012 (2012) 006; E. Neil, *Proc. Sci.*, LATTICE2011 (2011) 009; L. Del Debbio, *Proc. Sci.*, LATTICE2010 (2010) 004, and references therein.
- [2] T. Banks and A. Zaks, *Nucl. Phys.* **B196**, 189 (1982).
- [3] W. E. Caswell, *Phys. Rev. Lett.* **33**, 244 (1974).
- [4] Y. Iwasaki, K. Kanaya, S. Kaya, S. Sakai, and T. Yoshie, *Phys. Rev. D* **69**, 014507 (2004).
- [5] S. Catterall and F. Sannino, *Phys. Rev. D* **76**, 034504 (2007).
- [6] S. Catterall, J. Giedt, F. Sannino, and J. Schneible, *J. High Energy Phys.* **11** (2008) 009.
- [7] S. Catterall, J. Giedt, F. Sannino, and J. Schneible, arXiv:0910.4387.
- [8] T. Appelquist, G. T. Fleming, and E. T. Neil, *Phys. Rev. Lett.* **100**, 171607 (2008); **102**149902E (2009); *Phys. Rev. D* **79**, 076010 (2009).
- [9] T. Appelquist *et al.* (LSD Collaboration), *Phys. Rev. Lett.* **104**, 071601 (2010).
- [10] T. Appelquist, G. T. Fleming, M. F. Lin, E. T. Neil, and D. A. Schaich, *Phys. Rev. D* **84**, 054501 (2011).
- [11] T. Appelquist, R. C. Brower, M. I. Buchoff, M. Cheng, S. D. Cohen, G. T. Fleming, J. Kiskis, and M. Lin *et al.*, arXiv:1204.6000.
- [12] Z. Fodor, K. Holland, J. Kuti, D. Nogradi, and C. Schroeder, *Phys. Lett. B* **681**, 353 (2009).
- [13] Z. Fodor, K. Holland, J. Kuti, D. Nogradi, and C. Schroeder, *Proc. Sci.*, LATTICE2009 (2009) 058.
- [14] Z. Fodor, K. Holland, J. Kuti, D. Nogradi, and C. Schroeder, *J. High Energy Phys.* **11** (2009) 103.
- [15] Z. Fodor, K. Holland, J. Kuti, D. Nogradi, and C. Schroeder, *Phys. Lett. B* **703**, 348 (2011).
- [16] A. Deuzeman, M. P. Lombardo, and E. Pallante, *Phys. Lett. B* **670**, 41 (2008).
- [17] A. Deuzeman, M. P. Lombardo, and E. Pallante, *Phys. Rev. D* **82**, 074503 (2010).
- [18] K. Miura, M. P. Lombardo, and E. Pallante, *Phys. Lett. B* **710**, 676 (2012).
- [19] A. Deuzeman, M. P. Lombardo, T. N. da Silva, and E. Pallante, *Phys. Lett. B* **720**, 358 (2013).
- [20] P. de Forcrand, S. Kim, and W. Unger, *J. High Energy Phys.* **02** (2013) 051.
- [21] X.-Y. Jin and R. D. Mawhinney, *Proc. Sci.*, LATTICE2011 (2011) 066.
- [22] A. Hasenfratz, *Phys. Rev. D* **82**, 014506 (2010).
- [23] A. Hasenfratz, *Phys. Rev. Lett.* **108**, 061601 (2012).
- [24] A. Cheng, A. Hasenfratz, and D. Schaich, *Phys. Rev. D* **85**, 094509 (2012).
- [25] T. DeGrand and A. Hasenfratz, *Phys. Rev. D* **80**, 034506 (2009).
- [26] T. DeGrand, Y. Shamir, and B. Svetitsky, *Phys. Rev. D* **82**, 054503 (2010).
- [27] T. DeGrand, *Phys. Rev. D* **84**, 116901 (2011).
- [28] T. DeGrand, Y. Shamir, and B. Svetitsky, *Phys. Rev. D* **85**, 074506 (2012).
- [29] T. DeGrand, Y. Shamir, and B. Svetitsky, *Phys. Rev. D* **87**, 074507 (2013).
- [30] Y. Aoki, T. Aoyama, M. Kurachi, T. Maskawa, K.-i. Nagai, H. Ohki, A. Shibata, K. Yamawaki, and T. Yamazaki, *Phys. Rev. D* **86**, 054506 (2012).
- [31] L. Del Debbio, A. Patella, and C. Pica, *Phys. Rev. D* **81**, 094503 (2010).
- [32] L. Del Debbio, B. Lucini, A. Patella, C. Pica, and A. Rago, *Phys. Rev. D* **80**, 074507 (2009).
- [33] L. Del Debbio, B. Lucini, A. Patella, C. Pica, and A. Rago, *Phys. Rev. D* **82**, 014510 (2010).
- [34] F. Bursa, L. Del Debbio, L. Keegan, C. Pica, and T. Pickup, *Phys. Rev. D* **81**, 014505 (2010).
- [35] L. Del Debbio and R. Zwicky, *Phys. Rev. D* **82**, 014502 (2010).
- [36] F. Bursa, L. Del Debbio, L. Keegan, C. Pica, and T. Pickup, *Phys. Lett. B* **696**, 374 (2011).
- [37] L. Del Debbio and R. Zwicky, *Phys. Lett. B* **700**, 217 (2011).
- [38] F. Bursa, L. Del Debbio, D. Henty, E. Kerrane, B. Lucini, A. Patella, C. Pica, and T. Pickup, and A. Rago, *Phys. Rev. D* **84**, 034506 (2011).
- [39] A. Patella, *Phys. Rev. D* **86**, 025006 (2012).
- [40] M. I. Buchoff, *Phys. Rev. D* **85**, 074503 (2012).
- [41] M. Hayakawa, K. I. Ishikawa, Y. Osaki, S. Takeda, S. Uno, and N. Yamada, *Phys. Rev. D* **83**, 074509 (2011).
- [42] J. Giedt and E. Weinberg, *Phys. Rev. D* **84**, 074501 (2011).
- [43] J. Giedt and E. Weinberg, *Phys. Rev. D* **85**, 097503 (2012).
- [44] A. J. Hietanen, J. Rantaharju, K. Rummukainen, and K. Tuominen, *J. High Energy Phys.* **05** (2009) 025.
- [45] A. J. Hietanen, K. Rummukainen, and K. Tuominen, *Phys. Rev. D* **80**, 094504 (2009).
- [46] T. Karavirta, A. Mykkanen, J. Rantaharju, K. Rummukainen, and K. Tuominen, *J. High Energy Phys.* **06** (2011) 061.
- [47] T. Karavirta, J. Rantaharju, K. Rummukainen, and K. Tuominen, *J. High Energy Phys.* **05** (2012) 003.
- [48] T. Karavirta, K. Tuominen, and K. Rummukainen, *Phys. Rev. D* **85**, 054506 (2012).
- [49] A. Hasenfratz, A. Cheng, G. Petropoulos, and D. Schaich, *Proc. Sci.*, LATTICE2012 (2012) 034.
- [50] Z. Fodor, K. Holland, J. Kuti, D. Nogradi, C. Schroeder, and C. H. Wong, *Prog. Theor. Phys. Suppl.* **197**, 31 (2012).
- [51] Z. Fodor, K. Holland, J. Kuti, D. Nogradi, C. Schroeder, and C. H. Wong, *Phys. Lett. B* **718**, 657 (2012).
- [52] Z. Fodor, K. Holland, J. Kuti, D. Nogradi, C. Schroeder, and C. H. Wong, *Proc. Sci.*, LATTICE2012 (2012) 279.
- [53] E. Itou, *Prog. Theor. Exp. Phys.* **2013**, 083B01 (2013).
- [54] E. Itou, arXiv:1307.6645.
- [55] M. Luescher, P. Weisz, and U. Wolff, *Nucl. Phys.* **B359**, 221 (1991).
- [56] K.-I. Ishikawa, Y. Iwasaki, Y. Nakayama, and T. Yoshie, arXiv:1304.4345.
- [57] Y. Iwasaki, in *Strong Coupling Gauge Theories in the LHC Perspective (SCGT 12)*, edited by Y. Aoki, T. Maskawa, and K. Yamawaki (World Scientific, Singapore, 2014) p. 1.
- [58] M. Bochicchio, L. Maiani, G. Martinelli, G. Rossi, and M. Testa, *Nucl. Phys.* **B262**, 331 (1985).
- [59] S. Itoh, Y. Iwasaki, Y. Oyanagi, and T. Yoshié, *Nucl. Phys.* **B274**, 33 (1986).
- [60] Y. Iwasaki, K. Kanaya, S. Sakai, and T. Yoshié, *Phys. Rev. Lett.* **67**, 1494 (1991).
- [61] M. Hayakawa *et al.*, *Proc. Sci.*, LATTICE2010 (2010) 325.
- [62] M. A. Clark and A. D. Kennedy, *Phys. Rev. Lett.* **98**, 051601 (2007).
- [63] Y. Iwasaki, K. Kanaya, S. Kaya, S. Sakai, and T. Yoshié, *Phys. Rev. D* **54**, 7010 (1996).

- [64] K.-I. Ishikawa, Y. Iwasaki, Y. Nakayama, and T. Yoshié, *Phys. Rev. D* **87**, 071503 (2013).
- [65] T. Alho, M. Jarvinen, K. Kajantie, E. Kiritsis, and K. Tuominen, *J. High Energy Phys.* 01 (2013) 093.
- [66] J. Braun and H. Gies, *Phys. Lett. B* **645**, 53 (2007).
- [67] J. Braun and H. Gies, *J. High Energy Phys.* 06 (2006) 024.
- [68] J. Polchinski, *Nucl. Phys.* **B303**, 226 (1988).
- [69] Y. Nakayama, *Int. J. Mod. Phys. A* **25**, 4849 (2010).
- [70] Y. Nakayama, [arXiv:1302.0884](https://arxiv.org/abs/1302.0884).
- [71] L. Del Debbio and R. Zwicky, *Phys. Rev. D* **89**, 014503 (2014).
- [72] Y. Hosotani, *Phys. Lett.* **126B**, 309 (1983).
- [73] V. A. Miransky, *Phys. Rev. D* **59**, 105003 (1999).
- [74] G. Cacciapaglia, G. Marandella, and J. Terning, *J. High Energy Phys.* 02 (2009) 049.
- [75] M. Asakawa and T. Hatsuda, *Phys. Rev. Lett.* **92**, 012001 (2004); S. Datta, F. Karsch, P. Petreczky, I. Wetzorke, *Phys. Rev. D* **69**, 094507 (2004); H. T. Ding, A. Francis, O. Kaczmarek, F. Karsch, H. Satz, and W. Soeldner, *Phys. Rev. D* **86**, 014509 (2012); G. Aarts, C. Allton, S. Kim, M. P. Lombardo, M. B. Oktay, S. M. Ryan, D. K. Sinclair, and J.-I. Skullerud, *J. High Energy Phys.* 11 (2011) 103.
- [76] Y. Iwasaki, K. Kanaya, S. Sakai, and T. Yoshié, *Phys. Rev. Lett.* **69**, 21 (1992).
- [77] Y. Iwasaki, K. Kanaya, S. Sakai, and T. Yoshié, *Nucl. Phys. B, Proc. Suppl.* **30**, 327 (1993); Y. Iwasaki, K. Kanaya, S. Sakai, and T. Yoshié, *Nucl. Phys. B, Proc. Suppl.* **34**, 314 (1994); Y. Iwasaki, K. Kanaya, S. Kaya, S. Sakai, and T. Yoshié, *Nucl. Phys. B, Proc. Suppl.* **53**, 449 (1997).
- [78] Y. Iwasaki, in *Perspectives of Strong Coupling Gauge Theories*, edited by J. Nishimura and K. Yamawaki (World Scientific, Singapore, 1997), p. 135; Y. Iwasaki, K. Kanaya, S. Kaya, S. Sakai, and T. Yoshié, *Prog. Theor. Phys. Suppl.* **131**, 415 (1998); Y. Iwasaki, K. Kanaya, S. Kaya, T. Yoshié, and S. Sakai, in *Dynamics of Gauge Fields*, edited by A. Chodos *et al.* (Universal Academy Press, Tokyo, 2000), p. 145; Y. Iwasaki, in *Proceedings of International Workshop SCGT2002*, Nagoya, Japan, 2002), p. 10.
- [79] K.-I. Nagai, M. G. Carrillo-Ruiz, G. Koleva, and R. Lewis, *Phys. Rev. D* **80**, 074508 (2009).
- [80] K.-I. Nagai, M. G. Carrillo-Ruiz, G. Koleva, and R. Lewis, *Proc. Sci., LATTICE2010* (2010) 065.
- [81] T. Banks and A. Casher, *Nucl. Phys.* **B169**, 103 (1980).
- [82] L. Giusti and M. Lüscher, *J. High Energy Phys.* 03 (2009) 013.
- [83] O. Kaczmarek, F. Karsch, F. Zantow, and P. Petreczky, *Phys. Rev. D* **70**, 074505 (2004).
- [84] T. A. Ryttov and F. Sannino, *Phys. Rev. D* **78**, 065001 (2008).
- [85] D. B. Kaplan, J.-W. Lee, D. T. Son, and M. A. Stephanov, *Phys. Rev. D* **80**, 125005 (2009).
- [86] R. Pisarski and F. Wilczek, *Phys. Rev. D* **29**, 338 (1984).
- [87] Y. Iwasaki, K. Kanaya, S. Kaya, and T. Yoshié, *Phys. Rev. Lett.* **78**, 179 (1997).
- [88] A. Ali Khan *et al.* (CP-PACS Collaboration), *Phys. Rev. D* **63**, 034502 (2000).
- [89] S. Ejiri, F. Karsch, E. Laermann, C. Miao, S. Mukherjee, P. Petreczky, C. Schmidt, W. Soeldner, and W. Unger, *Phys. Rev. D* **80**, 094505 (2009); A. Bazavov *et al.*, *Phys. Rev. D* **85**, 054503 (2012).
- [90] S. Aoki, H. Fukaya, and Y. Taniguchi, *Phys. Rev. D* **86**, 114512 (2012).